(2)

METAL MATRIX COMPOSITE: STRENGTHENING MECHANISMS

ANNUAL REPORT

OF

CONTRACT NO. N00014-85-K-0007

FROM

THE OFFICE OF NAVAL RESEARCH

PREPARED BY

R. J. ARSENAULT
METALLURGICAL MATERIALS LABORATORY
UNIVERSITY OF MARYLAND
COLLEGE PARK, MARYLAND

OCTOBER 1989

Unclassified

SECURITY CLASSIFICATION OF THIS PAGE

REPORT DOCUMENTATION PAGE

1a. REPORT SECURITY CLASSIFICATION: Unclassified	1b. RESTRICTIVE MARKINGS
2a. SECURITY CLASSIFICATION AUTHORITY	3. DISTRIBUTION/AVAILABILITY OF REPORT
2b. DECLASSIFICATION/DOWNGRADING SCHEDULE	
4. PERFORMING ORGANIZATION REPORT NUMBER(S): MML-1989-1	5. MONITORING ORGANIZATION REPORT NUMBER(S)
6a. NAME OF PERFORMING ORGANIZATION: University of Maryland; 6b. OFFICE SYMBOL (If applicable)	7a. NAME OF MONITORING ORGANIZATION
6c. ADDRESS (City, State and ZIP Code): Chemical & Nuclear Engineering Bldg. University of Maryland College Park, Md 20742-2115	7b. ADDRESS (City, State and ZIP Code)
8a. NAME OF FUNDING/SPONSORING ORGANIZATION: Office of Naval Research; 8b. OFFICE SYMBOL (If applicable)	9. PROCUREMENT INSTRUMENT IDENTIFICATION NUMBER: N00014-85-K-0007
8c. ADDRESS (City, State and ZIP Code): Office of Naval Research Code 1131N Arlington, VA 22217	10. SOURCE OF FUNDING NOS.

PROGRAM ELEMENT NO.	PROJECT NO.	TASK NO.	WORK UNIT NO.

11. TITLE (Include Security Classification): Metal Matrix Composite: Strengthening Mechanisms

12. PERSONAL AUTHOR(S): Richard J. Arsenault

13a. TYPE OF REPORT	13b. TIME COVERED	14. DATE OF REPORT (Yr., Mo., Day)	15. PAGE COUNT
Annual	FROM Oct. 88 TO Sept. 89	1989 October	153

16. SUPPLEMENTARY NOTATION

17. COSATI CODES			18. SUBJECT TERMS (Continue on reverse if necessary and identify by block number)
FIELD	GROUP	SUB GR.	Metal Matrix Composites titanium; SiC/Al; TiB_2/NiAl

19. ABSTRACT (Continue on reverse if necessary and identify by block number)

All of the existing strengthening mechanisms that have been proposed to explain the increase in strength of discontinuous reinforcement composites are based on the assumption that the reinforcement does not deform. However, it appears that TiB_2 deforms at high temperature within the NiAl matrix.

It has also been observed that there is no apparent dislocation generation due to the difference in coefficient of thermal expansion between TiB_2 and NiAl.

A finite element method investigation has demonstrated how and why the deformation is localized in discontinuous reinforced composites.

The addition of discontinuous SiC to Al alloys can result in a five-fold increase in the yield stress and this increase in strength is readily accounted for by changes in the matrix strength.

20. DISTRIBUTION/AVAILABILITY OF ABSTRACT	21. ABSTRACT SECURITY CLASSIFICATION
UNCLASSIFIED/UNLIMITED ☒ SAME AS RPT. ☐ DTIC USERS ☐	Unclassified

22a. NAME OF RESPONSIBLE INDIVIDUAL	22b. TELEPHONE NUMBER (Include Area Code)	22c. OFFICE SYMBOL
Dr. S.G. Fishman	703-696-0285	ONR/1131

DD FORM 1473, 83 APR EDITION OF 1 JAN 73 IS OBSOLETE. Unclassified

SECURITY CLASSIFICATION OF THIS PAGE

Table of Contents

I. SUMMARY

In the following paragraphs, a brief summary of the advances in our understanding of the strengthening mechanisms of discontinuous composites will be given.

All of the existing strengthening mechanisms that have been proposed to explain the increase in strength of discontinuous reinforcement composites are based on the assumption that the reinforcement does not deform. We have found that there is an increase in dislocation density within TiB_2 (the reinforcement in NiAl) as a result of deformation of the composite at 1273 K. This increased dislocation density indicates that the TiB_2 is deforming during the deformation of the composite.

It has also been observed that there is no apparent dislocation generation due to the difference in coefficient of thermal expansion between TiB_2 and NiAl. However, there is evidence of dislocation generation about the TiB_2 particles (due to a modulus difference) during plastic deformation.

A finite element method investigation has demonstrated how and why the deformation is localized in discontinuous reinforced composite. This local deformation has been observed in SiC/Al and TiB_2/NiAl composite. Even though there is higher localized volume function of TiB_2 or SiC, this is the region (in the matrix) in which the higher density of slip lines and dislocations occur.

The addition of discontinuous SiC to Al alloys can result in a five-fold increase in the yield stress. The magnitude of the increase is obviously a function of the volume fraction and the particle size of the SiC. Previously, it was proposed that the strength increase due to SiC addition to Al alloys was the result of change in the matrix strength, i.e. an increase in dislocation density and a reduction of subgrain size. The data obtained from a series of experiments indicate that dislocation density increases with an increase in volume fraction of SiC and decreases with an increase in particle size. The subgrain size decreases as the volume fraction increases and increases as the particle size increases. There is a good correlation between the microstructural changes in the matrix and the changes in the yield

stress of the composites.

Following is a list of the publications and presentations and copies of the publications which resulted from the research supported by contract number N00014-85-K-0007 in the time period from October 1988 to September 1989.

II. PUBLICATIONS AND PRESENTATIONS

A. PUBLICATIONS

1. Book entitled **Metal Matrix Composites: Thermomechanical Behavior** 1989 (Co-author)

2. **Relationship Between Strengthening Mechanism And Fracture Toughness of Discontinuous SiC/Al Composites**
J. Comp. Tech. Research 10, 1988, 140.

3. **Effect of Particle Size on Fracture Toughness in SiC/Al Composite Materials**
Y. Flom and R. J. Arsenault
Acta Metal. 37, 1987, 2413.

4. **The Effect of External Mechanical Loading on the Change of the Matrix Residual Stresses in SiC/Al Composites**
N. Shi and R. J. Arsenault
Accepted for publication in *The 7th Int. Conf. on Composite Materials*, China.

5. **Fracture Toughness of SiC/Al Composite Materials**
Y. Flom, S. B. Wu and R. J. Arsenault
SAMPE Proc. (in press)

6. **Microstructure of TiB_2/NiAl**
L. Wang and R.J. Arsenault, submitted for publication in *Mater. Sci. Eng.*

7. **Dislocations in TiB_2**
L. Wang and R.J. Arsenault, submitted for publication in *Phil. Mag.*

8. **Localized Deformation of SiC/Al Composites**
R.J. Arsenault, N. Shi, C.R. Feng and L. Wang, submitted for publication in *Mater. Sci. Eng.*

9. **Strengthening of Composites Due to Microstructural Changes in the Matrix**
R.J. Arsenault, L. Wang and C. R. Feng, submitted for publication

B. PRESENTATIONS

1. Virginia Polytechnical Institute, 1989, "Strengthening Mechanisms in Discontinuous Metal Matrix Composites"

2. March APS Meeting, 1989, "Quantum Chemical Study of Adhesion at Al/SiC

Interface"
P. Jena, S. Li and R. J. Arsenault

3. Annual Meeting of AIME, 1989, "Strengthening of Discontinuous Metal Matrix Composites Due to Dislocations"
R. J. Arsenault, L. Wang and C. R. Feng

4. Eleventh Annual DMMC, 1989, "Microstructure of TiB_2/NiAl"
L. Wang and R. J. Arsenault

5. 47th Annual Meeting of EMSA, 1989, "Dislocation Structures in TiB_2/NiAl Composites Deformed at High Temperature"
L. Wang and R. J. Arsenault

6. 34th International SAMPE Meeting, 1989, "Fracture Toughness of SiC/Al Composite Materials"
Y. Flom, S. B. Wu and R. J. Arsenault

7. Fall Meeting of ASM/AIME, 1989, "Crack Tip Propagation in SiC/Al Composites"
S. B. Wu and R. J. Arsenault

8. Fall Meeting of ASM/AIME, 1989, "The Change of Residual Stress Due to Mechanical Loading"
N. Shi and R. J. Arsenault

III. PUBLICATIONS

Richard J. Arsenault[1]

Authorized Reprint 1988 from Journal of Composites Technology & Research, Winter 1988

Relationship Between Strengthening Mechanisms and Fracture Toughness of Discontinuous SiC/Al Composites

REFERENCE: Arsenault, R. J., **"Relationship Between Strengthening Mechanisms and Fracture Toughness of Discontinuous SiC/Al Composites,"** *Journal of Composites Technology & Research*, Vol. 10, No. 4, Winter 1988, pp. 140-145.

ABSTRACT: In all cases of discontinuous silicon carbide (SiC/Al) metal matrix it was shown that classical composite strengthening mechanisms could not be used to explain the data. A high dislocation density model was proposed to account for the strengthening, but other factors, such as residual stress and texture, could contribute. These were investigated, and it was shown that texture had no effect and residual stress reduced the tensile yield stress. The fracture process in the composites is controlled by fracture of the matrix up to SiC particle sizes of 20 μm and for larger SiC size particles fracture of SiC begins to dominate. The fracture process in the matrix is influenced by residual hydrostatic tension and high density of dislocations generated at SiC/Al interfaces. Crack initiation fracture toughness does not depend on SiC particle size, for particle sizes less than 20 μm. Crack growth resistance increases as the size of the SiC particles increases.

KEYWORDS: discontinuous SiC/Al composites, strengthening mechanisms, fracture toughness, residual stress, texture

The framework of a mechanism is slowly evolving to account for the strengthening caused by the addition of silicon carbide (SiC)[2] to an aluminum (Al) alloy matrix. However, it should be kept in mind that the number of detailed investigations of these composites is rather limited [*1-5*].

The basic strengthening mechanism is the high dislocation density, which is produced as a result of the differences in the thermal coefficients of expansion between SiC and aluminum, and the small subgrain size that results. There could be other contributing causes to the strengthening such as

(1) residual elastic stresses,
(2) differences in texture, and
(3) classical composite strengthening (load transfer).

Therefore, a listing of the components of the strengthening mechanisms can be proposed

$$\Delta\sigma_{YC} = \Delta\sigma_{DISL} + \Delta\sigma_{SC} \pm \Delta\sigma_{RES} + \Delta\sigma_{TEX} + \Delta\sigma_{COMP}$$

where $\Delta\sigma_{DISL}$ is the increase in strengthening caused by the increase in dislocation density resulting from the differences in thermal coefficients of expansion between the SiC and aluminum, $\Delta\sigma_{SC}$ is the increase in strengthening caused by the reduced subgrain size, $\Delta\sigma_{RES}$ is the change in yield stress caused by presence of the thermal residual stress that results from the difference in thermal coefficients of expansion of the matrix and reinforcement, $\Delta\sigma_{TEX}$ is the difference in strengthening caused by differences in texture between the 0 Vol% and the higher volume percent composites, and $\Delta\sigma_{COMP}$ is the strengthening caused by classical composite strengthening, for example, load transfer.

Dislocation generation about the SiC particle caused by differences in the coefficient of thermal expansion was modeled by a simple prismatic punching model [*6*]. Figure 1 is a schematic of a particle that can take on the shape of a cube, plate, or whisker, from which several dislocations have been "punched" out. If the strengthening caused by this simple prismatic punching [*6*] is considered then 20 Vol% spherical SiC with a diameter of 0.5 μm would produce a $\Delta\sigma$ of 133.9 MPa, and 20 Vol% of whisker of l/d of 2 with a diameter of 0.5 μm (which is the approximate average diameter of the whiskers in the composite) would produce a $\Delta\sigma$ of 124.2 MPa. The model predicts a higher strengthening for the spherical morphology as compared to the whisker morphology caused by the difference in volume of the SiC, not the volume fraction; the volume fraction of SiC remains the same.

The change in strength caused by a large decrease in subgrain size can be obtained from the experimental investigations of McQueen and Jonas [*7*].

An analytical model by Arsenault and Taya [*4*] based on an ellipsoidal-shaped SiC particle in the aluminum matrix was developed, which predicts that a tensile thermal residual stress should exist in the matrix for a whisker of l/d of 1.8 and that the longitudinal residual stress should be higher than the transverse residual stress. Also, in the case of composite containing spherical reinforcement there should be zero net residual stress.

A mechanism or mechanisms of fracture in these composites have not emerged as yet, and low ductility and fracture toughness of discontinuous SiC/Al composites remains a major obstacle to the practical application of these materials. Despite the significant improvement in the processing of SiC/Al composites in the recent years, fracture toughness is still in the range of 12 to 33 MPa $\cdot$ m$^{1/2}$ [*8-11*]. It is not clear how the interfacial SiC/Al bond strength, difference in CTE between SiC and aluminum, and size of the SiC reinforcement affect the toughness. It has already been established that the increase in the volume fraction of SiC particles or whiskers or both and the increase of the matrix strength adversely influence the toughness of SiC/Al composites [*10,12*].

The purpose of this investigation was to consider the above men-

[1]Professor, Engineering Materials Group, University of Maryland, College Park, MD 20742.
[2]In all cases the discussion is of discontinuous metal matrix composites.

0885-6804/88/0012-0140$02.50

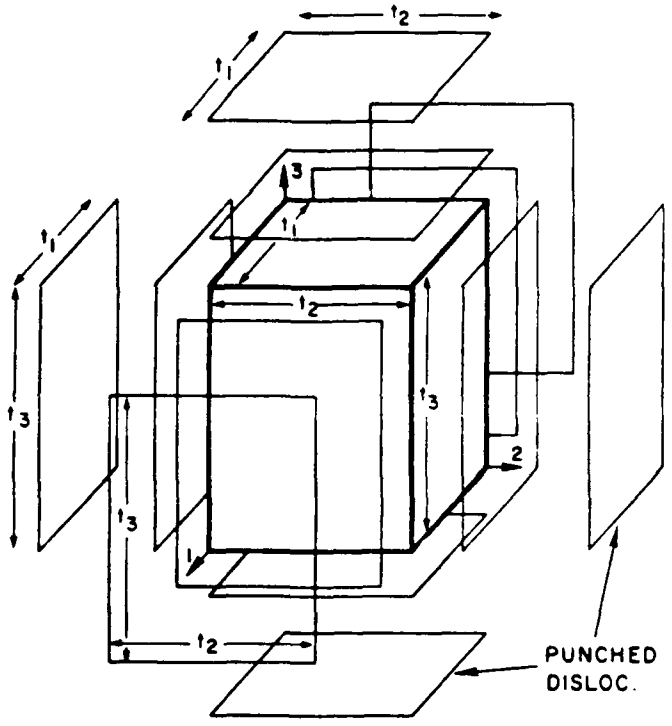

FIG. 1—*A schematic diagram of the particle and several prismatic punched dislocations.*

tioned three remaining strengthening items, that is, residual stress, texture, and composite strengthening. This paper will also examine the dependence of the toughness and tensile properties of the SiC/Al composites on size and morphology of the SiC reinforcement.

Materials, Test Methods, and Results

Two different SiC morphologies, whisker ($l/d \approx 1.8$ to 2.8 where $d \approx 0.5$ μm) and spherical (~0.5 μm in diameter), and three different matrices, 1100, 6061, and 7091 Al alloys, were used. In fracture toughness investigations, various sizes of SiC particles were used, and they will be described later.

The specimens used for the residual stress measurements were cylindrical, ~12.5 mm in diameter by ~25 mm long, and had four flats 3 mm wide machined along the length of the cylinder. The specimens were then annealed for 12 h at 803 K and furnace cooled. The residual stresses were determined by measuring the changes in the lattice parameters for the various composites. There is a recognizable error in this method, but it was found that standard techniques of using X-rays were completely useless. The standard techniques assumed the specimen has a uniform tensile or compressive stress [*13*], along the length of the specimen. However, in discontinuous composites this is not the case as Arsenault and Taya have shown [*4*], the residual stress varies from point to point within the specimen.

The actual experimental data obtained from an X-ray analysis is shown in Table 1. The X-ray results do indicate that the matrix is in tension and that the longitudinal residual stress is higher than the transverse residual stress. However, the X-ray data indicate a higher value of residual stress than predicted [*4*]. Also, the residual

TABLE 1—*The thermal residual stresses (tensile) as measured by X-ray diffraction techniques.*

Material	Transverse, MPa	Longitudinal, MPa
0 Vol% whisker SiC 6061 matrix	0.0	0.0
5 Vol% whisker SiC 6061 matrix	34.5	407.1
20 Vol% whisker SiC 6061 matrix	55.2	227.70
Wrought	0.0	0.0

stress will effect the yield stress. The model of Arsenault and Taya [*4*] predicts that the yield stress in tension will be less than that in compression for whisker SiC reinforced composites. If the SiC is in the form of spheres there should be no difference in tensile or compressive yield stress. In the case of the spherical SiC reinforced composite there are tensile and compressive residual stresses in the matrix, but they cancel each other so the NET residual stress is zero. Table 2 lists experimental data obtained from 1100 aluminum matrix specimens tested in the annealed condition. The surprising result is that in the case of spherical SiC composites, the tensile stress is higher than that of the compressive yield stress, whereas the difference predicted by the model is zero. However, the point to be made is that for the whisker case $\sigma_y^C > \sigma_y^T$. The model of Arsenault and Taya [*4*] successfully predicts the differences in the tensile and compressive yield stress because of the thermal residual stresses. However, the model is completely incapable of predicting the absolute magnitude of the increase in yield stress, for it does not have the capability of predicting the increase in the matrix strengthening.

A "texture" [*14*] investigation was undertaken, to determine if the presence of the reinforcement would produce a difference in texture from that of the unreinforced matrix material. If there is a difference in the texture between the composite and unreinforced matrix material there will be a difference in the yield strength of the composite and the unreinforced matrix material [*15*]. From a comparison of the data (Fig. 2) it is apparent that there is little difference in the texture of the 99.99% aluminum, 0 Vol%, 6061 aluminum alloy and 20 Vol% 6061 aluminum alloy matrix composite. Therefore "texture" does not produce any difference in the yield strength of the composite and the unreinforced material.

The remaining term to be considered is the $\Delta\sigma_{COMP}$, which is defined as classical composite strengthening or load transfer strengthening. The load transfer model developed by Taya and Arsenault [*5*] as stated before predicts very little strengthening. This model, which is based on Eshbely's model [*16*], handles load transfers in much greater detail than the shear lag model, and this certainly takes into account the end effects [*17*]. For the case of whis-

TABLE 2—*Difference in yield stress.*

Matrix	Vol%	$\Delta\sigma$,* MPa
1100	0	3.8
1100	20$_a$	42.9
1100	20$_b$	−15.46

*$\Delta\sigma = \sigma_y^C - \sigma_y^T$

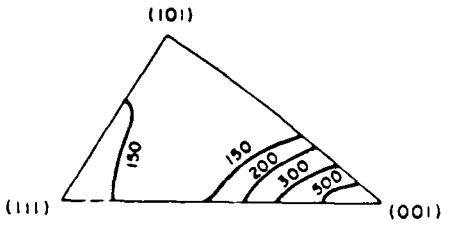

TEXTURE FOR EXTRUDED & ANNEALED
99.99% Al

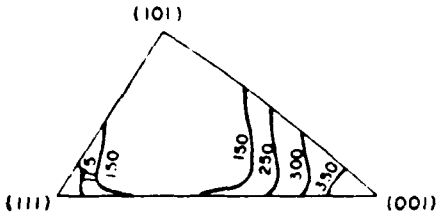

TEXTURE FOR EXTRUDED & ANNEALED
0V% SiC 1100 MATRIX

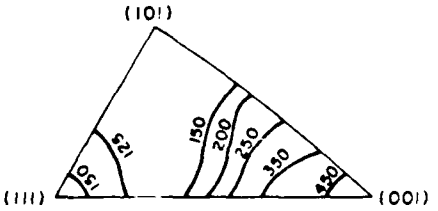

TEXTURE FOR EXTRUDED & ANNEALED
20V% SiC 1100 MATRIX

FIG. 2—*The texture of composites containing various volume fraction of SiC*

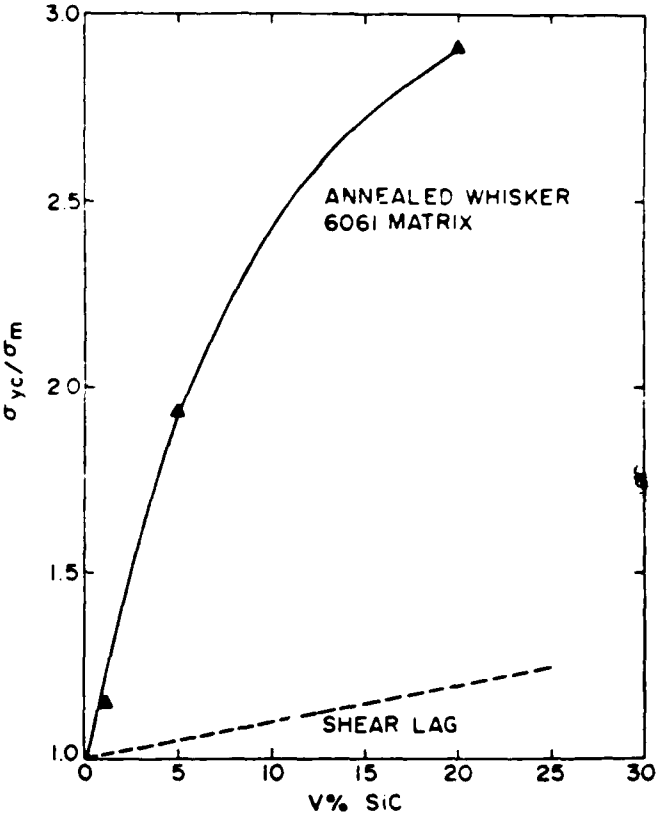

FIG. 3—*The yield stress as a function of volume fraction of SiC. The solid line is of the experimental results. The dashed line represents the yield stress as predicted by the shear lag model.*

TABLE 3—*Differences in yield stress for different matrices*

Matrix Material Annealed	$\Delta\sigma_y$,* MPa	% $\Delta\sigma_y$
1100	144.9	420
6061	100	181
7091	131.1	190

*$\Delta\sigma_y = \sigma_{y,\ 20\ Vol\%} - \sigma_{y,\ 0\ Vol\%}$

ker composite with a l/d of 1.8 (which was obtained from histograms [1]) the model predicts that the composite will have a slightly lower tensile yield stress than the matrix alloy with 0 Vol% SiC in it. The reason for this lower yield in the composite is due to the thermal residual stress. Figure 3 is a plot of yield stress versus volume fraction of SiC, and it is obvious that the experimentally observed strengthening is much greater than that predicted by the composite theory. Also, the composite theory predicts that if the shape of the reinforcement remains the same and volume fraction remains the same, the yield strength should be the same. However, experimentally, it was found that by changing the particle size from ~ 5 to 250 μm, the yield stress decreases from ~ 172.5 to ~ 69 MPa.

Another investigation was undertaken to determine the effect of different matrices on the strength of the composite. Composite rods were obtained from ARCO Silag containing 0 and 20 Vol% SiC whisker with 3 different Al alloy matrices, 1100, 6061, and 7091. The rods were machined into tension specimens and then annealed and furnace cooled. The difference in yield strength between the 20 and 0 Vol% are listed in Table 3. There is a slight decrease in the magnitude of the increase in strengthening when comparing 1100 and 6061 or 7091. It was expected that the higher yield stress of the 6061 and 7091 matrices, as compared to the 1100, would result in a lower production of dislocations and a higher value of the thermal residual elastic stress. Both of these effects would reduce the increase in tensile yield stress of 6061 and 7091 matrices, which is in agreement with experimental results.

In the fracture investigation, specimens containing various size SiC particles were used. The SiC particles have a general shape of a platelets with a length to thickness ratio of 2 to 3. SiC particles of 2.4, 3.2, 8, and 20 μm average length were mixed separately with 1100 aluminum powder and hot pressed, extruded and hot rolled to produce tension test specimens and compact tension specimens (CTS). The composites were produced within the Metallurgical

Materials Laboratory at the University of Maryland [*18*]. Also a SiC/Al composite containing 250-μm-size SiC particles was purchased from DWA (DWA Composites Specialties, Chatsworth, CA). The volume fraction of the SiC reinforcement was constant in all composites and equal to 20 Vol%. An 1100 aluminum alloy was selected in order to minimize the influence of the alloying elements, which would otherwise introduce additional complicating factors. Tension samples were machined in the rolling direction and tested at a standard crosshead speed of 0.05 cm/min. The CTS were machined, with a T-L [*19*] orientation, and tested using single specimen J integral testing technique in accordance with ASTM Test Method for J_{IC}, a Measure of Fracture Toughness (E 813) [*20*]. All specimens were tested in the annealed condition. It was initially assumed, based on previous results and theories [*21*] that the fracture toughness would increase with an increase in particle size, thereby making it impossible to do valid K_{IC} [*19*] measurements, since the sample thickness was confined to be 7 mm. Also, the energy separation technique developed at the University of Maryland [*22*] was utilized as a supplemental method of analyzing load-unload records to increase the confidence in the data obtained. The latter technique implies that the area under the load versus displacement curve, which corresponds to the work done by external load, can be separated into the stored elastic strain (potential) energy U_s, the elastic energy U_e released during crack extension, and the plastic energy U_p dissipated during crack extension as shown in Fig. 4.

The rate of the plastic energy dissipation $I = 1/B_N\, dU_p/da$ and the elastic energy release rate $G = 1/B_N\, dU_e/da$ represent the plastic and elastic parts of the J integral, that is, $J = I + G$, where B_N is the thickness of the CTS between the side grooves, and a is the crack length. Crack initiation fracture toughness can be determined as $K_{IC} = (GE_c/1 - \nu^2)^{1/2}$ [*23*], where E_c is the composite Young's modulus and ν is Poisson's ration ($\nu = 0.31$). Also, a direct evaluation of K_{IQ} is possible by taking maximum load P_m from the load-unload record and substituting into the expression $K_{IQ} = P_m/B_N(W)^{1/2} f(a/w)$ [*14*], where w is the width of the CTS and values of $f(a/w)$ are readily available. Crack growth fracture toughness is evaluated by dimensionless tearing modulus T, which is $T = E_c/\sigma_y^2\, dJ/da$, where σ_y is the composite yield stress and dJ/da is the slope of the stable crack extension portion of the J versus a plot constructed in accordance with ASTM E 813 [*23,24*]. Crack extension was determined using the unloading compliance technique [*12,14*]. In order to verify the calculated crack extension values, the tested CTS were exposed to elevated temperature and then fractured. Physical crack lengths are within 5 to 10% from the values calculated by the compliance technique.

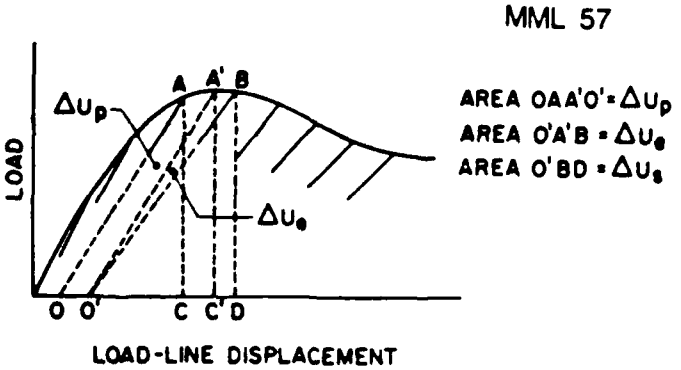

FIG. 4—*Schematic of the energy separation principle between two successive unloadings.*

Crack initiation fracture toughness measured as K_{IC} and K_{IQ} is plotted as a function of the average SiC particle size and is shown on Fig. 5.

The fact that both of these values show the same trend, that is, no dependence on the size of the SiC particles, if the particles are less than 20 μm in length, increases the confidence in the results obtained and supports the energy separation method as a new and powerful tool. The numerical difference ($K_{IC} \simeq 18$ MPa $\cdot$ m$^{1/2}$ and $K_{IQ} \simeq 23$ MPa $\cdot$ m$^{1/2}$) between the values of K_{IC} and K_{IQ} can be explained as follows. A finite notch with a root radius of $\simeq 150$ μm was machined in CTS in order to start the crack (as opposed to ASTM Test Method for Plane-Strain Fracture Toughness of Metallic Materials [E 399] requirement of a pre-fatigued crack starter resulting in a geometrically sharp crack [*19*]). Thus it is reasonable to expect higher values of K_{IQ}, which are obtained in accordance with ASTM E 399. Using the result of the study of the influence of notch acuity on the fracture initiation toughness [*10*] in SiC/Al composites we may write

$$K_{IQ} = K_{IC(r)} = K_{IC}\frac{(1 + r/2c)^{1/2}}{(1 + r/c)}$$

where $K_{IC(r)}$ is the initiation toughness of the notch with radius r, K_{IC} is the toughness of geometrically sharp crack, and c is the adjustable constant related to the microstructure. Substituting values for $K_{IC(r)} = 23$ MPa $\cdot$ m$^{1/2}$, $K_{IC} = 18$ MPa $\cdot$ m$^{1/2}$ and $r \cong 150$ μm, we obtain value for $c \cong 20$ μm. It is rather comparable with the size of the fracture process zone observed in 2.4-μm average SiC particle size composite [*25*]. Initiation fracture toughness for 250-μm SiC/Al composite is almost by the factor of 2 less than for the rest of the tested composites. This is apparently because of the premature cracking of 250-μm size SiC particles.

Crack growth resistance measured as tearing modulus T and plastic part I of the J integral is plotted versus the average size of SiC particles in Fig. 6.

The increase of the crack growth resistance with an increase of the SiC particle size means that there is an increase in energy dissipation during crack extension in the composite with a larger size of SiC particles. As tension test data show the yield stress of the SiC/Al composites drops with the increase of the SiC particle size. The same behavior was reported in literature for various alloys containing second phase particles [*26*]. The size of the plastic zone is inversely proportional to the square of the yield stress [*27*]. Thus as the size of SiC particles increase, the size of the plastic zone also increases resulting in the increase of dissipated plastic energy, which in turn increases the crack growth resistance.

Discussion and Conclusions

If the strengthening components are considered again, it is now necessary to consider the morphology of SiC. Table 4 is a listing of the strengthening components for the whisker case. The strengthening caused by $\Delta\sigma_{TEX}$ and $\Delta\sigma_{COMP}$ is equal to zero. The summation of the predicted strengthening and the observed strengthening are in very good agreement. Table 5 is a listing of the strengthening components for the spherical SiC case. The strengthening caused by $\Delta\sigma_{DISL}$ may be a little higher than the value given; however,

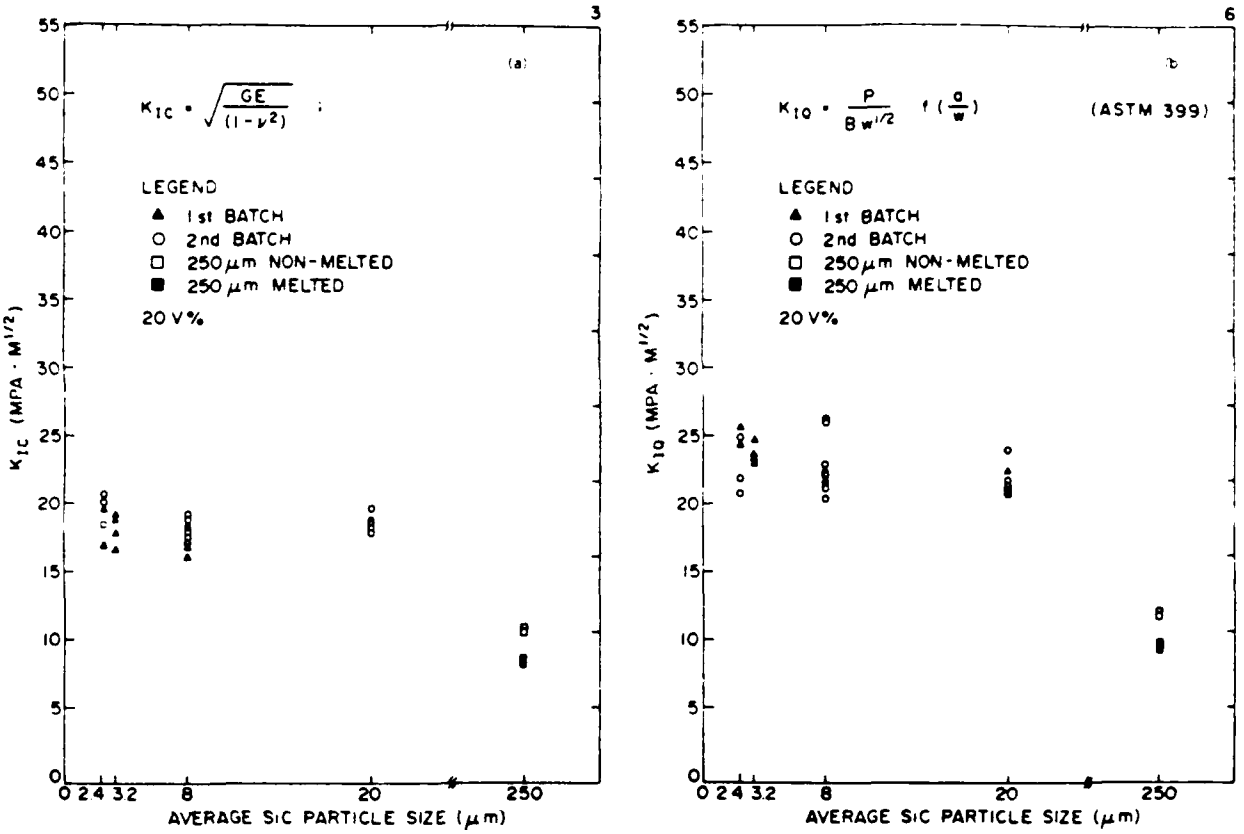

FIG. 5—*Crack initiation fracture toughness of SiC/Al composites measures as* K_{IC} (a) *and* K_{IQ} *(b).*

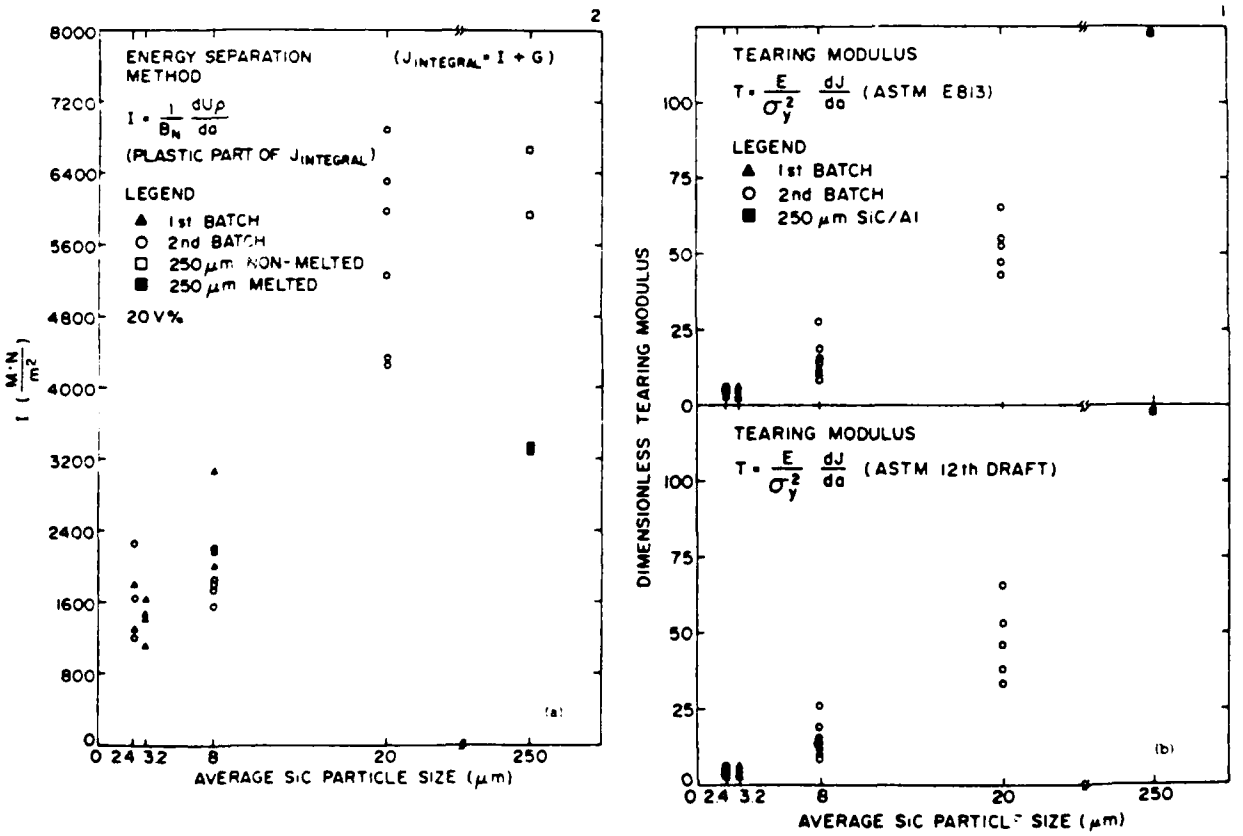

FIG. 6—*Crack growth resistance of SiC/Al composites measured as* (a) I *and* (b) T.

TABLE 4—*A listing of the strengthening components for the whisker SiC 1100 aluminum matrix.*

$\Delta\sigma_{YC} = \Delta\sigma_{DISL} + \Delta\sigma_{SC} \pm \Delta\sigma_{RES} + \Delta\sigma_{TEX} + \Delta\sigma_{COMP}$	
$\Delta\sigma_{DISL}$	= 117
$\Delta\sigma_{SC}$	= 55 MPa
$\Delta\sigma_{RES}$	= 34.5 MPa
$\Delta\sigma_{TEX}$	= 0
$\Delta\sigma_{COMP}$	= 0
$\Delta\sigma_{w}$	= 117 + 55 − 34.5 = 137.5 MPa
$\Delta\sigma_{YW\ EXP}$	= 144.9 MPa

TABLE 5—*A listing of the strengthening components for the spherical SiC in 1100 aluminum matrix*

$\Delta\sigma_{YC} = \Delta\sigma_{DISL} + \Delta\sigma_{SG} \pm \Delta\sigma_{RES} + \Delta\sigma_{TEX} + \Delta\sigma_{COMP}$	
$\Delta\sigma_{DISL}$	= 135 MPa
$\Delta\sigma_{SG}$	= 55 MPa
$\Delta\sigma_{RES}$	= 0
$\Delta\sigma_{TEX}$	= 0
$\Delta\sigma_{COMP}$	= 0
$\Delta\sigma_{w}$	= 135 + 55 = 190 MPa
$\Delta\sigma_{YS\ EXP}$	= 172.5 MPa

again the agreement between the predicted and experimental results is very good.

The data generated further support the concept that the strengthening mechanism is due to a higher dislocation density and a small subgrain size, which is the result of the difference in the thermal coefficient of expansion between SiC and aluminum. The thermal residual stress as measured by the X-ray technique indicates that the matrix is in tension. Also, a model based on load transfer is completely incapable of explaining the increase in strength due to the addition of SiC to the aluminum alloy matrix, in the composites used in the present investigation. The aspect ratio, in the whisker and platelet case, are too small to provide any effective local transfer.

Since the fracture toughness is independent of particle size and particle spacing (provided the particles are $< 20\ \mu m$), the data supports the contention that fracture process is controlled entirely within the matrix. In other words the fracture process (for the case of 20 μm and smaller SiC reinforcement composites) does not occur by the nucleation and growth of voids of SiC particles. This does not mean that the reinforcement has no effect on the fracture process. The reinforcement can produce a high dislocation within the matrix; therefore the fracture toughness of composite is related or equivalent to the fracture toughness of the cold worked matrix alloy. Also, the reinforcement results in a hydrostatic tension in the matrix, which also further reduces the fracture toughness [*28*].

Acknowledgment

This research was supported by the Office of Naval Research under Contract N00014-85-K-0907. The author wishes to acknowledge the continued support and encouragement of Dr. S. Fishman of the Office of Naval Research.

References

[1] Arsenault, R. J., *Material Science and Engineering*, Vol. C4, 1984, p. 171.
[2] Vogelsang, M., Arsenault, R. J., and Fisher, R. M., *Metallurgical Transactions*, Vol. 17A, 1986, p. 379.
[3] Arsenault, R. J. and Fisher, R. M., *Scripta Metallurgica*, Vol. 17, 1983, p. 67.
[4] Arsenault, R. J. and Taya, M., *Acta Metallurgica*, Vol. 35, 1987, p. 651.
[5] Taya, M. and Arsenault, R. J., *Scripta Metallurgica*, Vol. 21, 1987, p. 349.
[6] Arsenault, R. J. and Shi, N., *Materials Science & Engineering*, Vol. 81, 1986, p. 175.
[7] McQueen, H. and Jones, J. J., *Plastic Deformation of Materials*, R. J. Arsenault, Ed., Academic Press, New York, 1975, p. 416.
[8] Divecha, A. P., Fishman, S. G., and Karmarkar, S. D., *Journal of Metals*, Vol. 9, 1981, p. 12.
[9] Logsdon, W. A. and Liaw, P. K., "Tensile, Fracture Toughness and Fatigue Crack Growth Rate Properties of SiC Whisker and Particulate Reinforced Al Metal Matrix Composites," Westinghouse Scientific Paper 83-1D3-NODEM-P1, Dec. 1983.
[10] Crowe, C. R., Gray, R. A., and Hasson, D. F., *Proceedings of ICCM-V*, W. Harrigan, Ed., San Diego, CA, 1985.
[11] Hunt, W. H., Richmond, O., and Young, R. D., *ICCM 6*, Vol. 2, 1987, p. 2.209.
[12] McDanels, D. L., *Metallurgical Transactions A*, Vol. 16, 1985, p. 1105.
[13] Cohen, J. B., *Diffraction Methods in Materials Science*, Macmillan Series in Materials Science, 1966.
[14] Read-Hill, R. E., *Physical Metallurgy Principles*, 2nd ed., Brooks-Cole, 1973, p. 13.
[15] Reed, R. E. and McHargue, C. J., *Transactions of the AIME*, Vol. 242, 1968, p. 180.
[16] Eshelby, J. D., *Proceedings of the Royal Society of London*, Vol. A241, 1957, p. 376.
[17] Nardone, V. C. and Prewo, K. M., *Scripta Metallurgica*, Vol. 20, 1986, p. 43.
[18] Flom, Y., Ph.D. thesis, University of Maryland, College Park, MD, 1987.
[19] *1980 Annual Book of ASTM Standards*, 1980, p. 596.
[20] *1986 Annual Book of ASTM Standards*, Section 3, Vol. 03.01, E 813, 1986.
[21] Gerberich, W. W., "Interaction of Microstructure and Mechanisms in Defining K_{IC}, K_{ISCC}, or K_{Th} Values," in *Proceedings of the 113th AIME Conference*, J. M. Wells and J. B. Landes, Eds., 1985, p. 49.
[22] Mechklenburg, M. F., Joyce, J. A., and Albrecht, P., "Separation of Energies in Elastic-Plastic Fracture," presented at the Third International Symposium on Nonlinear Fracture Mechanics, American Society for Testing and Materials, Philadelphia, Knoxville, TN, Oct. 1986.
[23] Latzo, D. G. H., Turner, C. E., Landes, J. D., McCabe, D. E., and Hellen, T. K., *Post Yield Fracture Mechanics*, 2nd ed., Elsevier Publishers, New York, 1984.
[24] Ritchie, R. O. and Thompson, A. W., *Metallurgical Transactions A*, Vol. 16, 1985, p. 233.
[25] Feng, C. R., Wang, L., and Arsenault, R. J., to be published.
[26] Schoutens, J. E., *Introduction to Metal Matrix Composite Materials*, MMCIAC, 3rd ed., 1982.
[27] Thomason, P. F., *International Journal of Fracture Mechanics*, Vol. 7, 1971, p. 409.
[28] Cox, T. B. and Low, J. R., *Metallurgical Transactions*, Vol. 5, 1974, p. 1457.

EFFECT OF PARTICLE SIZE ON FRACTURE TOUGHNESS OF SIC/AL COMPOSITE MATERIAL[+]

Y. Flom* and R. J. Arsenault
Metallurgical Materials Laboratory
Engineering Materials Group
University of Maryland
College Park, MD 20742

ABSTRACT

Discontinuous SiC/Al composites with SiC particles of different sizes were fabricated in order to study the role of particle size on the fracture process. The fracture process is confined to a very narrow band and takes place within the matrix in composites containing small SiC particle sizes. In the composite reinforced with SiC particles of 20 μm and above fracture of SiC begins to dominate. The matrix is influenced by the high density of dislocations generated at SiC/Al interfaces due to the difference in coefficient of thermal expansion (CTE) between SiC and the Al matrix. Crack initiation fracture toughness does not depend on SiC particle size. Crack growth fracture toughness increases as the size of the SiC particle increase.

I. INTRODUCTION

During the past several decades there has been a considerable number of investigations of the fracture characteristics of two phase alloys where the second phase is a discreet precipitate or particulate[1-17]. The review by

---

* Presently at Goddard Space Flight Center, NASA, Greenbelt, MD.

+ This investigation was supported by the Office of Naval Research under Grant No. N00014-85-K-0007.

Shwalbe[13] and more recent publications by Bates[15], Gerberich[16] and Firrao and Roberti[17] are very informative on this subject. In ductile fracture, characterized by void nucleation and growth (VNG), the spacing between the void nucleating particles is generally considered to be a critical microstructural parameter that taken together with the tensile properties controls the toughness of a given material[11-17]. This can be represented by the following simplified expression[17]

$$K_{IC} = \left[a\sigma_y \epsilon_f^* E f(N)\right]^{1/2} s^{1/2} \qquad (1)$$

where K_{IC} is the plane strain fracture toughness, a is the numerical coefficient, σ_y is the yield stress, ϵ_f^* is the maximum strain acting at the crack tip, E is the Young's modulus, f(N) is some function of the strain-hardening exponent and s is the average inclusion spacing in the matrix. The experimental data collected by various investigators are usually given in terms of the volume fraction of the second phase particles (V) or less often in terms of s (see Fig. 1).

The dimple morphology of the fracture surfaces is the most common observation made by a number of researchers studying the fracture process in discontinuous+ SiC/Al composites[18-32]. This indicates that the VNG mechanism is active in these composites and therefore, corresponding theories (generalized by Eq. 1) should be applicable to describe the fracture process in SiC/Al composites. In the past, the investigations of the fracture toughness of SiC/Al composites were concerned with the matrix properties (heat treatment, amount of work, alloying elements, crack tip acuity) and the morphology of the

+ In all cases we shall be referring to discontinuous SiC/Al composites.

SiC reinforcement (shape and volume fraction).

The adverse influence of an increase of the volume fraction of SiC reinforcement on fracture toughness can be established rather well when one combines the data on fracture toughness testing available in the literature, as shown in Fig. 2.

A rather strict geometric consideration requires that all three microstructural variables V, s and particle size d be related. There are several expressions relating V, s and d available in the literature[1,14,33]. Since there is no substantial difference between these expressions, we have selected one derived by LeRoy et al[14] for the equiaxial particles:

$$s = 0.77\, dV^{-1/2} \qquad (2)$$

The data in Fig. 2 can now be considered as a function of the average center-to-center SiC particle spacing s, providing that the average SiC particle size remains constant which is generally the case in commercial composites. There would be approximately a of factor 3 increase in K_{IC} if the data in Fig. 2 is employed along with Eq. 2, and assuming that the average SiC particle size is about 5 μm[21]. Notice that in this case we are changing s by varying V.

Mathematically, a similar result can be achieved by keeping V constant and changing the particle size d. A similar trend is obtained, there is a linear increase of K_{IC} as d increases, assuming that voids are nucleated at SiC particles. Therefore, it appears that the fracture toughness of SiC/Al composites can be improved when the size of the SiC particles is increased, providing that at least one of the two following assumptions is met:

1) voids are nucleated by SiC particles and/or

2) the response of the matrix to changes of s remains the same regardless

of whether this change is caused by varying the volume fraction or the size of the SiC particles.

The purpose of this work, therefore, was to determine the influence of the size of SiC particles on fracture toughness of SiC/Al composites and to examine the applicability of the aforementioned assumptions.

II. MATERIALS

Inert gas atomized 1100 Al alloy (Valimet H-3) was mixed in succession with 2.4, 3.2, 8 and 20 μm average size SiC particles obtained from the Norton Co. An 1100 Al alloy was selected in order to minimize the influence of the alloying elements which would otherwise introduce additional complicating factors. The size distribution of the as received SiC powders were obtained by filtering onto 0.4 μm size Nuclepore filters, and photographing the filters in the SEM. Figure 3 shows histograms of SiC particles size distribution for all sizes used in present investigation. The SiC particles had an approximate platelet morphology. Mixtures of Al and SiC powders were hot pressed, hot extruded and hot rolled to produce tensile test and compact tension specimens. Details of the fabrication process are described elsewhere[34]. The volume fraction of the SiC reinforcement was constant in all composites and equal to 20 volume percent. Following the rolling process the densities of the specimens were determined using a Buoyancy method per ASTM C 693-74. Density measurements showed that composites were within 99% of theoretical density.

Also, a SiC/Al composite containing 250 μm size SiC particles purchased

from DWA* in the form of a 25 mm thick plate was sliced into plates ~ 6.5 mm × 12.5 mm × 304 mm. The "as rolled" and sliced plates were machined into compact tension specimens (CTS). Design of the CTS was based on ASTM standard E 813 and also on the latest ASTM developments in the area of elastic-plastic fracture toughness test methods[35,36] as shown in Fig. 4(a). All specimens were annealed at 803 K for 12 hours and furnace cooled prior to the mechanical testing.

III. TEST METHODS

The CTS were tested using the single specimen J-integral test method per ASTM standard E 813. Also, the energy separation technique (EST) was utilized as an additional tool in the load-unload records analysis[37]. The EST enables one to obtain values of plastic, I, and elastic, G, contributions to the total value of J-integral. It implies that the area under the load versus displacement curve which corresponds to the work done by external force can be separated into the stored elastic strain (potential) energy, U_s, the elastic energy, U_E, released during crack extension, and plastic energy, U_p, dissipated during the crack extension, as schematically shown in Fig. 5. A more detailed description of the EST is outside the scope of this paper and can be found elsewhere[37]. The rate of plastic energy dissipation, $I = 1/B_n \, dU_p/da$, and the elastic energy release rate, $G = 1/B_n \, dU_E/da$, represent the plastic and elastic parts of the J-integral, i.e. $J = I + G$, where B_n is the thickness of the CTS between the side grooves and a is the crack length. Crack initiation fracture toughness can be determined as[38]:

---

* DWA Composites Specialities, Inc.

$$K_{IC} = \left(\frac{G\,E_c}{1-\nu^2}\right)^{1/2} \tag{3}$$

where E_c is the composite Young's modulus and ν is the Poisson ratio (ν = 0.31). Also a direct evaluation of K_{IQ} is possible by taking maximum load P_M from the load-unload record and substituting into the expression[39]:

$$K_{IQ} = \frac{P_m\, f(a/w)}{B_n (w)^{1/2}} \tag{4}$$

where W is the width of the CTS as shown in Fig. 4(a) and values of f(a/w) are readily available. Crack growth fracture toughness is evaluated by a dimensionless tearing modulus, T, which is equal to[38,40]:

$$T = \frac{E_c}{\sigma_y^2}\frac{dJ}{da} \tag{5}$$

where σ_y is the composite yield stress and dJ/da is the slope of the stable crack extension portion of J versus a plot constructed in accordance with ASTM E813. Crack extension was determined by using the unloading compliance technique[35,38]. In order to verify the calculated crack extension values, the tested CTS were exposed to elevated temperature and then fractured (heat tinting method). Experimentally measured crack lengths were found to be within 5 to 10% from the values calculated by a compliance technique.

The interaction between the fracture path and SiC particles was analyzed by counting the number of SiC particles along a random path (RP) and the fracture path (FP), and by comparing SiC particle densities and size distributions. Particle size is represented by the longest dimension of the SiC particle. Random path particle count (RPPC) was performed by counting the particles along the perpendicular lines forming a square grid which was placed on the

micrographs of the metallographically polished cross sections of SiC/Al composites. Fracture path particle count (FPPC) was done by incorporating the SiC particles touching both matching flanks of the crack on the cross sections of the tested but not separated CTS. In addition, the upper limit number of SiC particles fractured by the crack could be reasonably estimated since both matching halves of the same crack were present on the micrograph. The latter was used to determine the percent of SiC particles fractured by the crack path using the following ratio:

$$\frac{\#\text{ of particles fractured by crack path}}{\text{FPPC}}$$

This technique is described in greater details in Ref. 34.

IV. EXPERIMENTAL RESULTS

A. SiC Particles - Matrix Interaction

The experimental data indicated that the ratio of SiC densities measured along RP and FP does not depend on the SiC particle size, i.e. the ratio RPPC/FPPC = constant = 0.75 for 2.4, 3.2, 8 and 20 μm average SiC size composites. This means that one finds more SiC particles along FP than along any other direction. Thus, the crack is attracted towards the SiC particles. In the case of the 250 μm SiC size composite there were too few SiC at the fracture surface to arrive at reproducible values, but ratio was small.

The significance of the specific value 0.75 is not fully understood. The occurrence of the attraction or deflection is determined by the sign of the triaxial stress state. In the case of a tensile triaxial stress state, the

crack front is attracted toward the particles[41]. The presence of the tensile triaxial stress state has been demonstrated by Shi and Arsenault[42].

The upper limit percentage of SiC particles fractured by the crack path remains around 8% for 2.4, 3.2, and 8 μm average SiC particle size composites and increases to ≈ 25% for 20 μm SiC/Al composites. However, in the case of 250 μm almost all SiC particles were fractured on the fracture surface. This result can be treated on the basis of the critical flaw size in the SiC used in the Griffith fracture mechanics. The probability of finding a critical flaw size in a small SiC particle is less than in the large one[43].

B. Fractography

Three characteristics were observed in the study of fracture surfaces: 1) fracture surfaces have a dimple morphology, 2) there are two dimple populations: the first, which is associated with SiC particles, and increases its size as the size of the SiC particles increases, and a second type consisting of very small dimples (≈ 1 μm) located in the space between the SiC related dimples, 3) cleavage of SiC particles becomes more evident as their size increases (see Fig. 6). The shape of the dimples is rather equiaxial.

Despite the correlation between the coarse dimples and SiC particles on the fracture surfaces of SiC/Al composites, not all the SiC particles were completely exposed. This corresponds to the earlier observations of the fracture surfaces of SiC/Al composites[19,23,25], and indicates good bonding between SiC and Al matrix.

C. Metallography

The examination of the polished cross sections of the tested tensile and CTS did not reveal the presence of the voids below the fracture surface (see Fig. 7). This means, that the fracture process is confined to an extremely narrow band and there is no apparent damage zone adjacent to the fracture surface which generally exists in the classical void nucleation and growth type fracture.

It is possible to stop a J-integral test and cut and polish the sample as schematically shown in Fig. 4b. It is then possible to determine how the crack propagates through the composite. (It should be clearly stated that crack was examined in the unloaded condition.)

There were only a few observations of "pull out" of the SiC particles from the Al matrix, which indicates a good SiC/Al interfacial bonding. Voids were not observed in the vicinity of and/or ahead of the crack tip. Instead, a series of short cracks could be seen in the matrix in front of the continuous crack as shown in Fig. 8. Apparently, this cracking takes place in the matrix ahead of the crack tip and it is believed that crack propagation occurs by connecting these discontinuous microcracks.

It seems that the short microcracks are associated with the clusters of SiC particles (see Fig. 8). Even though the distribution of the SiC particles is predominately homogeneous, on the microscale there are islands of high and low density of SiC particles. The clusters of the inclusions are considered to be the sites where the damage level reaches extreme values causing the fracture of the entire system[44]. The degree of plastic constraint within the clusters could be much higher than in the rest of the matrix as a result of: 1) high dislocation density due to the difference in CTE[42,45], and 2) increase of the

tensile triaxial stress state during the deformation due to the plastic constraint in the matrix between the particles. These factors make SiC clusters favorable for crack initiation sites.

D. Crack Initiation Fracture Toughness

Crack initiation fracture toughness measured as K_{IC} and K_{IQ} is plotted as a function of the average SiC particle size and shown in Fig. 9. The fact that both K_{IC} and K_{IQ} show the same trend, i.e. no dependence on the size of the SiC particles, increases the confidence in the results obtained and supports the energy separation method as a new and powerful tool.

The numerical difference ($K_{IC} \approx 18$ MPa $\cdot$ $m^{1/2}$ and $K_{IQ} \approx 23$ MPa $\cdot$ $m^{1/2}$) between the values of K_{IC} and K_{IQ} can be explained as follows. A finite notch with a root radius of $\approx$ 150 μm was machined in CTS in order to start the crack (in contrast with ASTM E 399 requirement of a fatigue precracking to form a geometrically sharp crack). Thus it is reasonable to expect higher values of K_{IQ} which are obtained in accordance with ASTM E 399. Using the result of the study of the influence of notch acuity on the fracture initiation toughness[23] in SiC/Al composites we can write

$$K_{IQ} = K_{IC(r)} = \frac{K_{IC}\left(1 + \frac{r}{2c}\right)^{3/2}}{(1 + r/c)} \qquad (6)$$

where K_{IC} is the intiation toughness of a geometrically sharp crack and c is the adjustable constant related to the microstructure. Substituting values for $K_{IC(r)} = 23$ MPa $\cdot$ $m^{1/2}$, $K_{IC} = 18$ MPa $\cdot$ $m^{1/2}$ and $r \approx 150$ μm, we obtain c = 20 μm. This value is within the range of the microcracking ahead of the crack tip in a 2.4 μm average SiC particle size composite.

Initiation fracture toughness of a 250 μm SiC/Al composite is almost a factor of 2 less than the rest of the tested composites. This is apparently due to the premature cracking of 250 μm SiC particles.

E. Crack Growth Fracture Toughness

Crack growth fracture toughness defined as tearing modulus, T, and plastic part (I) of J-integral versus the average size of SiC particles is plotted in Fig. 10. The increase of the crack growth toughness with the increase of the SiC particle size means that more energy is dissipated during crack extension in the composite with a larger size of SiC particles.

V. DISCUSSION

In this section we will address crack initiation and propagation toughness as measured by K_{IC} and tearing modulus T, respectively. Throughout this section the attempt will be made to show that the size of the SiC particles in SiC/Al composite does not have a strong influence on the mechanisms affecting the K_{IC} portion of the toughness of SiC/Al composite, but that the particle size has an influence on the tearing modulus (T). The influence of high dislocation densities on K_{IC} and T will also be considered. Finally a brief description of the separation mechanism will be given.

A. Crack Initation Toughness K_{IC}

The experimental results of this investigation have indicated that crack initiation fracture toughness K_{IC} is independent of the SiC particle size

(within the range of SiC sizes tested). In order to understand this result it is instructive to consider local energy dissipation mechanisms associated with the crack extension in SiC/Al composite. We are using the term "local" to emphasize the area in the vicinity of the crack tip. The plastic deformation in the bulk of the SiC/Al specimen is not included since it is separated out by using the energy separation technique (EST).

The elastic energy release rate G consists of the several terms that can account for energy dissipation. These terms can be identified as:

$$G = \gamma_s + \gamma_v + \gamma_{PLzone} + \gamma_{CTS} \qquad (7)$$

where γ_s is the energy consumed in creation of the new surfaces, γ_v is the energy consumed in the formation of the void sheet, γ_{PLzone} is the energy dissipated into plastic deformation around the crack tip and γ_{CTS} represents crack tip shielding effects described by Ritchie et al.[46]. It is rather well established that the γ_s term[38] is very small in metallic systems compared with $\gamma_{PLzone} + \gamma_v$. Evaluation of γ_{CTS} is quite complicated and requires the consideration of the extrinsic toughening mechanisms affecting the conditions at the crack tip in SiC/Al system. Following Ritchie's nomenclature[46] these mechanisms can be divided into four groups: 1) crack deflection and meandering, 2) zone shielding, 3) contact shielding, 4) local plastic deformation and void formation.

In the next few paragraphs we will examine how the change in SiC particle size may influence these mechanisms. Before we proceed, however, one important comment should be made. The term "toughening" mechanisms used in this manuscript is the original term employed by Ritchie[46]. In order to avoid possible confusion we decided to retain this terminology even though the

presence of these mechanisms in SiC/Al composites does not result in the improvement of the toughness of the composite over that of the matrix material.

1. Crack Deflection and Meandering

Crack deflection by SiC particles was observed in the present work. Cotterell and Rice showed[47] that the change in the stress intensity at the crack tip is a function of the kink angle θ. No observable differences in the crack deflection angle were noticed in the present work in SiC/Al composites containing small or large SiC particles. In addition to the kink angle it is possible that the kink length (ℓ) is also an important factor[46].

If the length, ℓ, of the deflected portion of the crack is considered then the following analysis (not very rigorous but still useful) can be performed. Using the idealized geometry of the crack deflection depicted in Fig. 11 the total length L of the kinked crack can be expressed as:

$$L = 2N\ell \ , \tag{8}$$

where N is the total number of particles along the crack path. Again from the geometry in Fig. 11 one can see that

$$\ell = \frac{1}{\sin\theta}\left(\frac{1}{2}d + \eta d\right) \ , \tag{9}$$

where the term (1/2d + ηd) represents the amplitude of the crack deflection, and η is the coefficient determining the extent of the crack deflection by the SiC particle. It seems that η depends on the elastic properties of the silicon carbide and aluminum and can be considered independent of the size of SiC

particle. It is possible to express N as:

$$N = \frac{B\ V_p}{d} \tag{10}$$

where B is the thickness of the specimen, V_p is the volume fraction of the SiC particles (remains constant) and d is the size of the SiC particle. Substituting Eqs. 8 and 9 into Eq. 10 we obtain:

$$L = 2\ \frac{B\ V_p}{\sin\theta}\ (\frac{1}{2} + n)\ , \tag{11}$$

As one can see Eq. 11 does not contain parameter d, i.e. L is size independent. Therefore the analysis above show that the influence of the crack deflection on the toughness of SiC/Al system is independent of SiC particle size.

2. Zone shielding

Some of the mechanisms in this group such as transformation toughening and crack field void formation are not active in SiC/Al system. Others like crack wake plasticity, and the effects of dislocation density will be addressed later.

The mechanism of microcrack toughening will be considered here again in terms of the SiC particle size. The microcracking (consisting of both types, cleavage of SiC particles and matrix microcracking) of the composite in front of the crack tip reduces the stress intensity at the crack tip if it occurs in the correct orientation[48]. It seems, therefore, that when SiC size increases, the increased cleavage of the SiC particles should result in further reduction of the stress intensity at the crack tip, i.e., the toughness (K_{IC}) should increase. On the other hand, the larger the SiC particles the more the total

crack path is consumed by the cleaved SiC particles. This means that the larger portion of the composite fails now in a brittle, SiC-like manner. Clearly, these two events are working in opposite directions. It can be speculated, therefore, based on these qualitative considerations that as SiC particle size increases these two opposing events compensate each other and their combined effect is such that the influence of microcracking on K_{IC} is SiC size insensitive. It is realized, however, that quantitative analysis should be perform to check the validity of this speculation.

3. Contact Shielding

This type of extrinsic toughening (due to wedging, bridging, and sliding) would be more relevant to cyclic loading, and therefore, will not be considered here.

4. Local Plastic Deformation and Void Formation

Davidson has shown[49] that $\gamma_v + \gamma_{PLzone}$ could be the most important factors in absorbing the energy around the crack. The evaluation of γ_v can be done following the approach suggested by Davidson[49] for calculation of the work of forming the void sheet:

$$W_v = W_o\left(\frac{\pi}{3}\frac{b}{h}\right)^m h\left[1 - \frac{1}{2}\frac{W_o m^2}{E}\left(\frac{b}{h}\right)^{m-2}\right] , \qquad (12)$$

where W_v is the work per unit area of void sheet formation, $W_o = \frac{\sigma_1 \varepsilon_1}{m(\varepsilon_1)^m}$ σ_1 and ε_1 are stress and strain picked from the stress-strain curve at some convenient point; $m = n + 1$, where n is the strain hardening coefficient, b is

the depth of the dimple and h is the height of the volume affected by the dimple formation[49].

Since we observed basically two populations of dimples, Eq. 12 has to be modified to account for this. We can write:

$$W_v = W_o\{K_1(\frac{\pi}{3}\frac{b_1}{h_1})^m h_1[1 - \frac{1}{2}\frac{W_o m^2}{E}(\frac{b_1}{h_1})^{m-2}] + K_2(\frac{\pi}{3}\frac{b_2}{h_2})^m h_2[1 - \frac{1}{2}\frac{W_o m^2}{E}(\frac{b_2}{h_2})^{m-2}]\}\ , \tag{13}$$

where subscripts 1 and 2 represent small (size does not change) and large dimples (size increases as SiC particle size increases), respectively. Coefficients K_1 and K_2 represent the fraction of the total fracture surface occupied by small or large dimples. In order to estimate K_1 and K_2 we need to involve the results of the SiC particle count. Recall that RPPC/FPPC is equal to 0.75, which means that 1.333 times more SiC particles can be found on the fracture surface than on any random plane cut through the SiC/Al composite. The fracturing of the SiC particles also has to be taken into account. Thus:

$$K_2 = 0.27(1 - \chi) \tag{14}$$

where factor 0.27 comes from the product of (volume fraction) × 1.333 or 0.20 × 1.333 = 0.27 and χ is the fraction of SiC particles fractured by the crack front. $K_1 = 1 - 0.27 = 0.73$. Since the systematic determination of the dimple geometry was not part of this work the accurate calculation of Eq. 13 is not possible. It is possible, however, to make an order of magnitude type estimate using the approximate average number of dimple dimensions obtained as a result of tedious observation of fracture surfaces of the subject SiC/Al

composite. The shape of the dimples is considered to be an ellipsoid with the minor to major axis ratios of 1/3 and 1/5 for small and large dimples, accordingly. By letting $d/3 \leq h_2 \leq d$ (where d is the largest dimension of the SiC particle) and $0.3\ \mu m \leq h_1 \leq 1\ \mu m$ for lower and upper bound[49] we can estimate W_v:

$W_v \approx 0.9 \times 10^{-4}$ MPa • m for 2.4 μm size SiC, lower bound

$W_v \approx 1 \times 10^{-4}$ Mpa • m for 20 μm size SiC, upper bound

As we can see W_v (or γ_v) remains practically independent of SiC particle size and represents only a small fraction of $G = 3.2 \times 10^{-3}$ Mpa • m obtained experimentally in the present work. Thus, the work to form the void sheet makes a rather insignificant contribution to the energy absorbed during crack extension in SiC/Al composite.

It seems, therefore, that most of the energy is absorbed within the plastic zone around the crack tip (γ_{PLzone}). In order to estimate this energy one has to know the distribution of the plastic strain in a direction perpendicular to the direction of crack propagation[49]. Preliminary data indicates that in the region immediately adjacent to the crack the plastic strain is large, as evidenced by very large dislocation density[50]. Also it was observed that the dislocation density was the same in the immediate region of fracture for two different volume fractions of SiC reinforcements[50] (SiC particle size was the same). Based on these results we can assume that as the particle size increases, i.e. an interparticle spacing increases (V = const.), the density of dislocation in the immediate region of the crack remains the same. Therefore γ_{PLzone} is independent of particle size.

We have shown that the γ_v, γ_{PLzone}, and γ_{CTS} which are the main contributing factors to G and directly related to K_{IC} (Eq. 3), are independent of particle size. Contrary to this, the classial VNG theory predicts that K_{IC} should increase as the particle size increases.

B. Propagation Fracture Toughness

The increase in crack growth fracture toughness (measured as I and T) with an increase of the SiC particle size can be treated on the basis of the relationship between the dislocation density and the spacing of the SiC particles demonstrated by Arsenault and Shi[45]. From their work one can see that the increase in the tearing modulus with an increase in particle size is the result of the increased plastic deformation that can be accommodated in the matrix as the interparticle spacing increases.

C. Separation Process

Based on the data collected in the present investigation, the crack propagation in the SiC/Al composite can be described as follows. The crack extension takes place after a certain amount of the damage in the form of discontinuous microcracks is accumulated ahead of the continuous crack tip. The crack propagates when these microcracks are connected by microvoid coalescence which explains the dimpled appearance of the fracture surface. The crack front is attracted towards the SiC particles due to tensile triaxial stress state present around the SiC particles as a result of differential thermal contraction of the SiC and Al matrix on the cooling down from the fabrication temperature.

VI. CONCLUSIONS

From the data generated in this investigation we arrived at five general conclusions.

1. An increase of SiC particle size did not improve K_{IC} fracture toughness of SiC/Al composite. K_{IC} was independent of SiC particle size up to 20 μm average size.
2. The crack growth toughness, i.e. the tearing modulus and plastic work, increased as the SiC particle size increased.
3. No evidence of void nucleation at SiC particles was found.
4. SiC/Al composite is a more complicated system than it appears: i) the sites of void nucleation were not well defined, and ii) the two alternative ways of increasing interparticle spacing did not produce the same results:
   - If the particle size was constant, and the volume fraction was increased and spacing decreased, then K_{IC} decreased[18-23,32].
   - If the particle size and spacing were increased, and volume fraction was held constant, then K_{IC} remained constant.
5. It can be speculated that K_{IC} depended mainly on the volume fraction of SiC particles.

ACKNOWLEDGEMENTS

The authors wish to acknowledge the assistance of Drs. S. B. Wu and C. R. Feng. They wish to acknowlege the support of the Office of Naval Research Grant No. N00014-85-K-0007 and the encouragement of Dr. S. Fishman.

References

1. B. I. Edelson and W. M. Baldwin, Trans. ASM, 55, 230 (1962).
2. J. Gurland and J. Plateau, Trans. ASM, 56, 442 (1963).
3. A. Gangullee and J. Gurland, J. Trans. Met. Soc. AIME, 239, 269 (1967).
4. J. Gurland, Trans. Met. Soc. AIME, 227, 1146 (1963).
5. C. T. Liu and J. Gurland, J. Trans. Met. Soc. AIME, 224, 1535 (1968).
6. C. T. Liu and J. Gurland, Trans. ASM, 61, 156 (1968).
7. J. Gurland, "Fracture of Metal-Matrix Particulate Composites" in Modern Composite Materials, eds. L. J. Broutman and R. H. Krock, Adison-Wesley, New York, 1969.
8. I. L. Mogford, Metallurgical Reviews, 114, 12, 49 (1967).
9. R. H. Van Stone, R. H. Merchant, and J. R. Low, Jr., ASTM STP 556, 93 (1974).
10. T. B. Cox and J. R. Low, Met. Trans., 5, 1457 (1974).
11. G. T. Hahn and A. R. Rosenfield, Met. Trans. A, 6, 653 (1975).
12. G. G. Garret and J. F. Knott, Met. Trans. A, 9, 1187 (1978).
13. K. H. Schwalbe, Eng. Frac. Mech., 9, 795 (1977).
14. G. LeRoy, J. D. Embury, G. Edwards, and M. F. Ashby, Acta Met., 29, 1509 (1981).
15. R. C. Bates, "Modeling of Ductile Fracture by Microvoid Coalescence for Prediction of Fracture Toughness" in Proc. 113th AIME Conf., eds., J. M. Wells and J. B. Landes, 117 (1985).
16. W. W. Gerberich, "Interaction of Microstructure and Mechanism in Defining K_{IC}, K_{ISCC} or K_{th} Values" in Proc. 113th AIME Conf., eds., J. M. Wells and J. B. Landes, 49 (1985).

17. D. Firrao and R. Roberti, "On the Mechanism of Ductile Fracture Nucleation Ahead of Sharp Crack" in Proc. 113th AIME Conf., eds., J. J. M. Wells and J. B. Landes, 165 (1985).

18. A. P. Divecha, S. G. Fishman, and S. D. Karmarkar, J. of Metals, 9, 12 (1981).

19. W. A. Longston, and P. K. Liaw, Westinghouse Scientific Paper 83-1D3-NODEM-P1, December 1983.

20. H. L. Marcus, "Microscopic Study of the Influence of the Impurities on Interface Bonding", Report No. UTCMSE-84-1, University of Texas, 1984.

21. J. E. Schoutens, "Discontinuous Silicon Carbide Reinforced Aluminum Metal Matrix Composites Data Review", MMCIAC Publication No. 000461, December 1984.

22. T. J. Hsieh, "Effect of Precracking Procedure on Fracture Toughness of SiC/Al Composite", M.S. Thesis, University of Maryland, 1985.

23. C. R. Crowe, R. A. Gray, and D. F. Hasson, Proceedings of ICCM-5, ed. by W. Harrigan, San Diego, 1985, p. 843.

24. D. L. McDaniels, Met. Trans. A, 16, 1105 (1985).

25. T. G. Nieh, R. A. Rainen, and D. J. Chellman, Proceedings of ICCM-5, ed. by W. Harrigan, San Diego, 825 (1985).

26. S. R. Nutt and J. M. Duva, Scripta Met., 20, 1055 (1986).

27. R. J. Arsenault and Y. Flom, "Role of Interfaces in SiC/Al Composites", Proc. Symposium "Phase Boundary Effects on Deformation, TMS AIME, Toronto, Canada, 13 (1985).

28. S. V. Nair, J. K. Tien, and R. C. Bates, Int. Met. Rev., 30, 6, 275 (1985).

29. C. P. You, A. W. Thompson, and I. M. Bernstein, Scripta Met., 21, 181 (1987).

30. Y. Flom and R. J. Arsenault, "Fracture of SiC/Al Composites", Proc. ICCM-VI, vol. 2, Elsevier Ltd., London, 1987.

31. J. J. Lewandovski, C. Liu, and W. H. Hunt, Jr., "Microstructural Effects on the Fracture Micromechanism in 7XXX Al P/M-SiC Particulate Metal Matrix Composite", in Powder Metallurgy Composites, eds., M. Kumar, K. Vedula, and A. M. Ritter, TMS AIME, 1987.

32. Y. Flom, B. H. Parker, and C. Chu, "Fracture Toughness of 40 Volume Percent Particulate SiC/Al Composites", paper in preparation, NASA, Goddard Space Flight Center, 1987.

33. E. E. Underwood, Quantitative Stereology, Addison-Wesley, 1970.

34. Y. Flom, "Fracture Toughness of SiC/Al Composites", Ph.D. Thesis, University of Maryland, 1987.

35. 1986 Annual Book of ASTM Standards, Section 3, Volume 03.01, Standard E813.

36. ASTM E24.08 Subcommittee, Standard Test Method for Determining J-R Curves, 12th Draft, July 1985.

37. M. F. Mecklenburg, J. A. Joyce, and P. Albrecht, "Separation of Energies in Elastic-Plastic Fracture", presented on 3rd International Symposium on Nonlinear Fracture Mechanics, ASTM, Knoxville, TN, October 1986.

38. D. G. H. Latzo, C. E. Turner, J. D. Landes, D. E. McCabe, and T. K. Hellen, "Post Yield Fracture Mechanics", 2nd Ed., Elsevier Pub., NY, 1984.

39. 1986 Annual Book of ASTM Standards, Section 3, Volume 03.01, Standard E399.

40. R. O. Richie, and A. W. Thompson, Met. Trans. A, 16, 233 (1985).

41. K. T. Faber and A. G. Evans, Acta Met., 31, 565 (1983).

42. N. Shi and R. J. Arsenault, to be published.

43. R. W. Davidge, "Mechanical Behavior of Ceramics", Cambridge University Press, 1980.

44. J. D. Embury and G. Burger, "The Role of Microstructure in the Fracture of Structural Steels", in the Proceedings of a Conference on Inclusions and Residuals in Steels: Effects on Fabrication and Service Behavior, Ottawa, March, 1985.

45. R. J. Arsenault and N. Shi, Mat. Sci. & Eng., 81, 175 (1986).

46. R. O. Ritchie and W. Yu, In Small Fatigue Cracks, R. O. Ritchie and J. Lankford, eds., 1986, TMS-AIME, Warrendale, PA.

47. B. Cotterell and J. R. Rice, Int. J. Fract., 16, 155 (1980).

48. C. Chin, Private Communications, SRI, January 1988.

49. D. L. Davidson, Met. Trans., 18A, 2115 (1987).

50. C. R. Feng, "Dislocation Density and High Temperature Creep of Aluminum Alloy and Fracture of SiC/Al Composite", Ph.D. Thesis, University of Maryland, 1987.

List of Figures

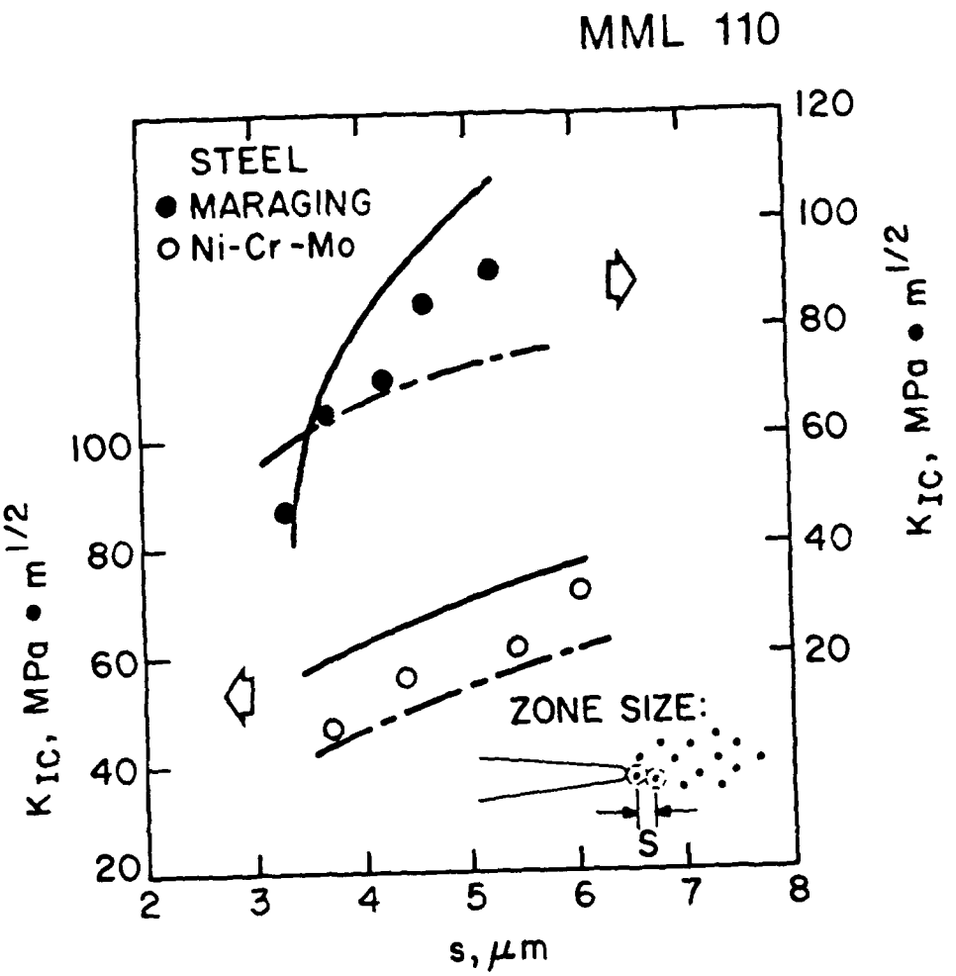

Fig. 1. Fracture toughness as a function of the "process" zone size. When VNG mechanism is active the process zone size is equated with the average spacing s between void nucleating particles (Gerberich, Ref. 16). Various forms of Eq. 1 are employed by Gerberich to predict the fracture toughness values (solid and dashed lines) and compare them with the experimental data reported by Shwalbe and Spitzig.

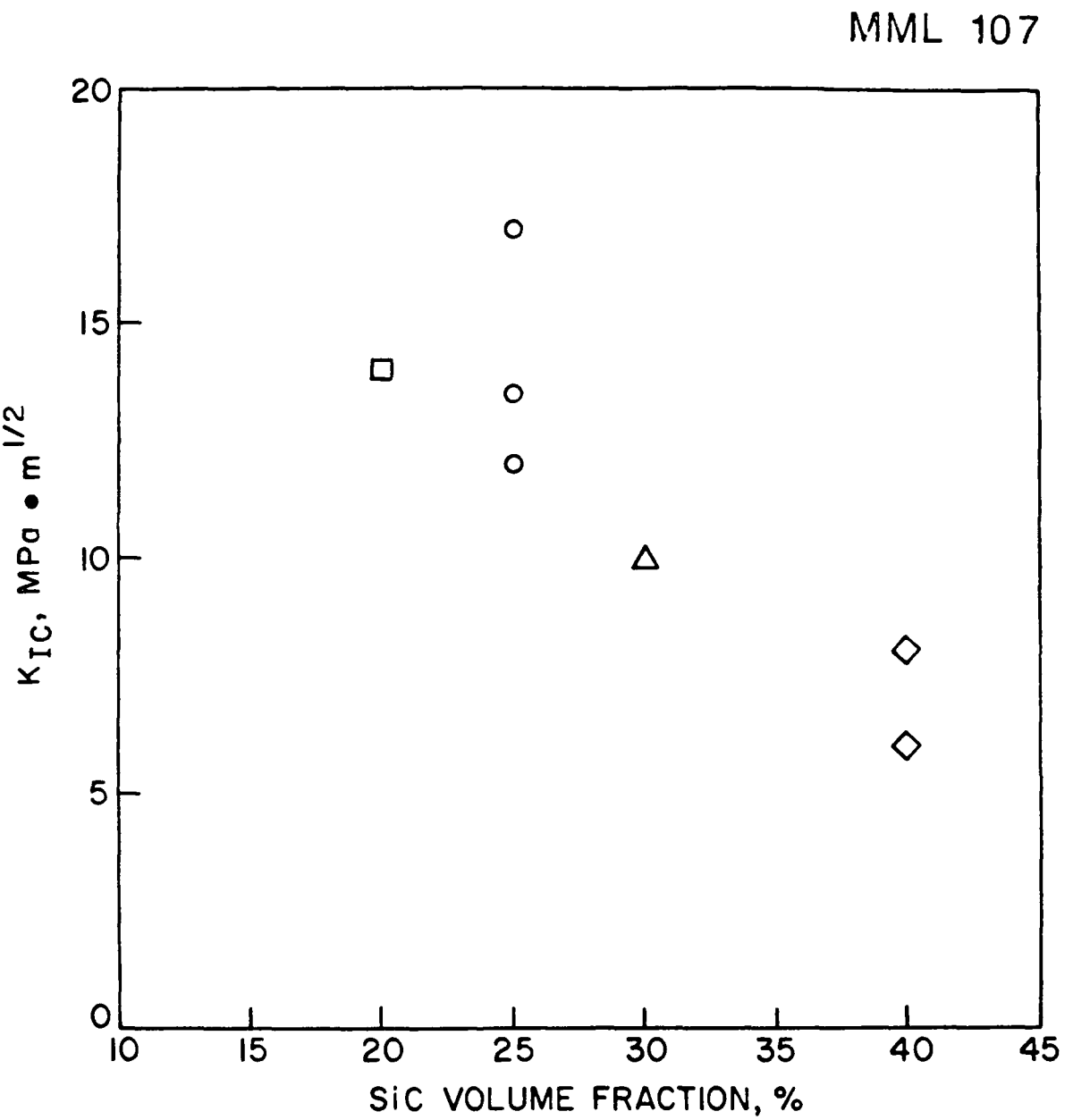

Fig. 2. Fracture toughness as a function of SiC volume fraction for SiC/Al composites. The shortage of the experimental data on the subject resulted in rather small number of data points presented in this graph (Refs. 18-23, 32).

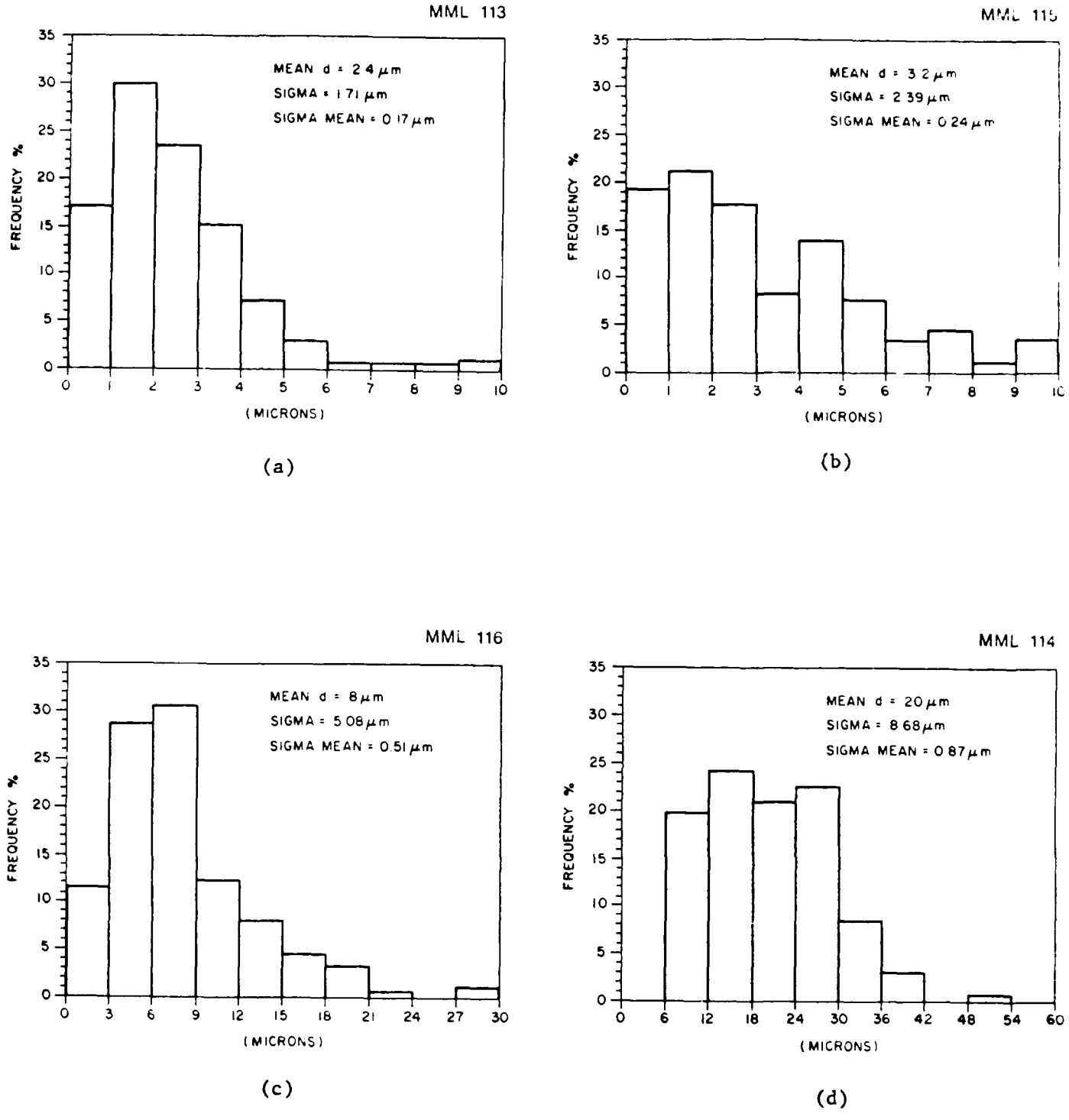

Fig. 3. Size distribution histograms of as-received 2.4 μm (a), 3.2 μm (b), 8 μm (c) and 20 μm (d) SiC particles.

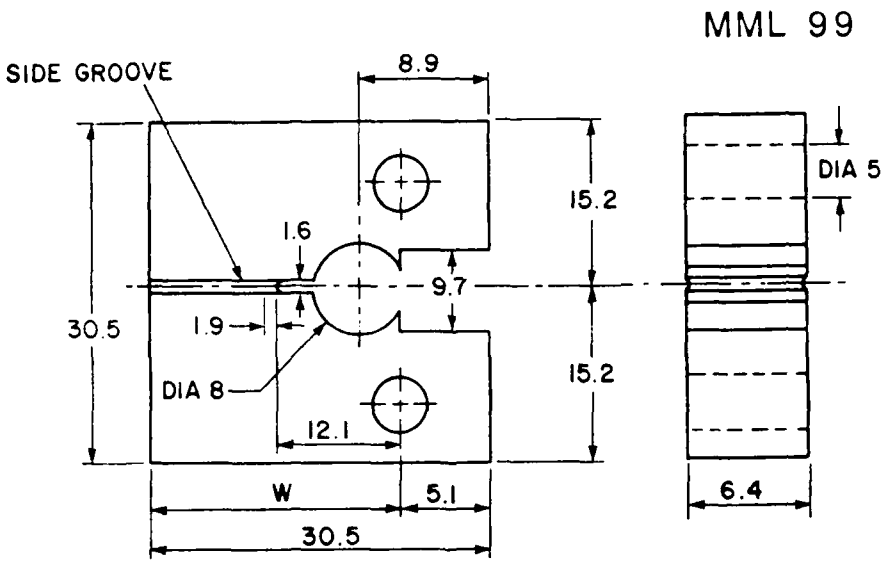

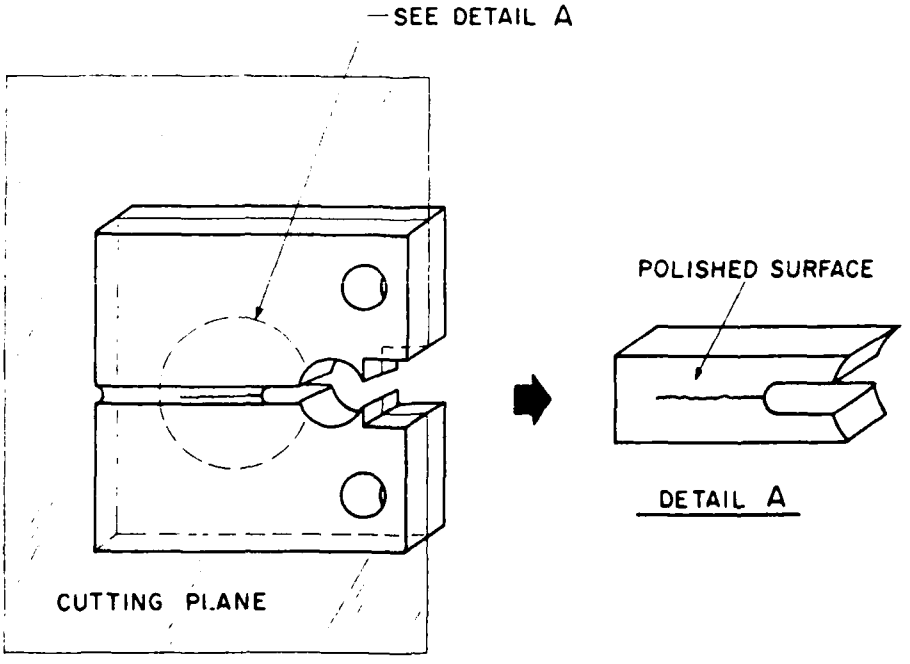

Fig. 4. Compact tension specimen (CTS) geometry (a) and the area of metallographic analysis (b).

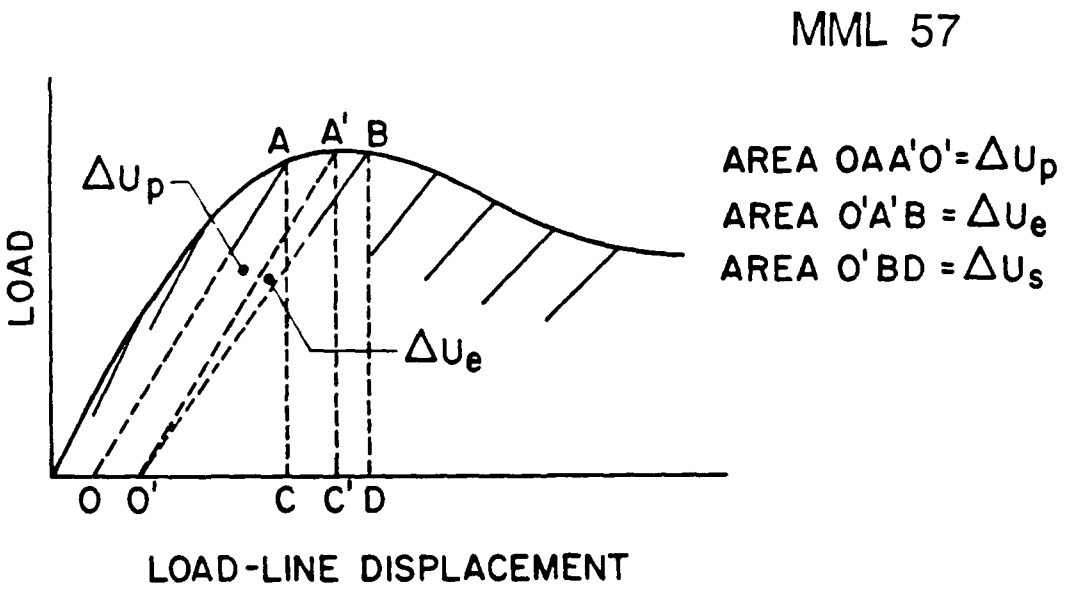

Fig. 5. Schematic of the energy separation principle between two successive unloadings.

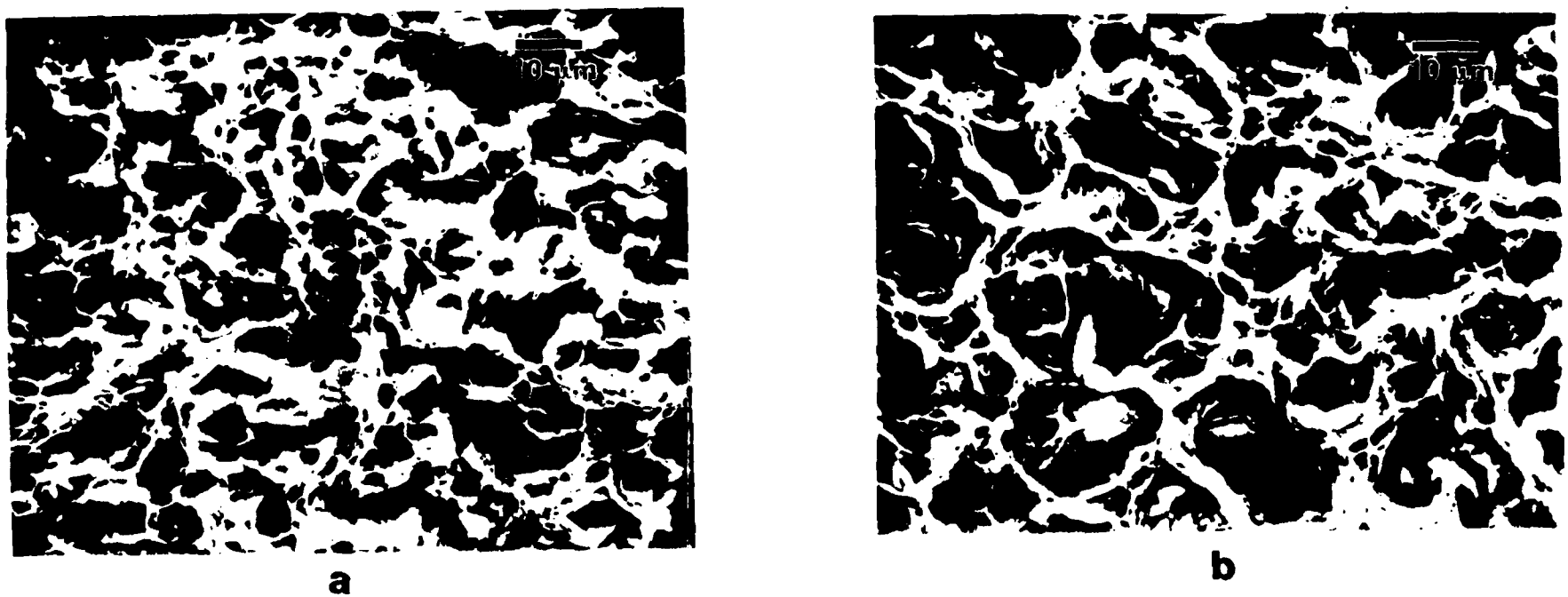

Fig. 6. Fracture surface of 3.2 μm (a) and 20 μm (b) average size SiC/Al composites.

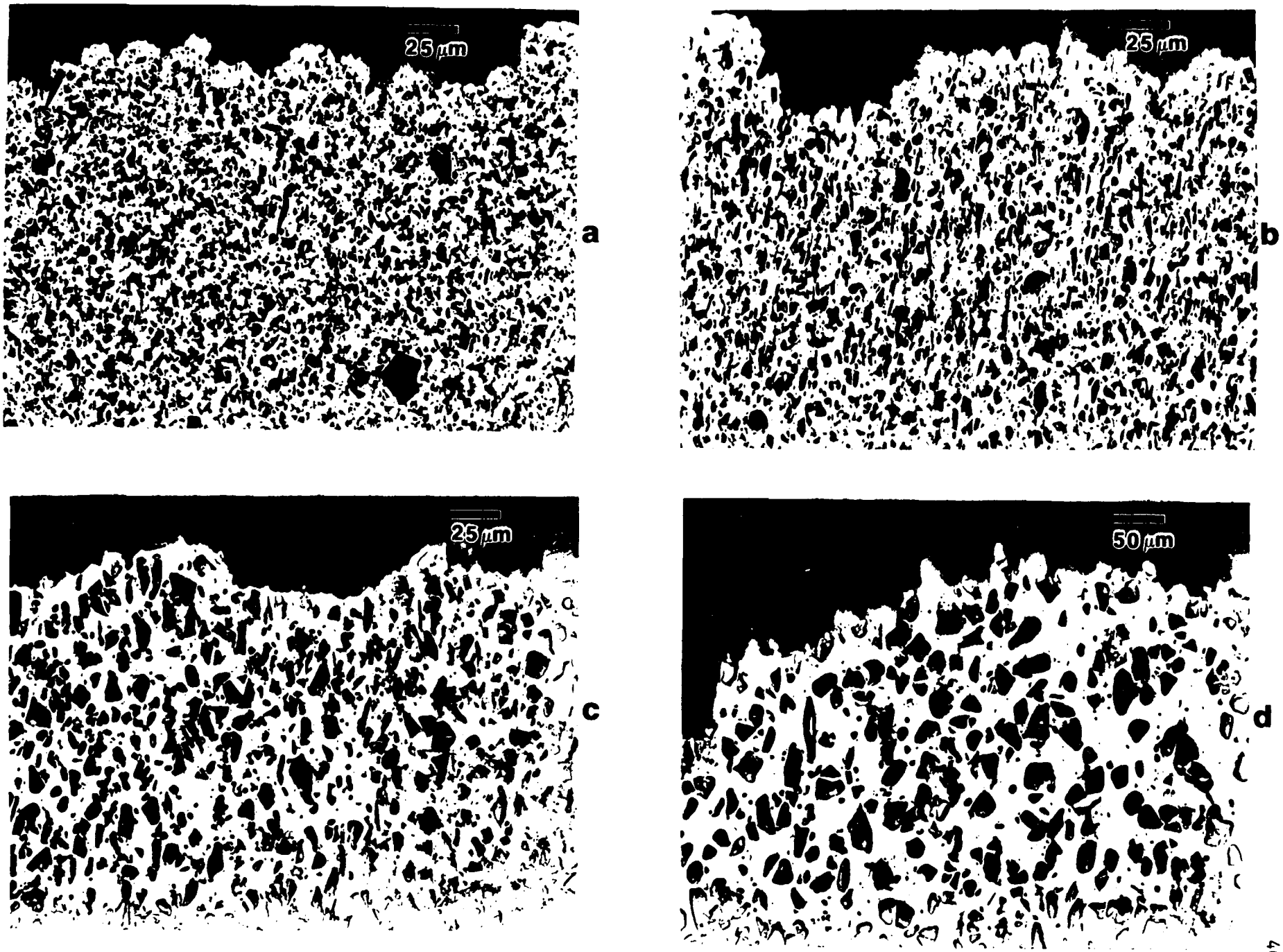

Fig. 7. Polished cross sections of 2.4, 3.2, 8 and 20 μm particle size tested SiC/Al composites (a, b, c, and d, respectively).

Fig. 8. Polished cross section showing crack tip region in 20 μm SiC particle size tested but not separate SiC/Al composite compact tension specimen.

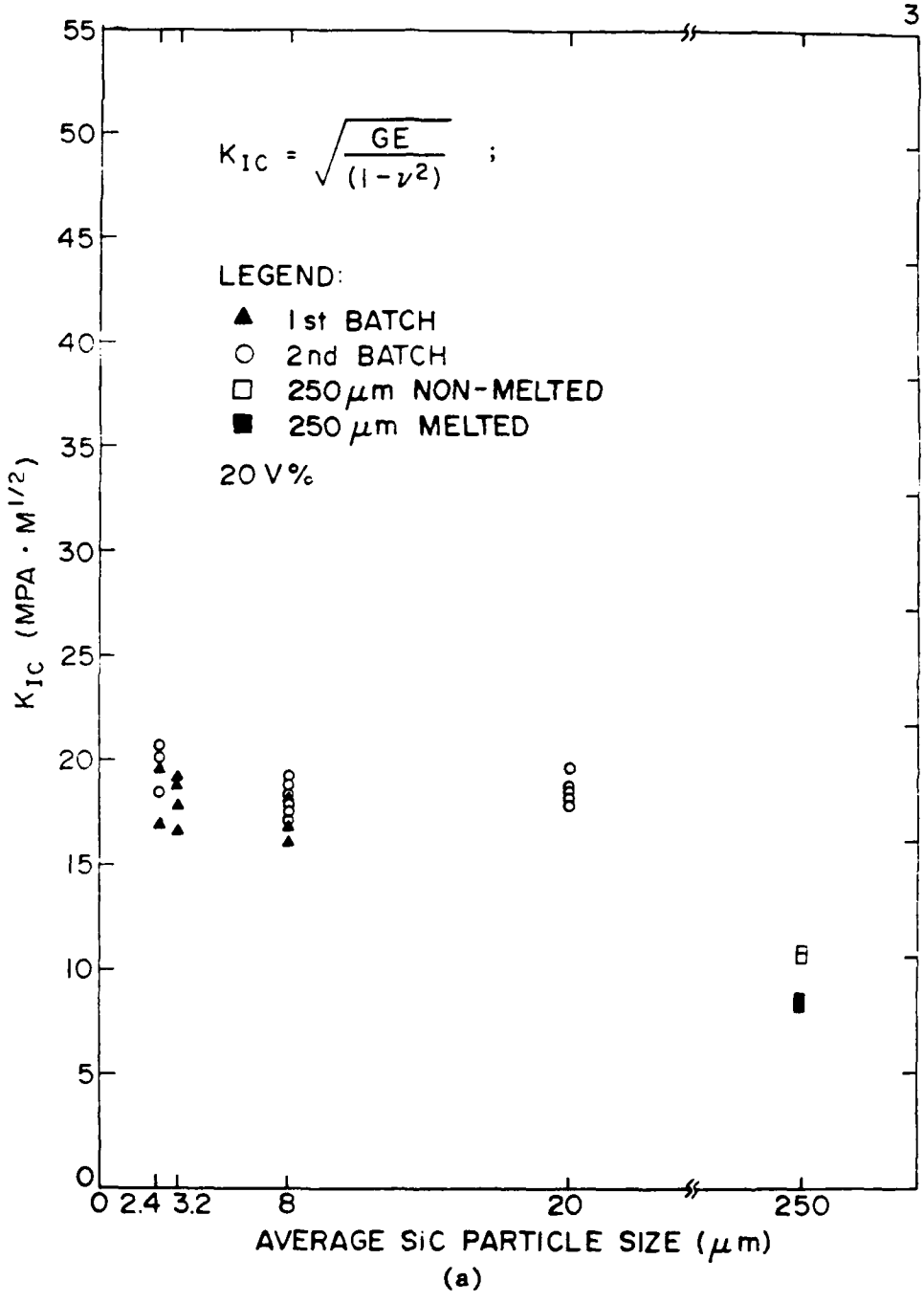

(a)

Fig. 9. Crack initiation fracture toughness of SiC/Al composites measured as K_{IC} (a) and K_{IQ} (b).

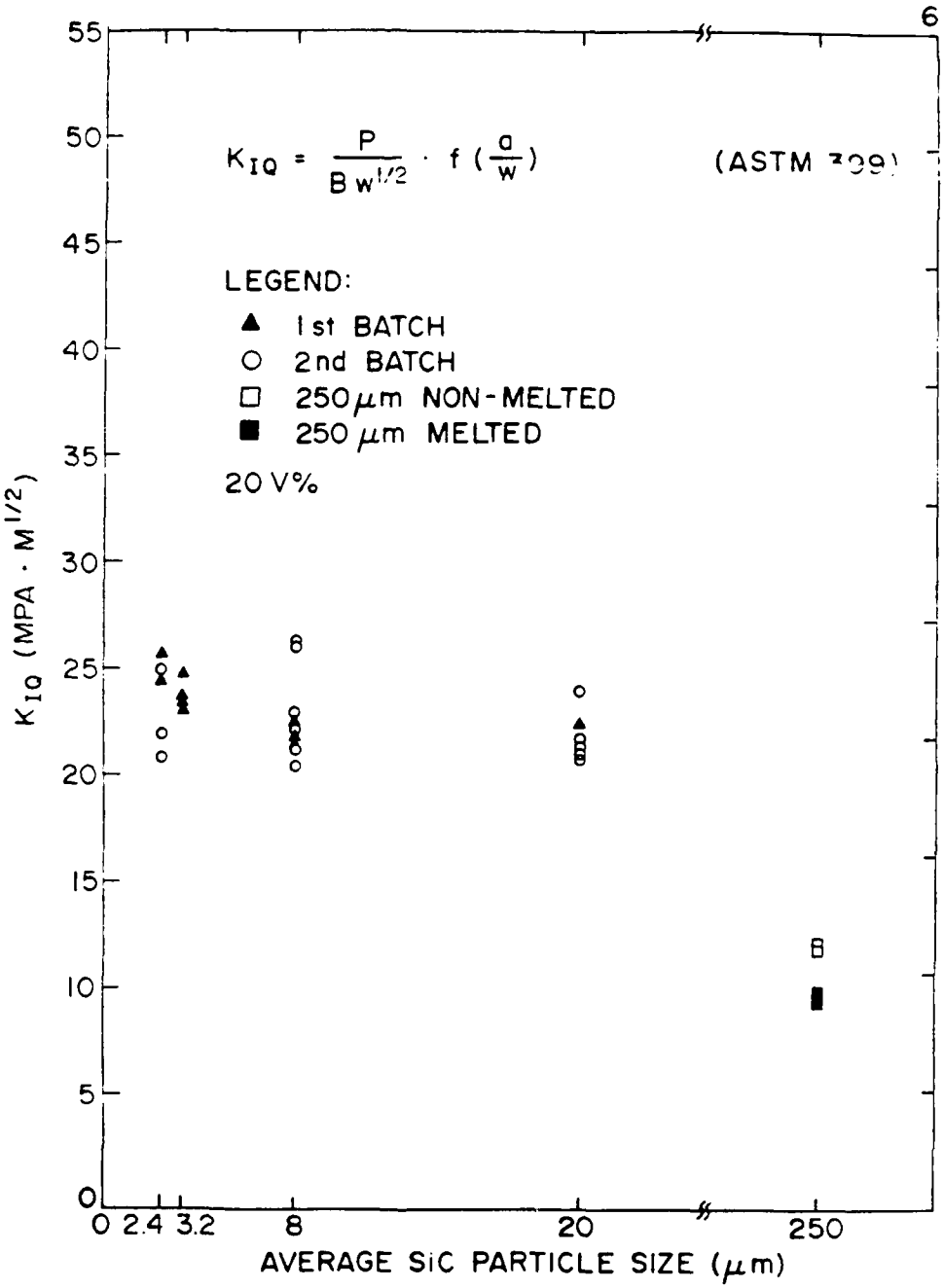

(b)

Fig. 9. Crack initiation fracture toughness of SiC/Al composites measured as K_{IC} (a) and K_{IQ} (b).

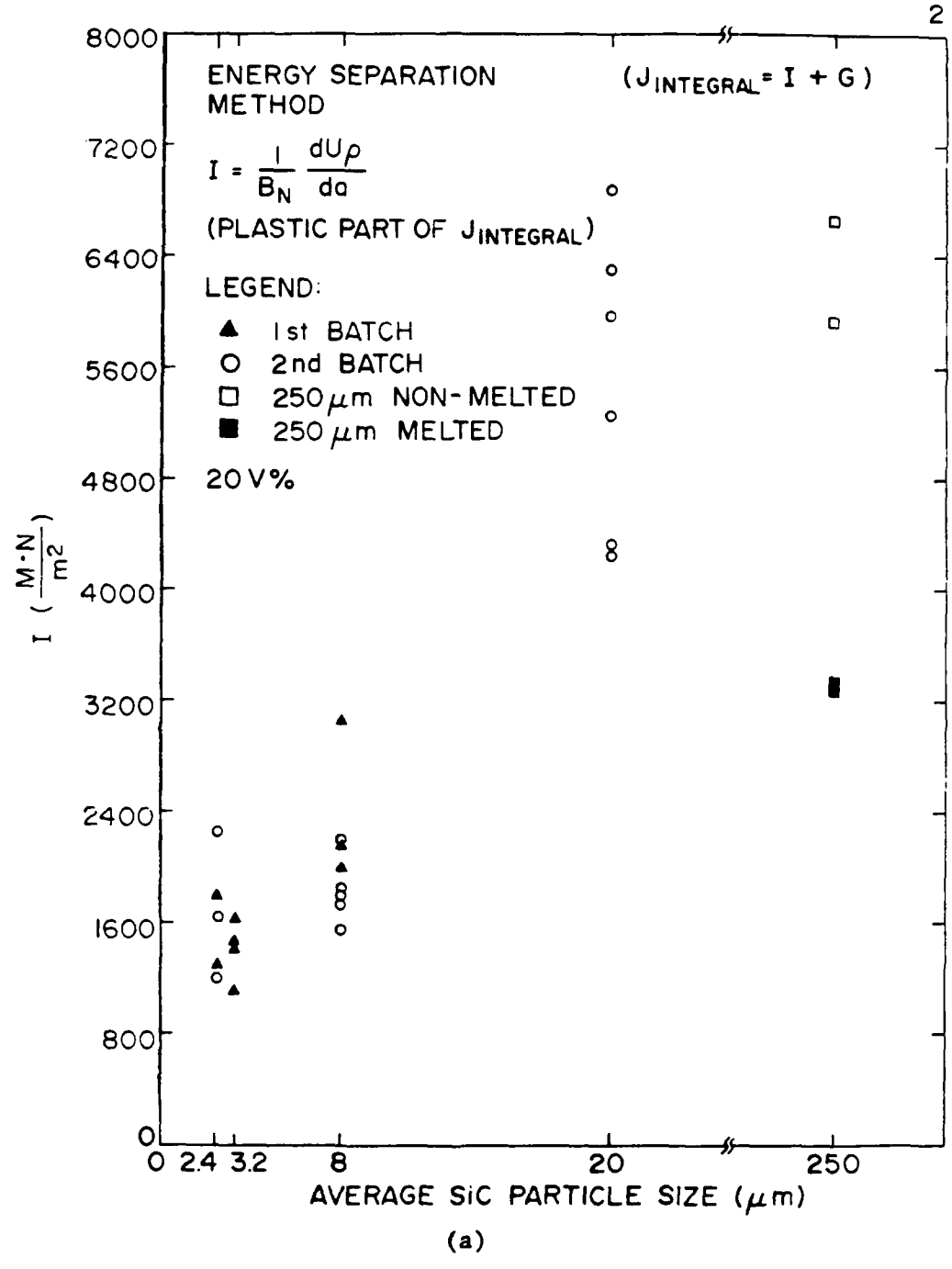

(a)

Fig. 10. Crack growth fracture toughness of SiC/Al composites measured as I (a) and T (b).

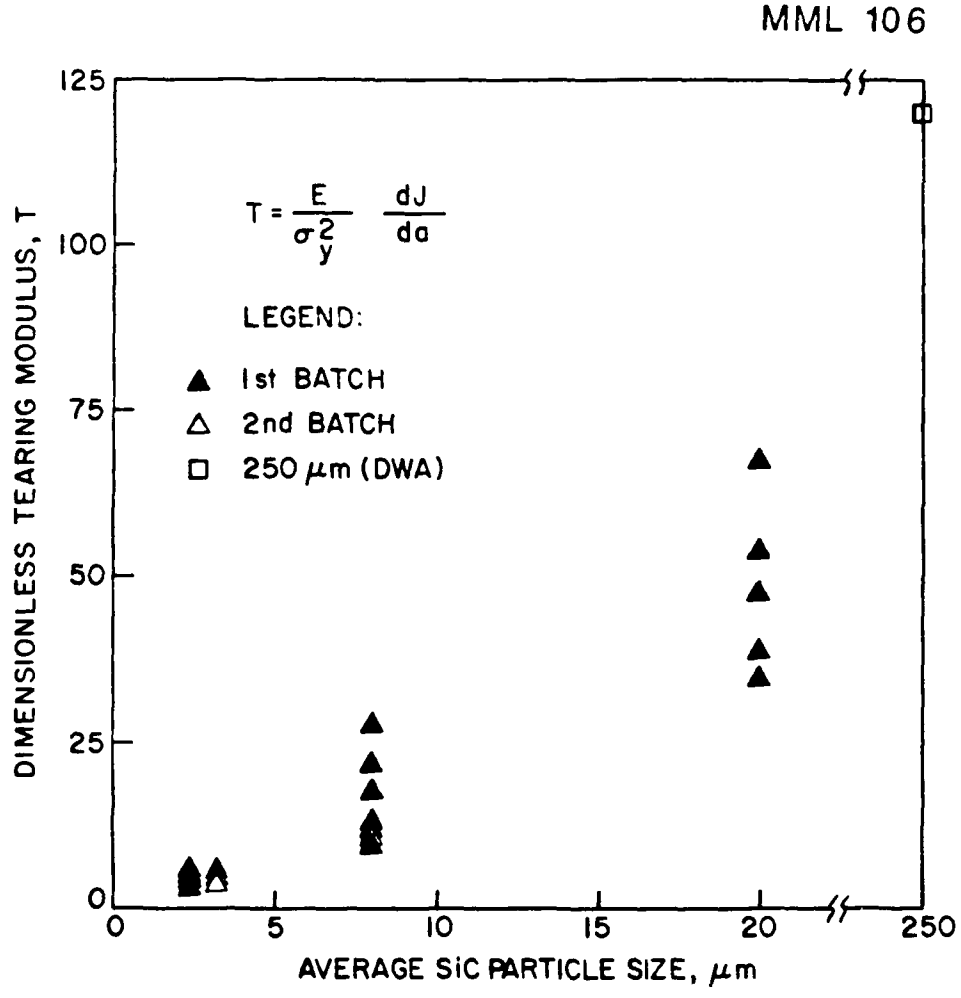

(b)

Fig. 10. Crack growth fracture toughness of SiC/Al composites measured as I (a) and T (b).

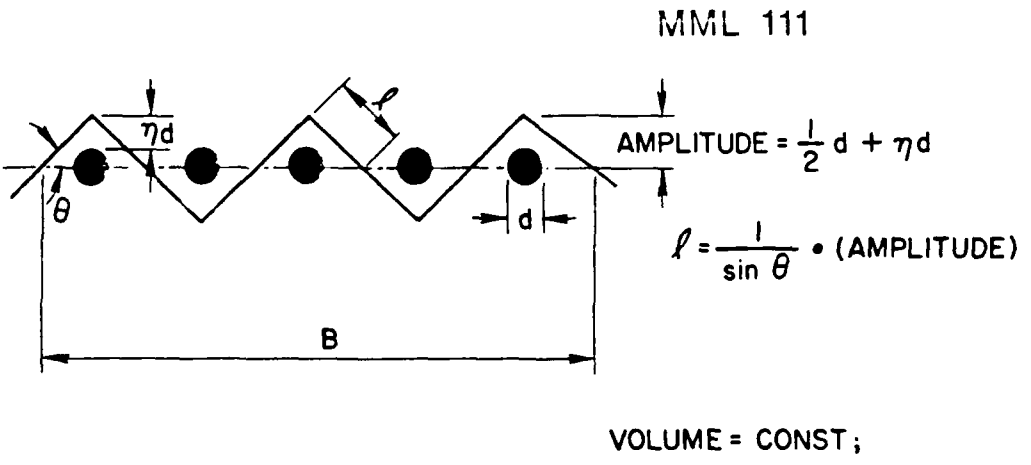

Fig. 11. Idealized geometry of the crack deflection by SiC particles.

THE EFFECT OF EXTERNAL MECHANICAL LOADING ON THE CHANGE OF THE MATRIX RESIDUAL STRESSES IN SiC/Al COMPOSITES

N. Shi and R.J. Arsenault
Metallurgical Materials Laboratory
University of Maryland
College Park, Maryland 20742 USA

ABSTRACT

The change of the average matrix residual stress as a function of two particular kinds of simple loading history was investigated, i.e. tension and compression. The major factor which controls the pattern of the change is presented.

INTRODUCTION

Previous experimental investigations of the deformation behavior of the short fiber reinforced SiC/Al composites have indicated that the constitutive behavior of these composites is distinctly different under applied uniaxial compressive and tensile loadings. It is generally found that the compressive yield strength of these composites is larger than that of the tensile yield strength while the Young's modulus for compression is smaller than that in tension[1,2]. It has been pointed out by various researchers[1-4] that the differences in response of the SiC/Al composite material to tensile or compressive load is closely related to the matrix thermal residual stresses. The previous analytical and experimental results indicate that in whisker reinforced composites the average thermal residual stress in the loading direction (z) in the matrix is in tension[2,4]. However, the change of residual stresses which may be a principal factor that affects the flow properties of the composites as a function of applied load has not been reported in the literature. It is therefore the primary goal of this investigation to analytically evaluate such a change in the magnitude of the matrix residual stresses. Throughout the analysis, it is understood that the term "residual stress" is referring to the phrase "the average matrix residual stress in loading direction Z."

FINITE ELEMENT (FEM) MODELING PROCEDURES

In our previous research[5], it was shown that a two-dimensional FEM model could qualitatively reproduce the changes in characteristic constitutive and flow properties of the whisker reinforced SiC/Al composites when the system is subject to either a uniaxial tensile or compressive loading. Based on the assumption that the change of the flow properties are largely controlled by the change in residual stresses, it is also conceivable that the change of residual stress can be qualitatively predicted.

In the present residual stress analysis, the ADINA finite element analysis code was used. The parameters used in this simulation correspond to annealed 6061 aluminum reinforced by SiC whiskers. The samples were initially thermally treated by setting a zero stress state at 773 K and then cooling down to 293 K and loaded either in

tension or compression to determine the materials' response under the influence of the thermal residual stresses. Such a response is characterized by macroscopically generating stress-strain curves which can be compared with experimental curves[5] and microscopically analyzing the change of the residual stresses after the external load is removed.

The composites are assumed to be two-dimensional infinite array of hexagonal packed parallelpipeds imbedded into the matrix. If the volume fraction of whisker is constant, it has been shown[5] that a small variation in interparticle spacing will not greatly affect the material's property. Therefore, in the subsequent analysis, the interparticle spacing was not selected as a critical parameter.

In the current analysis, 20V% SiC whisker composites with whisker aspect ratio equal to 4 were investigated. A multi-constraint boundary condition was employed so that only a quadrant of the material which contains the SiC whisker, as shown in Fig. 1, was considered to represent the whole infinite array.

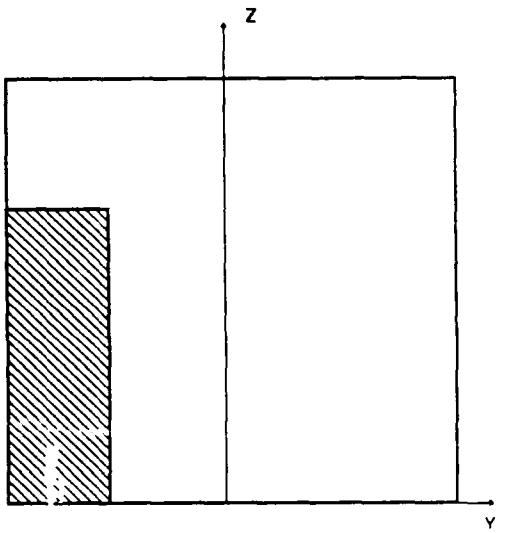

Fig. 1 Diagram of the composite unit cell for FEM calculation where the shaded area represents a quadrant of the SiC whisker and the remainder is Al.

RESIDUAL STRESS ANALYSIS

The average matrix residual stress is obtained in such a way that the stress values generated by FEM were averaged over the entire volume of the matrix. It was found that the average matrix residual stress along the tensile axes will drop initially and then will increase or decrease depending on the nature of the external loading(Fig. 2).

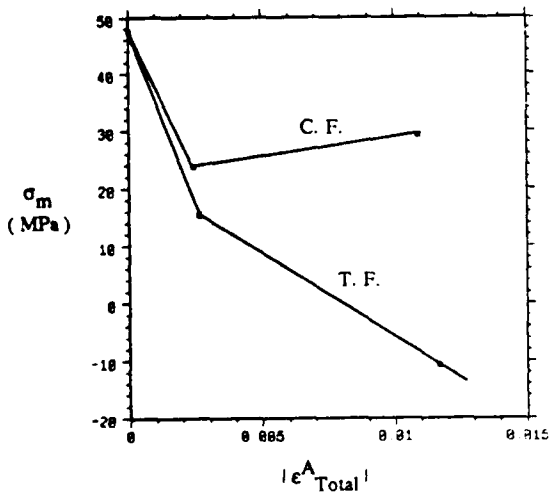

Fig. 2 A prediction of the change in the average thermal residual stress as function of eternal strain. C.F. is for initially tested in compression and T.F. is for tested in tension first.

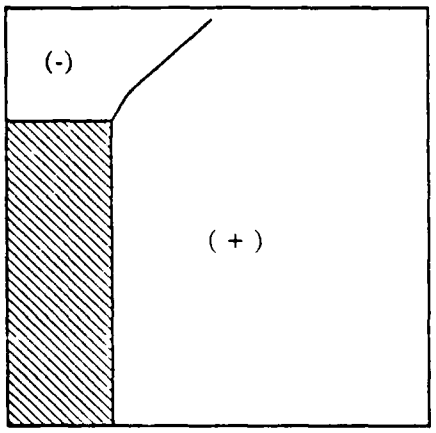

Fig. 3 Schematic diagram of the thermal residual stress arrangement where compressive residual stress is at the end of the fiber and the rest of the matrix is under tension.

and Fig. 3 shows a schematic of the thermal residual stress arrangement where at the whisker end the matrix is under compression while the rest of the matrix is under tension.

THEORETICAL EVALUATION OF THE CHANGE OF RESIDUAL STRESS UPON EXTERNAL LOADING

In this section, an analytical investigation was undertaken in order to obtain a physical understanding as to why there is an asymmetrical behavior due to plastic straining, i.e. compressive loading is not a mirror image of the tensile loading[1,3]. It was intended to depict the actual main physical process through the simplest model possible.

It is the authors' belief that the effect of the volume mismatch between the SiC particle and the Al matrix should be responsible for the asymmetric behaviors of the composites. Therefore, a simple discontinuous composite model based on such an idea was developed. It is assumed that a piece of SiC whisker is embedded into Al matrix, as shown in Fig. 1, except there is no bonding between SiC and Al along the whisker axes. Thus, there would be no shear load transfer and the boundary between tension and the compression zone is assumed to be the extension of SiC/Al interface along the whisker axes. Moreover, the shear stress at the zone boundary is assumed to be negligible. Also, a multi-constraint type of boundary condition was adopted as in the FEM analysis.

By following the same physical cooling and the subsequent mechanical loading process as described in the previous FEM section, the thermal residual stress can be determined as:

For the case of tension first:

$$\begin{cases} \sigma_{w_R} = \sigma_{y_m} + \dfrac{E_w E_{m_T}}{F_c E_w + F_w E_{m_T}} \epsilon_{cp}^{A} - \dfrac{E_m E_w}{F_c E_w + F_w E_m} \dfrac{\sigma_c^{A}}{E_c^{E}} \\ \sigma_{m_R} = -\dfrac{1-V_T}{V_T} \sigma_{w_R} \end{cases} \tag{1}$$

For the case of compression first:

$$\begin{cases} \sigma_{w_R} = \dfrac{-V_t}{1-V_t}\ \sigma_{m_{R_T}} + \dfrac{E_w E_{m_T}}{F_C E_w + F_w E_{m_T}}\ \epsilon^{A}_{Total} - \dfrac{E_m E_w}{F_C E_w + F_w E_m}\ \dfrac{\sigma^{A}_{c}}{E^{E}_{c}} \\ \sigma_{m_R} = -\ \dfrac{1-V_T}{V_T}\ \sigma_{w_R} \end{cases} \tag{2}$$

In both Eq. 1 and Eq. 2, σ_{w_R} and σ_{m_R} represent the residual stress in loading direction in the whisker and matrix, respectively. E_w and E_m are the Young's modulus for the whisker and matrix, E_{m_T} is the work hardening rate for the matrix, α_w and α_m are the coefficients of thermal expansion for the whisker and matrix. σ_{y_m} is the yield stress for the matrix, and E^{E}_{c} is the all-elastic Young's modulus of the composite without thermal residual stress as opposed to the apparent composite Young's modulus in which part of the matrix started plastically deforming right at the beginning of the loading

$$E^{E}_{c} = \frac{(1-V_T)E_m E_w}{F_C E_w + F_w E_m} + V_T E_m \tag{3}$$

where V_T is the volume fraction of the tension zone, and

$$F_C = \frac{V_C^2\ V_w}{V_w + V_C} \qquad F_w = \frac{V_C V_w^2}{V_w + V_C} \tag{4}$$

V_C and V_w are the volume fractions of compression zone and SiC whisker, respectively. Furthermore, $\sigma_{m_{R_T}}$ is the thermal residual stress in the tension zone. When ΔT is large enough to have induced plasticity which is true for the SiC/Al system[6,7]

$$\sigma_{m_{R_T}} = \frac{F_w(\alpha_w-\alpha_m)\Delta T + \sigma_{y_m} F_w\left[\frac{1}{E_{m_T}} - \frac{1}{E_m}\right]}{\left[\ \frac{1}{E_{m_T}} + F_C\ \frac{V_T}{1-V_T}\ \frac{1}{E_{m_T}} + F_w\ \frac{V_T}{(1-V_T)}\ \frac{1}{E_w}\ \right]} \tag{5}$$

and the average matrix residual stress ($\bar{\sigma}_m$) will be

$$\bar{\sigma}_m = \sigma_{m_R}\ V_T \frac{F_w}{1-V_w} \tag{6}$$

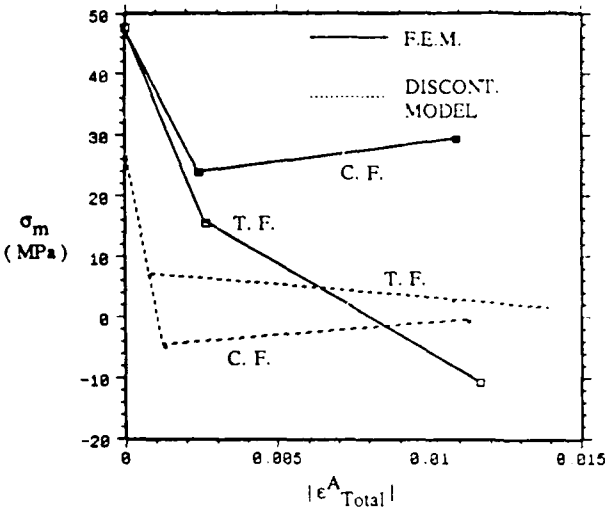

Fig. 4 A comparison between FEM and analytical results of average residual stress as function of total strain.

Fig. 4 shows the schematic curve for Eq. (6) if Eqs. 1 and 2 are considered.

DISCUSSION

From a consideration of Fig. 4, it is clear that the discontinuous composite model gives good qualitative agreement with the FEM data on the slope of the change of the residual stress. To be more specific, not only that the average residual stress drop is evident, but the slope change can also be correctly predicted. To understand the underlying mechanism for the change in residual stress, it is helpful to define a term as average matrix effective stress ($\bar{\sigma}_{m_{eff}}$) based on a weighted averaging scheme where an expression for the loading rate $(\partial\sigma_z/\partial p)^2$ may be used as a weighting function, where σ_z is the stress component in the loading direction corresponding to applied load p. Reevaluating the FEM results in the previous section by this scheme, it can be found that the ratio of the average matrix residual stress over the average effective residual stress ($\bar{\sigma}_m/\bar{\sigma}_{m_{eff}}$) is greater than $\left[(\bar{\sigma}_m/\bar{\sigma}_{m_{eff}})\big|_{p=0} = 1.55\right]$. This simply means that in order to maintain the volume compatibility, the compression zone at the whisker end will respond faster than the rest of the matrix, i.e. higher stress (strain) rate. This local stress (strain) rate inhomogeneity will later alter the residual stress arrangement after unloading.

Furthermore, it is worthwhile to point out that in the case of compression first, there is a sign change in slope $\partial\sigma_m/\partial\epsilon^A_{Total}$ after the composite starts yielding, which is predicted by both FEM and the discontinuous composite model. This is an indication that the interaction between tension and the compression zone becomes totally different. Once the macro-yielding is observed, a fact which has to be considered is that the matrix material is deforming plastically throughout regardless of initial sign of the residual stress. It is also interesting to point out that while the tendency of residual stress change is agreeable with both FEM and discontinuous composite model, the actual magnitude of the residual stresses predicted by the analytical model is much smaller than that predicted by the FEM. It is speculated that the absence of interfacial bonding in the model is

the key reason for the discrepancy. This discrepancy may be solved by assuming a set of effective materials' constant to the matrix material near the interface (tension zone).

CONCLUSION

In summary, (1) the predicted change of the average residual stress is asymmetrical, i.e. regardless of sign of the loading, the magnitude of the average residual stress drops upon initial elastic deformation, and it will increase or decrease depending on whether the loading history is compressive or tensile, and (2) the change of the residual stress predicted by FEM is generally comparable to that predicted by the theoretical model which is based on the volume mismatch between the reinforcement and the matrix. This indicates that such volume incompatibility is the controlling factor to the change of the residual stress.

ACKNOWLEDGEMENT

The authors would like to thank Prof. C. Schwartz of the University of Maryland for his encouragement in using the ADINA program and the Computer Science Center of the University of Maryland for its support on computer time.

REFERENCES

1. Arsenault RJ and Wu SB, Mater Sci and Eng, 96 (1987) 77.
2. Arsenault RJ and Taya M, Acta Met, 35 (1987) 651.
3. Withers PJ, Pedersen OB, Brown LM and Stobbs WM, to be published in Mater Sci and Eng.
4. Ledbetter HM and Austin MW, Mater Sci Eng, 89 (1987) 53-61.
5. Shi N, Sarfarazi M and Arsenault RJ, to be submitted to the "International Journal of Plasticity."
6. Arsenault RJ and Shi N, Mater Sci and Eng, 81 (1986) 175-187.
7. Flom Y and Arsenault RJ, Mater Sci and Eng, 75 (1985) 151-167.

FRACTURE TOUGHNESS IN SIC/AL COMPOSITE MATERIAL*

Y. Flom,** S.B. Wu and R.J. Arsenault

Metallurgical Materials Laboratory

Engineering Materials Group

University of Maryland

College Park, Maryland 20742-2111

Abstract

Crack initiation fracture toughness does not depend on SiC particle size. Crack growth fracture toughness increases as the size of the SiC particle increases. The fracture process is confined to a very narrow band and takes place within the matrix. In the case of composite reinforced with SiC particles of 20 μm and above fracture of SiC begins to dominate. The matrix is influenced by a triaxial tension in the matrix and a high density of dislocations generated at SiC/Al interfaces due to the difference in coefficient of thermal expansion (CTE) between SiC and the Al matrix.

1. INTRODUCTION

If ductile fracture is characterized by void nucleation and growth (VNG), then the spacing between the void nucleating particles is generally considered to be a critical microstructural parameter that taken together with the tensile properties controls the toughness of a given materials[1-7]. This can be represented by the following simplified expression[7]

---

* This investigation was supported by the Office of Naval Research under Grant No. N00015-87-K-0007.

** Presently at Goddard Space Flight Center, NASA, Greenbelt, MD

$$K_{IC} = [a\sigma_y \epsilon_f^* Ef(N)]^{\frac{1}{2}} s^{\frac{1}{2}} \quad (1)$$

where K_{IC} is the plane strain fracture toughness, a is the numerical coefficient, σ_y is the yield stress, ϵ_f is the maximum strain acting at the crack tip, E is the Young's modulus, f(N) is some function of the strain-hardening exponent and s is the average inclusion spacing in the matrix. The experimental data collected by various investigators are usually given in terms of the volume fraction of the second phase particles (V) or less often in terms of s (see Fig. 1).

The dimple morphology of the fracture surfaces is the most common observation made by a number of researchers studying the fracture process in discontinuous* SiC/Al composites[8-22]. This indicates that the VNG mechanism is active in these composites and therefore, corresponding theories (generalized by Eq. 1) should be applicable to describe the fracture process in SiC/Al composites. In the past, the investigations of the fracture toughness of SiC/Al composites were

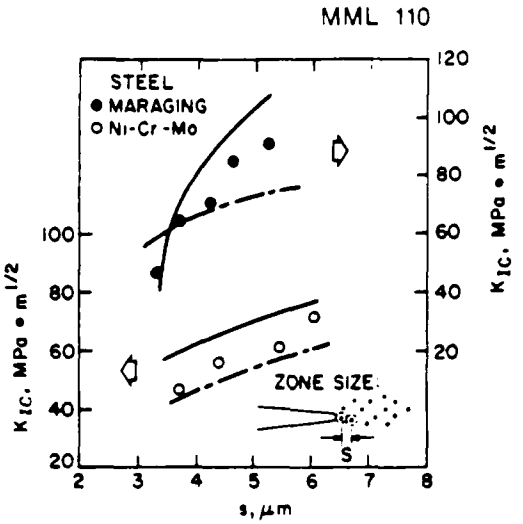

Fig. 1 Fracture toughness as a function of the "process" zone size. Various forms of Eq. 1 are employed to predict the fracture toughness values (solid and dashed lines) and compare them with the experimental data.

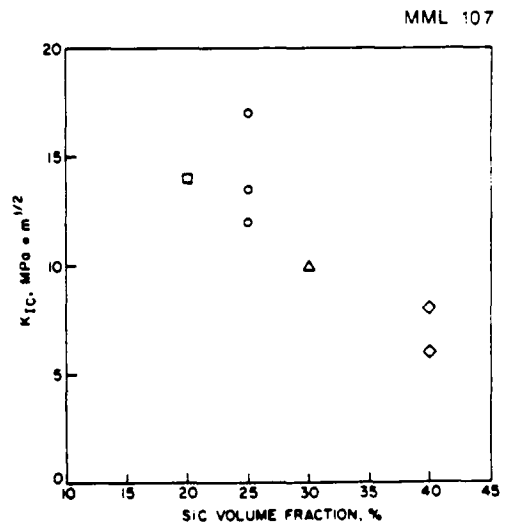

Fig. 2 Fracture toughness as a function of SiC volume fraction for SiC/Al composites (Refs. 8-13,22).

---

* In all cases, we shall be referring to discontinuous SiC/Al composites.

concerned with the matrix properties (heat treatment, amount of work, alloying elements, crack tip acuity) and the morphology of the SiC reinforcement (shape and volume fraction).

The adverse influence of an increase of the volume fraction of SiC reinforcement on fracture toughness can be established rather well when one combines the data on fracture toughness testing available in the literature, as shown in Fig. 2.

A rather strict geometric consideration requires that all three microstructural variables , V, s and particle size, d, be related. There are several expressions relating V, s and d available in the literature[4,23,24]. SiC/Al composites.

Since there is no substantial difference between these expressions, we select one derived by LeRoy et al.[4] for the equiaxial particles:

$$s = 0.77\ d V^{-\frac{1}{2}} \qquad (2)$$

Data in Fig. 2 can now be replotted as a function of the average center-to-center SiC particle spacing, s, providing that the average SiC particle size remains

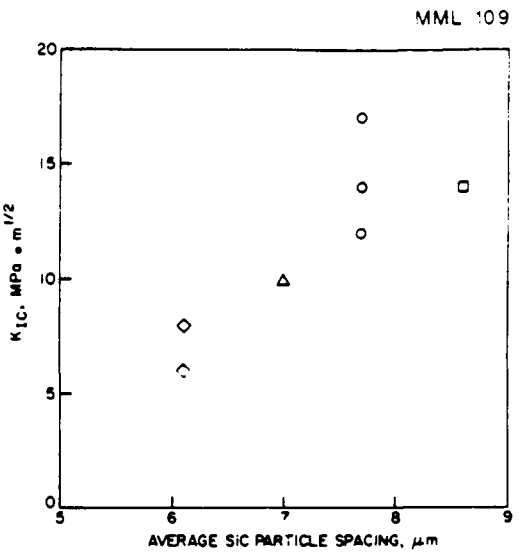

Fig. 3 Fracture toughness as a function of the average SiC particle spacing s. The experimental data in Fig is replotted using Eq. 2 and keeping SiC particle size d constant, equal to 5 μm.

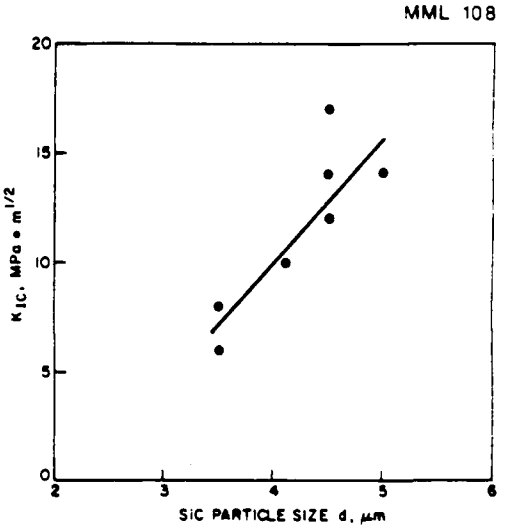

Fig. 4 Prediction of fracture toughness as a function of the average SiC particle size d. Volume fraction of SiC is constant and equaled to 20% (arbitrarily chosen).

constant which is generally the case in commercial composites. Figure 3 shows the dependence of K_{IC} on s which was plotted using the data in Fig. 2 and Eq. 2 assuming that the average SiC particle size is about 5 μm[11]. Notice that in this case we are changing s by varying V.

Mathematically, a similar result can be achieved by keeping V constant and changing the particle size d. In accordance with Eq. 2, by increasing d, we proportionally increase s. Thus, a plot similar to one shown in Fig. 3 should result if the size of SiC particles is increased and their volume fraction is kept constant (see Fig. 4). A similar trend can be obtained by plotting K_{IC} as a function of s employing Eq. 1 (which is based on VNG theories of ductile fracture) assuming that fracture toughness of SiC/Al composites can be improved when the size of the SiC particles is increased, providing that at least one of the two following assumptions is met:

1) Voids are nucleated by SiC particles and/or
2) the response of the matrix to changes of s remains the same regardless of whether this change is caused by varying the volume fraction or the size of the SiC particles.

The purpose of this work, therefore, was to determine the influence of the size of SiC particles on fracture toughness of SiC/Al composites and to examine the applicability of the aforementioned assumptions.

2. MATERIALS

Inert gas atomized 1100 Al alloy (Valimet H-3) was mixed in succession with 2.4, 3.2, 8 and 20 μm average size SiC particles obtained from the Norton Company. An 1100 Al alloy was selected in order to minimize the influence of the alloying elements which would other wise introduce additional complicating factors. As received SiC powders were filtered onto 0.4 μm size Nuclepore filters for size distribution, and distributions were fairly broad (25). Mixtures of Al and SiC powders were hot pressed, hot extruded and hot rolled to produce tensile test and compact tension specimens. Details of the fabrication process are described elsewhere[25]. The volume fraction of the SiC reinforcement was constant in all composites and equal to

20 V%.

Also, a SiC/Al composite containing 250 μm size SiC particles was purchased from DWA* in the form of a 25 mm thick plate was sliced into plates ~ 6.5 mm × 12.5 mm × 304 mm. The "as rolled" and sliced plates were machined into tensile test and compact tension specimens (CTS). Design of the CTS was based on ASTM E813 standard and also on the latest ASTM developments in the area of elastic-plastic fracture toughness test methods[26,27] and shown in Fig. 5(a).
All specimens were annealed at 803 K for 12 hours and furnace cooled prior to the mechanical testing.

3. TEST METHODS

The CTS were tested using single specimen J-integral test method per ASTM E813 standard. Also, the energy separation technique (EST) was utilized as a additional tool in the load-unload records analysis. The latter technique is quite new and is currently under intensive study by the fracture mechanics community [28]. The EST enables one to obtain values of plastic, I, and elastic,

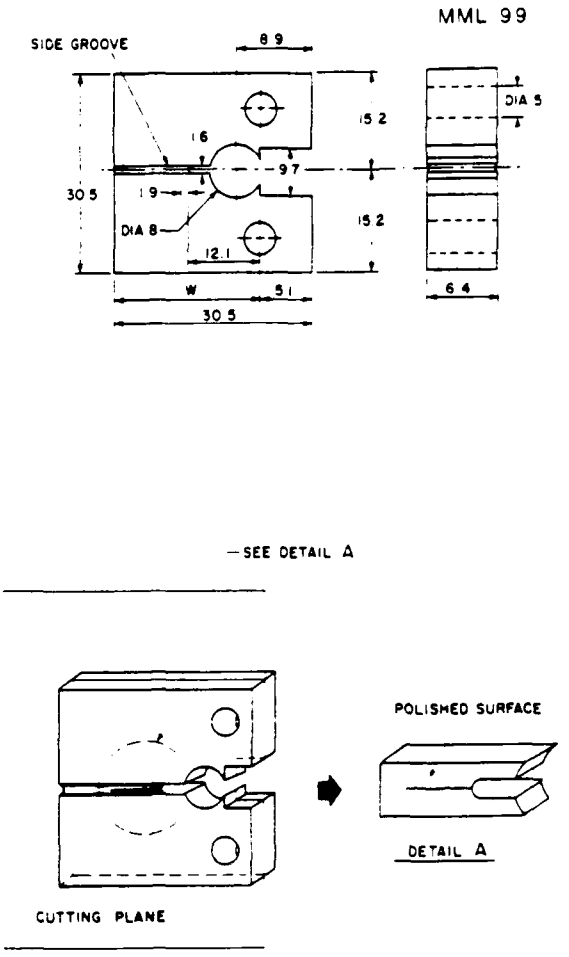

Fig. 5 Compact tension specimen (CTS) geometry (a) and the area of metallographic analysis (b).

---

* DWA Composites Specialities, Inc.

G, contributions to the total value of J-integral. It implies that the area under the load vs. displacement curve which corresponds to the work done by external force can be separated into the stored elastic strain (potential) energy, U_S, the elastic energy, U_E, released during crack during crack extension, and plastic energy, U_p dissipated during the crack extension. A more detailed description of the EST is outside the scope of this paper and can be found elsewhere[28]. The rate of plastic energy dissipation $I = 1/B_n \, dU_p/da$ and the elastic energy release rate $G = 1/B_n \, dU_E/da$ represent the plastic and elastic parts of the J-integral, i.e., $J = I+G$, where B_n is the thickness of the CTS between the side grooves and a is the crack length. Crack growth fracture toughness is evaluated by a dimensionless tearing modulus, T, which is equal to (29,30)

$$T = \frac{E_c}{\sigma_y^2} \frac{dJ}{da} \qquad (3)$$

where σ_y is the composite yield stress and dJ/da is the slope of the stable crack extension portion of J vs. a plot constructed in accordance with ASTM E813. Crack extension was determined by using the unloading compliance technique[26,29]. In order to verify the calculated crack extension values, the tested CTS were exposed to elevated temperature and then fractured (heat tinting method). Experimentally measured crack lengths were found to be within 5 to 10% from the values calculated by a compliance technique.

A mini-tensile stage was obtained so that a precracked CTS could be load and crack propagation observed on the optical microscope. The sample was cut as shown in Fig. 5b and then metallographically polished. The area in front of the crack was photomapped and then the CTS was loaded and photomapped again.

4. EXPERIMENTAL RESULTS

4.1 Crack Extension

The CTS were section-polished and loaded such that the crack propagation could be observed under load.

In the case of the composite containing small size SiC particles, i.e. <20 μm, there are three general observations: 1) there is very little, if not zero crack tip blunting or opening prior to propagation; 2) there is very little indication of void

formation at the particle-matrix interface, and 3) there is very little indication that particles are fractured as a result of the crack tip advance.

4.2 Crack Initiation Fracture Toughness

Crack initiation fracture toughness measured as K_{IC} and K_{IQ} is plotted as a function of the average SiC particle size and shown in Fig. 6. The fact that both K_{IC} and K_{IQ} show the same trend, i.e., no dependence on the size of the SiC particles, increases the confidence in the results obtained and supports the energy separation method as a new and powerful tool.

4.3 Crack Growth Fracture Toughness

Crack growth fracture toughness defined as tearing modulus (T) and plastic part (I) of J-integral is plotted vs. the average size of SiC particles in Fig. 7. The increase of the crack growth toughness with the increase of the SiC particle size means that more energy is dissipated during crack extension in the composite with a larger size of SiC particles.

5. DISCUSSION

5.1 Crack Initiation Toughness K_{IC}

The experimental results of this investigation have indicated that crack initiation fracture toughness K_{IC} is independent of the SiC particle size (within the range of SiC sizes tested). In order to understand this result it is instructive to consider local energy dissipation mechanisms associated with the crack extension in SiC/Al composite. We are using the term "local" to emphasize the area in the vicinity of the crack tip. The plastic deformation in the bulk of the SiC/Al specimen is not included since it is separated out by using the energy separation technique (EST).

The elastic energy release rate G consists of the several terms that can account for energy dissipation. These terms can be identified as:

$$G = \gamma_s + \gamma_v + \gamma_{PLzone} + \gamma_{CTS} \qquad (4)$$

where γ_s is the energy consumed in creation of the new surfaces, γ_v is the energy consumed in the formation of the void sheet, γ_{PLzone} is the energy dissipated into plastic deformation around the crack tip and γ_{CTS} represents crack tip shielding effects described by Ritchie et al.[31]. It is

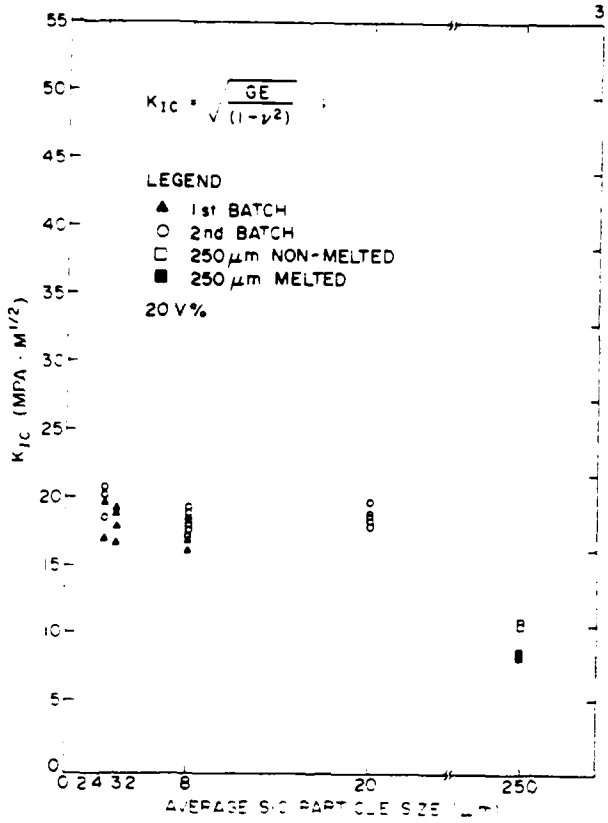

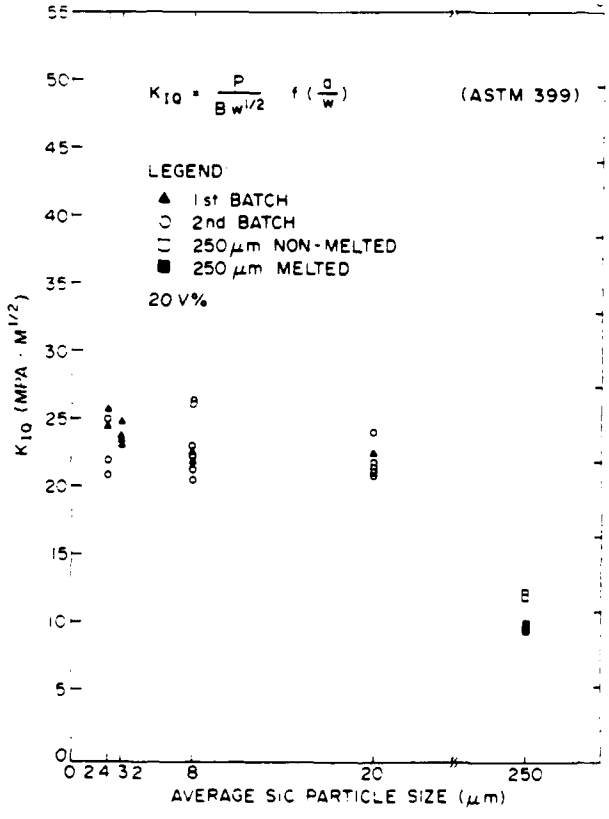

Fig. 6. Crack initiation fracture toughness of SiC/Al composites measured as K_{IC} (a) and K_{IQ} (b).

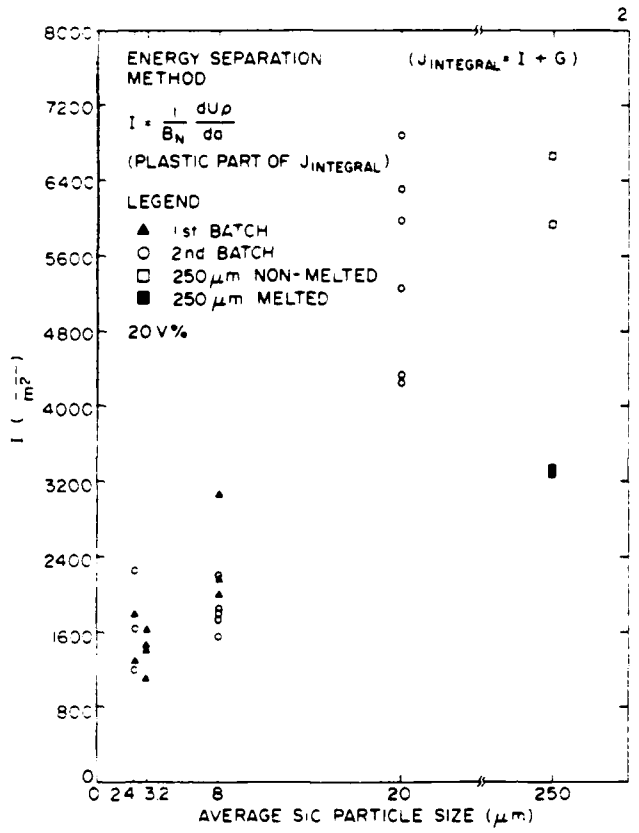

Fig. 7 Crack growth fracture toughness of SiC/Al composites measured as I (a) and T (b).

fracture toughness (measured as I and T) with an increase of the SiC particle size can be treated on the basis of the relationship between the dislocation density and the spacing of the SiC particles. The crack growth fracture toughness is related primarily to the extent of plastic deformation at a distance away from the crack. The amount of plastic deformation that can occur within the matrix depends upon the amount of plastic deformation in the matrix (i.e., due to ΔCTE) prior to crack propagation. If we

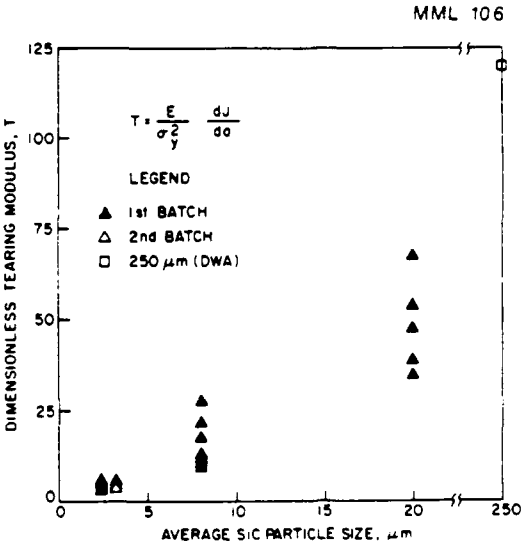

rather well established that the γ_s term[29] is very small in metallic systems compared with $\gamma_{PLzone}+\gamma_v$. Evaluation of γ_{CTS} is quite complicated and requires the consideration of the extrinsic toughening mechanisms affecting the conditions at the crack tip in the SiC/Al system. Following Ritchie's nomenclature[31] these mechanisms can be divided into four groups: 1) crack deflection and meandering, 2) zone shielding, 3) contact shielding, and 4) local plastic deformation and void formation.

5.2 Propagation Fracture Toughness

The increase in crack growth

equate dislocation density and the amount of plastic deformation then it is possible to determine the amount of plastic deformation permissible in the matrix as a function of particle size, due to external deformation, i.e., as a result of tensile or compact tension testing. In other words, if there is a low dislocation density in the sample prior to testing then the amount of deformation tion that the matrix can accumulate will be large. Arsenault and Shi[32] have shown this, by using a simple prismatic punching model.

6. CONCLUSIONS

From the data generated in this investigation we can arrive at four general conclusions.

1) Increase of SiC particle size did not improve K_{IC} fracture toughness of SiC/Al composite. K_{IC} is independent of SiC particle size up to 20 μm average size.
2) No evidence of void nucleation at SiC particles was found.
3) SiC/Al composite is a more complicated system than it appears: a) the sites of void nucleation are not well defined, and b) the two alternative ways of increasing interparticle spacing, S, do not produce the same results. V↑ S↓ and K_{IC}↓ (d = constant). d↑ S↓ but K_{IC} does not change (v = constant).
4. It can be speculated that K_{IC} depends mainly on the volume fraction of SiC particles.

7. ACKNOWLEDGEMENTS

The authors wish to acknowledge the assistance of Dr. C.R. Feng. They also wish to acknowledge the support of the Office of Naval Research, Grant No. N00014-85-K-0007 and the encouragement of Dr. S. Fishman.

8. REFERENCES

1. Hahn, G.T. and Rosenfield, A.R., Metal. Trans. A, 6, 653 (1975).
2. Garret, G.G. and Knott, J.F., Metal. Trans. A, 9, 1187 (1978).
3. Schwalbe, K.H., Eng. Frac. Mech., 9, 795 (1977).
4. LeRoy, G., Embury, J.D., Edwards, G. and Ashby, M.F., Acta Metal. 29, 1509 (1981).
5. Bates, R.C., "Modeling of Ductile Fracture by Microvoid Coalescense for Prediction of Fracture Toughness," in Proc. 113th AIME Conf., Wells, J.M. and Landes, J.B., eds., 1985, p. 117.

6. Gerberich, W.W., "Interaction of Microstructure and Mechanism in Defining K_{IC}, K_{ISCC} or K_{th} Values", in Proc. 113th AIME Conf., Wells, J.M. and Landes, J.B., eds., 1985, p. 49.
7. Firrao, D. and Roberti, R. "On the Mechanism of Ductile Fracture Nucleation Ahead of Sharp Crack" in Proc. 113th AIME Conf., Wells, J.M. and Landes, J.B., eds., 1985, p. 165.
8. Divecha, A.P., Fishman, S.G. and Karmarkar, S.D., J. of Metals, 9, 12 (1981).
9. Longston, W.A. and Liaw, P.K., Westinghouse Sci. Paper, 83-ID3-NODEM-P1, (Dec. 1983).
10. Marcus, H.L., "Microscopic Study of the Influence of the Impurities on Interface Bonding," Report No. UTCM-SE-84-1, U. of Texas, 1984.
11. Schoutens, J.E., "Discontinuous Silicon Carbide Reinforced Aluminum Metal Matrix Composites Data Review," MMCIAC Publ. No. 000461, Dec. 1984.
12. Hsieh, T.J. "Effect of Precracking Procedure on Fracture Toughness of SiC/Al Composite," M.S. Thesis, U. of Maryland, (1985).
13. Crowe, C.R., Gray, R.A. and Hasson, D.F., Proc. ICCM-5, Harrigan, W. ed., San Diego, 1985.
14. McDanels, D.L., Metal. Trans. A 16, 1105 (1985).
15. Nieh, T.G., Rainen, R.A. and Chellman, D.J., Proc. ICCM-5, Harrigan, W., ed., San Diego, 1985, p. 825.
16. Nutt, S.R. and Duva, J.M., Scripta Metal. 20, 1055 (1986).
17. Arsenault, R.J. and Flom, Y., "Role of Interfaces in SiC/Al Composites," Proc. Sym. "Phase Boundary Effects on Deformation," TMS AIME, Toronto, Canada, 1985, p. 13.
18. Nair, S.V., Tien, J.K. and Bates, R.C., Int. Met. Rev. 30, 6, 275 (1985).
19. You, C.P., Thompson, A.W. and Bernstein, I.M., Scripta Metal. 21, 181 (1987).
20. Flom, Y. and Arsenault, R.J., "Fracture of SiC/Al Composites," Proc. ICCM-VI, 2 Elsevier, London, 1987.
21. Lewandovski, J.J., Liu, C. and Hunt, W.H., Jr., "Microstructural Effects on the Fracture Micromechanism in 7XXX Al P/M-SiC Particulate Metal Matrix Composite," in

Powder Metallurgy Composites, Kumar, M., Vedula, K., and Ritter, A.M., eds., TMS AIME, 1987.

22. Flom, Y., Parker, B.H. and Chu, C., "Fracture Toughness of 40 Volume Percent Particulate SiC/Al Composites," paper in preparation, NASA, Goddard Space Flight Center, 1987.
23. Edelson, B.I. and Baldwin, W.M., Trans. ASM, 55 230 (1962).
24. Underwood, E.E., Quantitative Stereology, Addison-Wesley, 1970.
25. Flom, Y., "Fracture Toughness of SiC/Al Composites," Ph.D. Thesis, U. of Maryland, 1987.
26. 1986 Annual Book of ASTM Standards, 03.01, sec. 3, Standard E813.
27. ASTM E24.08 Subcommittee, Standard Test Method for Determining J-R Curves, 12th draft, July 1985.
28. Mecklenburg, M.F., Joyce, J.A. and Albrecht, P., "Separation of Energies in Elastic-Plastic Fracture," at 3rd Inter. Sym. on Linear Fracture Mechanics, ASTM, Knoxville, TN, Oct. 1986.
29. Latzo, D.G.H., Turner, C.E., Landes, J.D., McCabe, D.E. and Hellen, T.K., "Post Yield Fracture Mechanics," 2nd Ed., Elsevier Publ., NY, 1984.
30. Standard E399 of ref. 26.
31. Ritchie, R.O. and Yu, W., "In Small Fatigue Cracks," Ritchie, R.O. and Lankford, eds., TNS-AIME, Warrendale, PA, 1986.
32. Arsenault, R.J. and Shi, N., Mater. Sci. Eng. 81 175 (1986).

BIOGRAPHIES

R.J. Arsenault, Professor

R.J. Arsenault is the director of the Metallurgical Materials Laboratory. His research centers around fundamental investigations of plastic deformation and fracture. During the last several years, he has pioneered the research efforts to determine the strengthening mechanisms in metal matrix composites.

Y. Flom Dr. Flom received his Ph.D. from the University of Maryland and is presently conducting research on high temperature super conductors at NASA, Goddard.

S.B. Wu Dr. Wu is a research associate at the University of Maryland where he is conducting research on high temperature composite materials.

MICROSTRUCTURE OF TiB_2/NiAl*

L. WANG and R.J. ARSENAULT
Metallurgical Materials Laboratory, University of Maryland, College Park, Maryland 20742

ABSTRACT

The addition of 20 volume percent titanium diboride in particulate form (1-3 μm) to nickel aluminide (TiB_2/NiAl) results in a twofold increase in the high temperature strength of NiAl. There are at least two theories that have been proposed to account for the high temperature strength of discontinuous reinforced metal matrix composites. However, they can not be adequately used as a basis to explain the observed strengthening.

An investigation was undertaken of NiAl, 10 V% TiB_2/NiAl and 20 V% TiB_2/NiAl in the annealed condition and after deformation, allowed to cool slowly. There is a low dislocation density in the annealed samples and the dislocation density did increase slightly as a result of deformation. However, deformation did produce some intriguing dislocation arrangements; for example, it was found that there was a high dislocation density within the TiB_2 in the deformed higher volume fraction composites and the dislocation density within NiAl matrix was not uniform.

1. Introduction

1.1 Background

The interest in intermetallic compounds for high temperature applications extends back in time for a number of years [1] and there has been a continued interest [2-26]. There are numerous obvious advantages for the consideration of intermetallic compounds, i.e. they have good oxidation resistance at high temperatures. However, they are not widely used in structural applications, but they are, e.g. NiAl, used as coatings on super alloys for oxidation resistance. The reason that NiAl is not used in high temperature structural applications is that its strength is at least a factor of 10 weaker than conventional super

* This research was supported by the Office of Naval Research under contract No. N00014-K-85-0007.

alloys. For example, at 1300 K and a strain rate of 10^{-5} sec^{-1}, the stress required for UDIMET 115 [27] is ~ 200 MPa, whereas for NiAl, it is <20 MPa [26].

Another deterrent to the use of NiAl in structural application is its lack of ductility, especially in the large grain size condition [13]. The fracture toughness as measured by Charpy impact testing is about 0.08 ft.-lbs. (0.1J) [28]. It was assumed that the fracture toughness of SiC measured by Charpy impact testing was low, but in that case, the fracture toughness is 1 ft.-lb. [29].

The lack of high temperature strength and the low temperature ductility can probably be improved by the addition of TiB_2, i.e. to produce a discontinuous composite of TiB_2/NiAl. The major advantage of TiB_2 is that it is inert with respect to the NiAl matrix, and in high temperature applications, the matrix should not react with the reinforcement. If a reaction takes place, it is possible that reinforcement will be consumed during the reaction.

1.2. Mechanism or mechanisms of strengthening

The high temperature creep of composites as an indication of the high temperature strength of composites have all been analyzed in terms of a classical continuum composite strengthening mechanism [30]. Simply, this means that there is a reduction of the stress in the matrix due to the load transfer to the reinforcement. However, if these mechanisms are applied to a discontinuous spherical reinforcement, the load transfer is very small, i.e. 5%, which would mean that the predicted decrease in the creep rate of the spherical reinforced composite would be very small compared to that of the matrix material.

If one attempted to perform a more rigorous analysis by the use of the Eshelby method, there is a restriction which is presently placed on the Eshelby method which requires that the matrix has to be treated as a neutonian fluid, i.e. the stress exponent (n) would have to be one (1). The observed stress exponents are much greater than one, in the range of 5 to 20 [31].

Another approach would be to consider the dislocation mechanisms that have been

proposed to predict creep behavior. However, very few detailed mechanisms have been proposed which take into account the presence of large second phase particles [31,32].

From a consideration of a dislocation climb over second phase particles, it is possible to obtain the following equation [31] for the creep rate:

$$\frac{\dot{\epsilon}}{D} = \frac{(1+\nu)^{2/3}}{2.83\pi} \frac{\lambda^{8/3} b^{7-3} E\rho_m}{r^2 kT} \left[\frac{\sigma_e}{E}\right]^{5/3} \times \frac{1}{1-(1+\nu)^{4/3}\left[\frac{\lambda}{b}\right]^{4/3}\left[\frac{\sigma_e}{E}\right]^{4/3}} \quad (1)$$

where D is the diffusion coefficient for the matrix, ν is the Poisson's ratio, λ is the interparticle spacing, E is the Young's modulus of the matrix, ρ_m is the density of mobile dislocations, σ_e is the effective climb stress, b is the Burger's vector, r is the radius of the particle and kT are the Boltzmann's constant and the temperature, respectively. If it is assumed that the second phase is approximately spherical, then there is a simple relationship [33] between λ and r.

$$\lambda = 0.306\, r \left[\frac{\pi}{V_f}\right]^{\frac{1}{2}} \quad (2)$$

where V_f is the volume fraction of the reinforcement. As one would intuitively guess, for a constant V_f, the $\dot{\epsilon}/D$ is greater for a larger size reinforcement, and $\dot{\epsilon}/D$ decreases with an increase in the volume fraction of reinforcement. If the actual $\dot{\epsilon}$ vs. σ_e is determined for a composite of 20 V% and 0.5 μm radius particles in the NiAl matrix, then Eq. 1 predicts a stress for a $\dot{\epsilon}$ of $10^{-7}\,sec^{-1}$ of $<6.9\times10^{-3}$ MPa. This stress is ~ 3 orders of magnitude smaller than the strength of the matrix. There are other possible dislocation models which have been proposed by Blum and Reppich [32], but the result is that if the Orowan stress is

low for the composite, the effect of the reinforcement on the creep rate is small.

There have been a few TEM investigations of dislocations overcoming large particles at high temperatures; however, details of the rate controlling mechanisms are not given [33].

It can be concluded that there is a large difference in the predicted high temperature strengths, i.e. as manifested by the creep rates of discontinuous composites as predicted by the continuum mechanics and dislocation models. If we consider the preliminary data obtained, there is approximately a factor of two increase of the strength of composite (20 V%) vs. the matrix.

The purpose of this investigation was to determine the microstructures of TiB_2/NiAl samples which were deformed at high temperatures, and from these determinations obtain some insight into the possible strengthening mechanism.

2. Materials

The materials used in this investigation were purchased from the Martin Marietta Corporation, and consisted of 0, 10, 20 and 30 V% TiB_2 in NiAl. The material was ground into compression samples with a height to diameter (h/d) ratio of 1½-2 and were compression tested at 1143 K and 1273 K at various strain levels. Samples also were annealed at the test temperature for periods of time from 2 hours to 12 hours.

3. Testing methods

The samples were tested in compression at various strain rates ranging from 10^{-4} to 10^{-2} sec^{-1} at 1143 and 1273 K.

After compression testing and/or after annealing, samples were cut into 3 mm discs with a thickness of 0.5 mm by an electrical discharge machine. After lightly grinding to remove the debris on the surface, the discs were dimple ground until the thickness reached 0.07 ~ 0.1 mm in the center. The final electro-polishing was performed by using 5% perchloric acid ethanol solution at 253 K or below until a small hole appeared at the center of the sample. The applied voltage was 50 ~ 70 V.

Also, an investigation was carried out both optically and by scanning electron microscopy (SEM) to determine the particle size and distribution. This was also followed by an X-ray powder diffraction investigation to determine the content of TiB_2.

The transmission electron microscopy (TEM) was carried out at the high voltage electron microscopy (HVEM) facility at Argonne National Laboratory.

4. Experimental results and discussion

The yield stress (σ_y) which is only slightly less than the ultimate stress, was determined as a function of volume fraction of TiB_2 and strain rate. As expected, σ_y increases with increasing volume fraction (Fig. 1) and increasing strain rate. However, the increase in σ_y with increasing volume fraction of TiB_2 is greater at faster strain rates.

In Figs. 2-5 are SEM micrographs of 0, 10, 20 and 30 V% TiB_2/NiAl samples. There are particulates in the 0 V% which are not TiB_2. These have been tentatively identified as α-Al_2O_3 from an examination of TEM selected area diffraction patterns. The other dark spots in Fig. 1 are holes which are created by an etching effect. It can be seen that the volume fraction of the second phase can be as high as 10 V%. The dark particles in Figs. 3, 4 and 5 are the TiB_2. In Figs. 6-8 are X-ray powder diffraction patterns obtained from 0, 20 and 30 V% TiB_2 powder samples. The purpose of the X-ray investigation was to obtain some insight as to what were in the SEM micrographs, i.e. an attempt to determine the nature of the other particles.

In Figs. 9 and 10 are 0 V% samples deformed 30% at 1143 K (870° C). It is evident that the second phase particles are acting as barriers to dislocation motion. Figures 11 and 12 are again of 0 V% TiB_2/NiAl matrix samples showing the formation of a network which is prevalent in these alloys. Also, it is evident that the dislocation structure is not planar, i.e. no well defined slip plane, and the dislocations have convoluted shapes as shown in Fig. 12.

Also, a phenomenon which is only observed in 0 V% NiAl matrix samples, especially the ones which were deformed at higher strain rates, are bands or regions of very high dislocation density which we define as shear bands. Figure 13 is an example of these shear

bands in a sample which was deformed at 1143 K. These shear bands appear to go straight across the grain boundary without any apparent shifting of the grain boundary or of the shear band.

If we now consider the samples containing TiB_2 particulate, several things become evident. Figure 15 is a low magnification TEM micrograph of a 20 V% TiB_2/NiAl which was deformed 30%. There is a very high dislocation density in the area with higher than average volume fraction of TiB_2, whereas in regions of lower than average TiB_2 concentration, there is a very low dislocation density. Also, it is evident in these pictures that within the TiB_2, there is a large number of dislocations.

This difference in dislocation density which depends upon the local volume fraction of TiB_2 is evident in Figs. 16 and 17 where there are two different volume fractions of TiB_2. Figure 16 contains a very high dislocation density in the matrix, whereas in Fig. 17, there is a very low dislocation density in the matrix.

Returning to a consideration of plastic deformation which occurs in the TiB_2, there are several unique observations as shown in Figs. 18-19. First, the TiB_2 particles are not uniformly deformed in all cases. Secondly, in the TiB_2 particles which contain a variable dislocation density, there is a variable dislocation density in the surrounding matrix. There is an inverse relationship if a portion of a particle has a high dislocation density, then the dislocation density in the matrix immediately surrounding this portion of the particle has a low dislocation density. Whereas, if a portion of the particle has a low dislocation density, then the matrix immediately surrounding this portion of the particle has a high dislocation density.

As stated in the introduction, the purpose of this investigation was to determine the changes in microstructure of TiB_2/NiAl composites deformed at high temperatures for the purpose of obtaining insight into possible strengthening mechanisms in this composite. The results obtained do not appear to support any of the presently proposed mechanisms. The theories of Taya et al. [30] which are based on the load transfer concept require that there

should be zero or very little plastic deformation of the reinforcement. This requirement does not seem to be satisfied due to high dislocations within the TiB_2 particles. The theories of dislocation climb based on climb over second phase particles are inadequate, for they predict strengthening which is three orders of magnitude too small [31,32]. Finally, the theories of composite strengthening proposed by Arsenault et al. [34-42] based on an increased dislocation density and reduced subgrain size cannot be applied, for the increase in the dislocation density is too small and the change in subgrain size is not large enough. Therefore, an entirely new approach to causes of strengthening will have to be considered.

5. Conclusions

From a consideration of the data, there are several conclusions which we can arrive at. First, in regard to the NiAl matrix:

(1) There are other particles present within the matrix and it could be as high as 10 V%,

(2) The Burgers vector is a {100} type with no defined slip plane,

(3) Deformation at low strain rates results in no large change in dislocation densities; at higher strain rates, shear bonds are observed in the 0 V% TiB_2/NiAl.

Second, in regard to the TiB_2 NiAl composites:

(1) There is heterogeneous distribution of dislocations in the TiB_2/NiAl deformed samples,

(2) TiB_2 are deformed,

(3) At present, a strengthening mechanism is not obvious.

Acknowledgement

This research was supported by the Office of Naval Research under contract No. N00014-K-85-0007. The positive interactions with Dr. S. Fishman of the Office of Naval Research are to be greatly acknowledged. The authors wish to acknowledge the assistance

of Dr. S.B. Wu in the performance of the high temperature compression tests. The authors wish to acknowledge the continued support of the Argonne National Laboratory HVEM facility, especially, Dr. E. Ryan.

References

1. J.H. Westbrook, *J. Electrochem. Soc. 103* (1956) 54.

2. E.M. Grala, *Investigations of NiAl and Ni_3Al in Mechanical Properties of Intermetallic Compounds*, (ed.) J.H. Westbrook, J. Wiley, New York, NY, 1960 pp. 358-404.

3. E.P. Lautenschlager, D.A. Kiewit and J.O. Brittain, *Trans. Metall. Soc. AIME 233* (1965) 1297.

4. A.G. Rozner and R.J. Wasilewski, *J. Inst. Metals 94* (1966) 169.

5. A. Ball and R.E. Smallman, *Acta Metall. 14* (1966) 1349.

6. R.R. Vandervoort, A.K. Mukherjee and J.E. Dorn, *Trans. ASM 59* (1966) 930.

7. R.T. Pascoe and C.W.A. Newey, *Metall. Sci. J. 2* (1968) 138.

8. P.R. Strutt, R.A. Dodd and G.M. Rowe, *Creep in Stoichiometric NiAl*, Second Int. Conf. on the Strength of Metals and Alloys, III, ASM, Metals Park, OH, 1971 pp. 1057-61.

9. W.J. Yang and R.A. Dodd, *Metall. Sci. J. 7* (1973) 41.

10. L.A. Hocking, P.R. Strutt and R.A. Dodd, *J. Inst. Metals 99* (1971) 98.

11. J. Bevk, R.A. Dodd and P.R. Strutt, *Met. Trans. 4* (1973) 159.

12. H.L. Fraser, R.E. Smallman and M.H. Loretto, *Phil. Mag. 28* (1973) 651.

13. E.M. Schulson and D.R. Barker, *Scripta Metall. 17* (1983) 519.

14. J.D. Whittenberger, *Mater. Sci. Eng. 57* (1983) 77.

15. J.D. Whittenberger, *Mater. Sci. Eng. 73* (1985) 87-96.

16. W.R. Kanne, Jr., P.R. Strutt and F.A. Dodd, *Trans. AIME 245* (1969) 1259.

17. R.T. Pascoe and C.W.A. Newey, *Metall. Sci. J. 5* (1971) 50.

18. G.F. Hancock and B.R. McDonnell, *Phys. Status solidi (a) 4* (1971) 143.

19. A.E. Berkowitz, F.E. Jaumot, Jr. and F.C. Nix, *Phys. Rev. 95* (1954) 1185.

20. A. Lutze-Birk and H. Jacobi, *Scripta Metall. 9* (1975) 761.

21. S. Shankar and L.L. Siegle, *Metall. Trans. A 9A* (1978) 1467.

22. A. Lasalmonie, *J. Mater. Sci. 17* (1982) 2419.

23. E.P. Lautenschalager, T.C. Tisone and J.O. Brittain, *Phys. Status Solidi 20* (1967) 443.

24. O.D. Sherby, R.H. Klundt and A.K. Miller, *Metall. Trans. A. 8A* (1977) 843.

25. J.D. Whittenberger, *Mater. Sci. Eng. 77* (1986) 103.

26. J.D. Whittenberger, *J. Mater. Sci. 22* (1987) 394.

27. R.R. Jensen and J.K. Tien, *Metall. Trans. 16A* (1985) 1049.

28. R.W. Guard and A.M. Turkalo, *Mechanical Properties of Intermetallic Compounds*, (ed.) J.H. Westbrook, John Wiley, New York, NY, 1960, p. 141.

29. Unpublished investigation, University of Maryland.

30. M. Taya and L. Lilholt, to be published.

31. J.H. Hassenlet and W. Nix, *Acta. Metall. 25* (1977) 595.

32. W. Blum and B. Reppich, *Creep Behavior of Crystalline Solids*, (ed.) B. Wilshire and R. Evans, Pineridge Press, 1985, p. 85.

33. F.J. Humphreys and P.B. Hirsch, *Fourth Int. Conf. on Strength of Metals and Alloys 1*, 1976, p. 204.

34. R.J. Arsenault, *Mater. Sci. Eng. 6* (1984) 171.

35. R.J. Arsenault and M. Taya, *Acta Metall. 35* (1987) 651.

36. M. Vogelsang, R.J. Arsenault and R.M. Fisher, *Metall. Trans. 17A* (1986) 379.

37. R.J. Arsenault and S.B. Wu, *Mater. Sci. Eng. 96* (1987) 77.

38. R.J. Arsenault and N. Shi, *Mater. Sci. Eng. 81* (1986) 175.

39. Y. Flom and R.J. Arsenault, *Mater. Sci. Eng. 75* (1985) 151.

40. Y. Flom and R.J. Arsenault, *Mater. Sci. Eng. 77* (1986) 191.

41. M. Taya and R.J. Arsenault, *Scripta Metall. 21* (1987) 349.

42. R.J. Arsenault, *J. Comp. Tech. Res. 10* (1988) 140.

Fig. 19 Transmission electron microscope micrograph of the same area as in Fig. 17, except deformed end of TiB_2 particle with a practically dislocation-free area surrounding matrix.

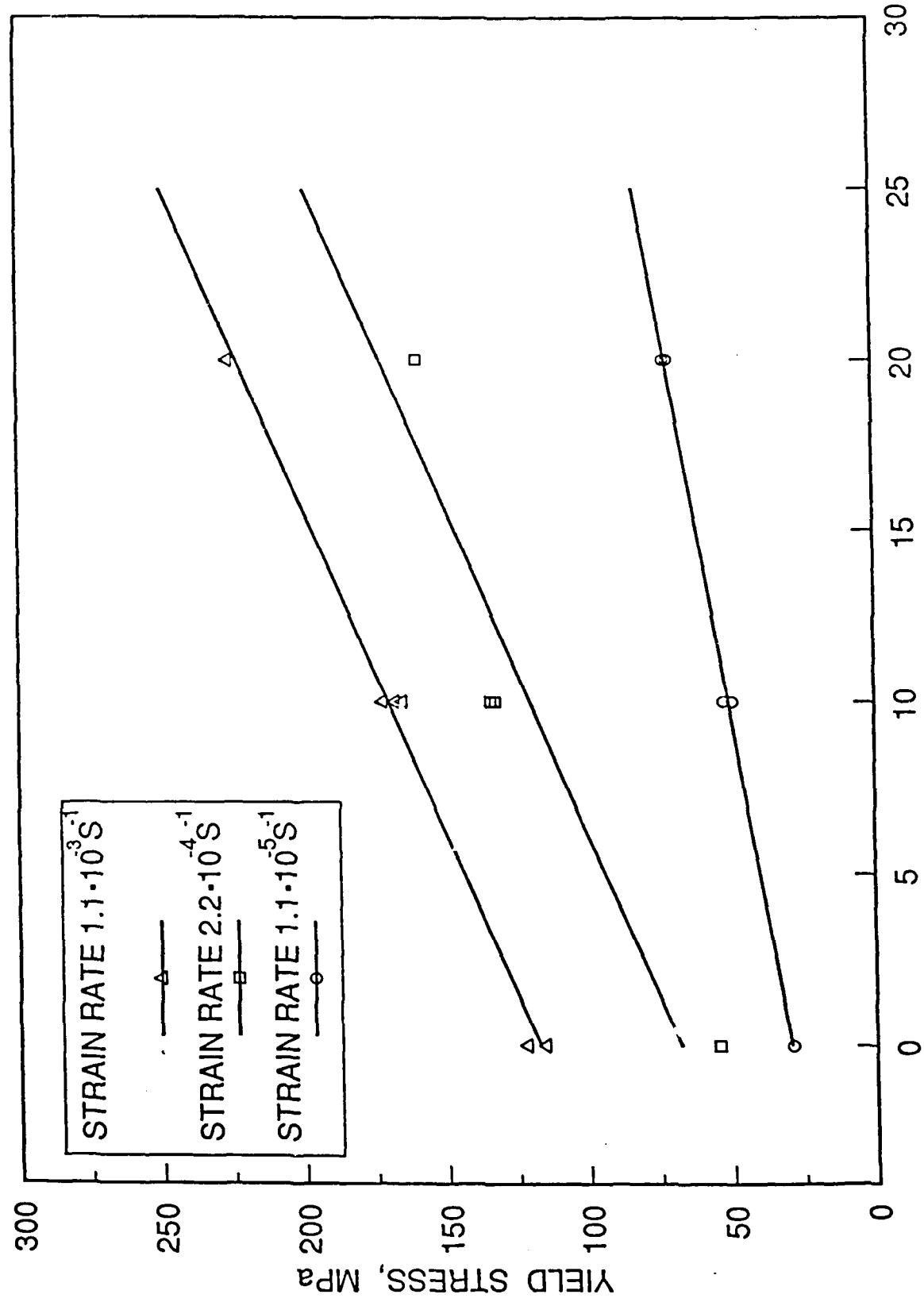

Fig. 1 The yield stress of TiB_2/NiAl composites as a function of strain rate and volume fraction of TiB_2/NiAl sample.

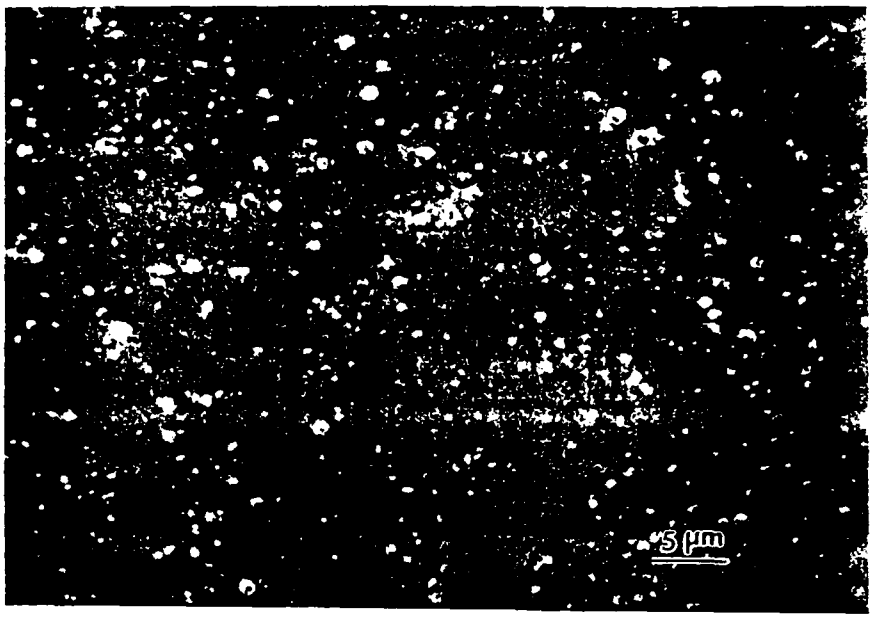

Fig. 2 Scanning electron microscope micrograph of 0 V% TiB_2/NiAl sample.

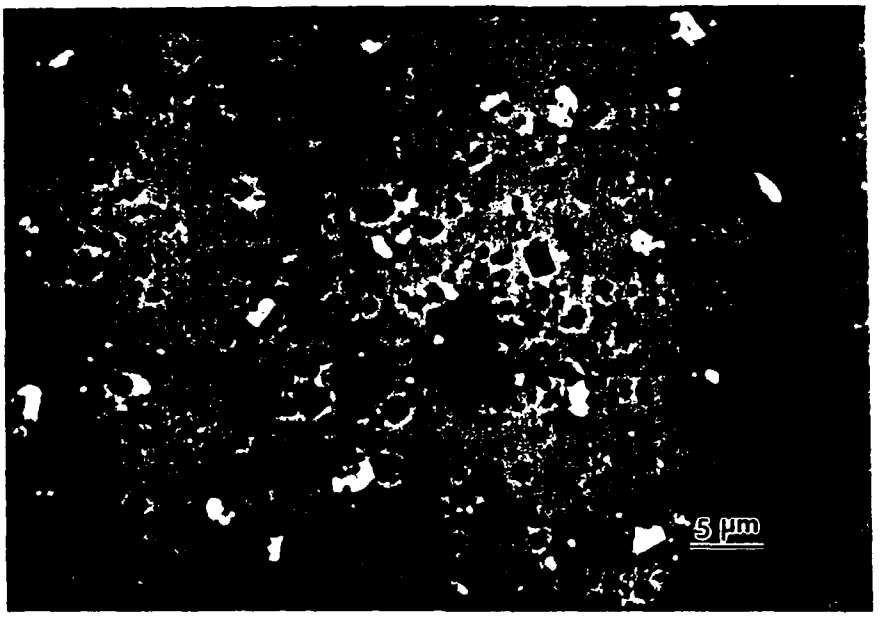

Fig. 3 Scanning electron microscope micrograph of 10 V% TiB_2/NiAl sample.

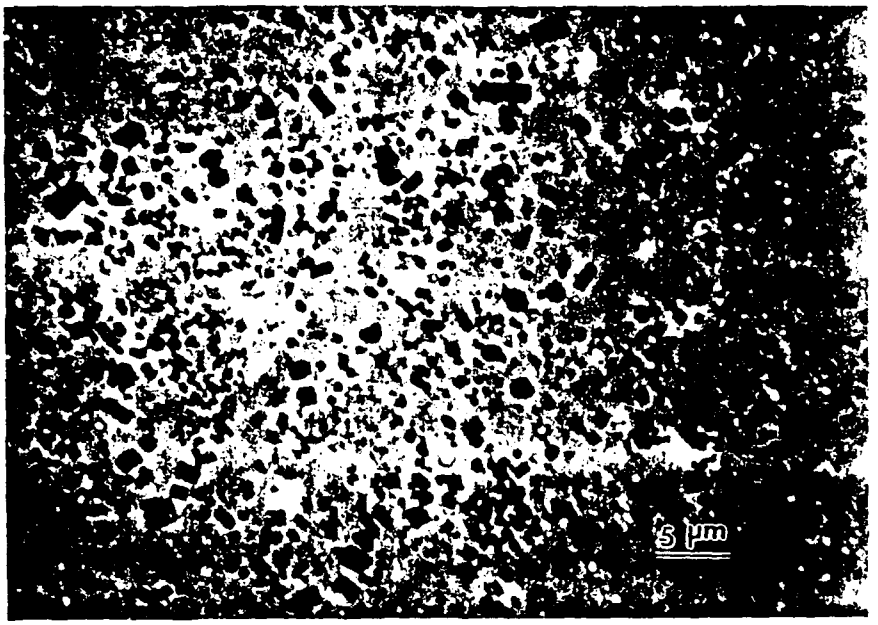

Fig. 4 Scanning electron microscope micrograph of 20 V% TiB_2/NiAl sample.

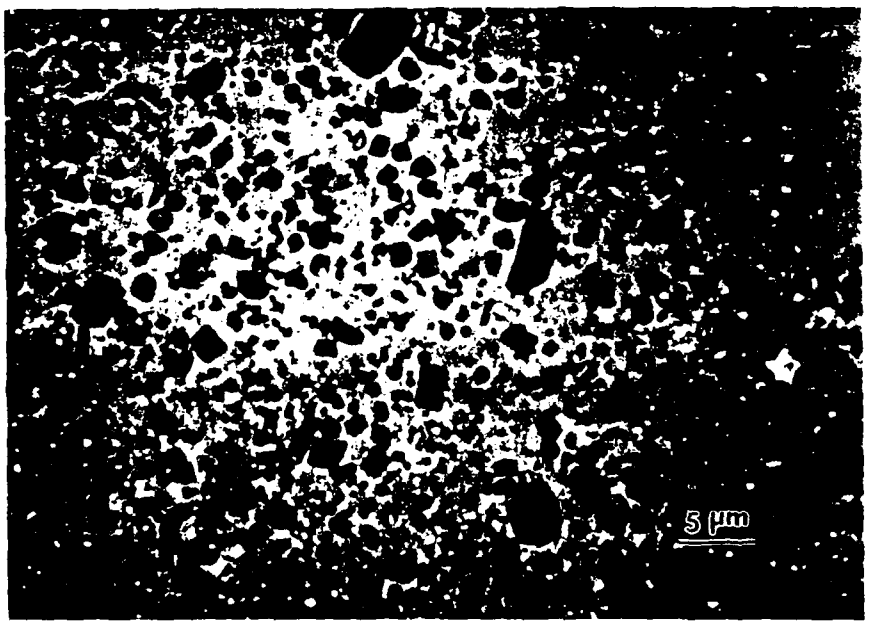

Fig. 5 Scanning electron microscope micrograph of 30 V% TiB_2/NiAl sample.

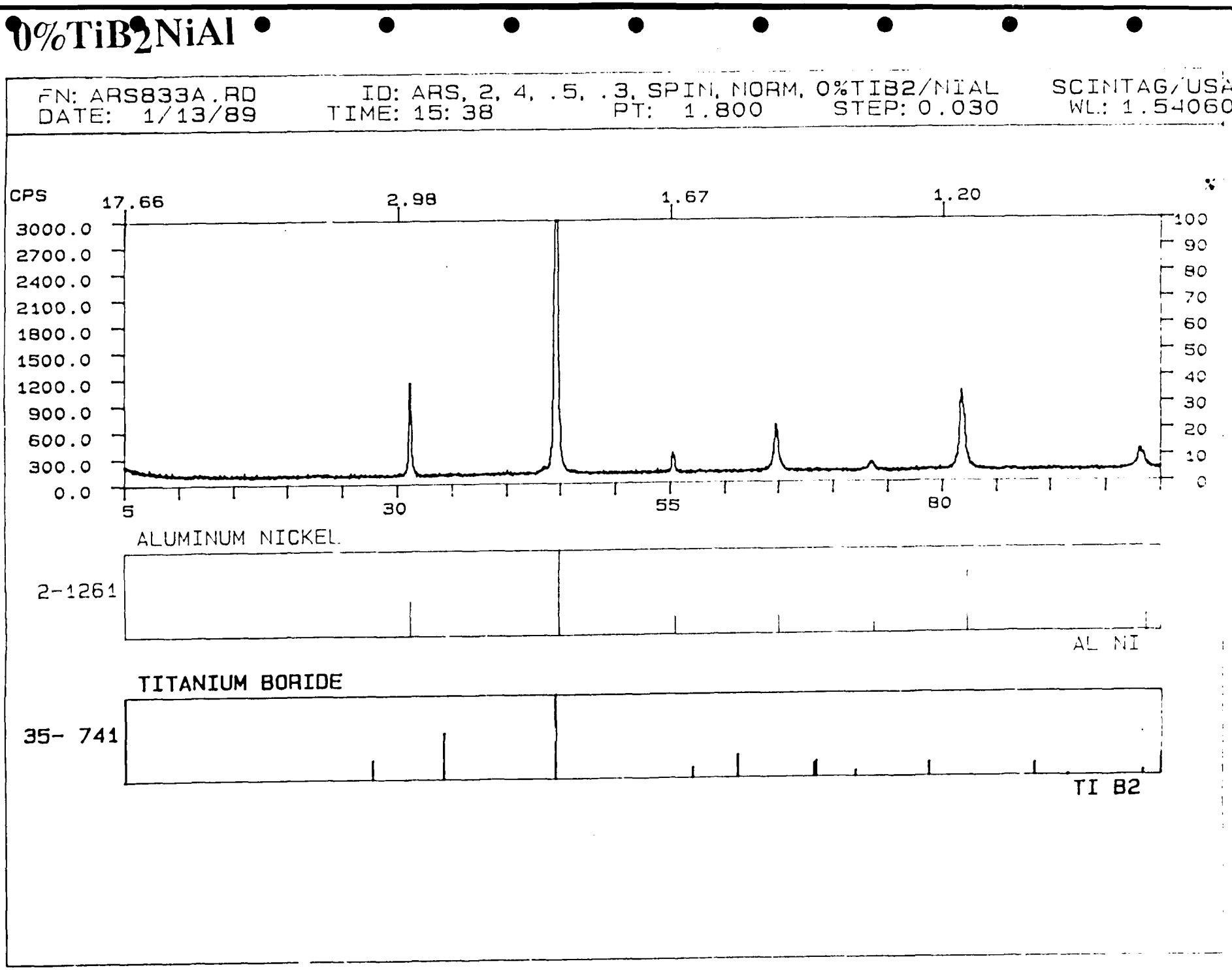

Fig. 6 X-ray powder diffraction pattern obtained from 0 V% TiB_2/NiAl powder sample.

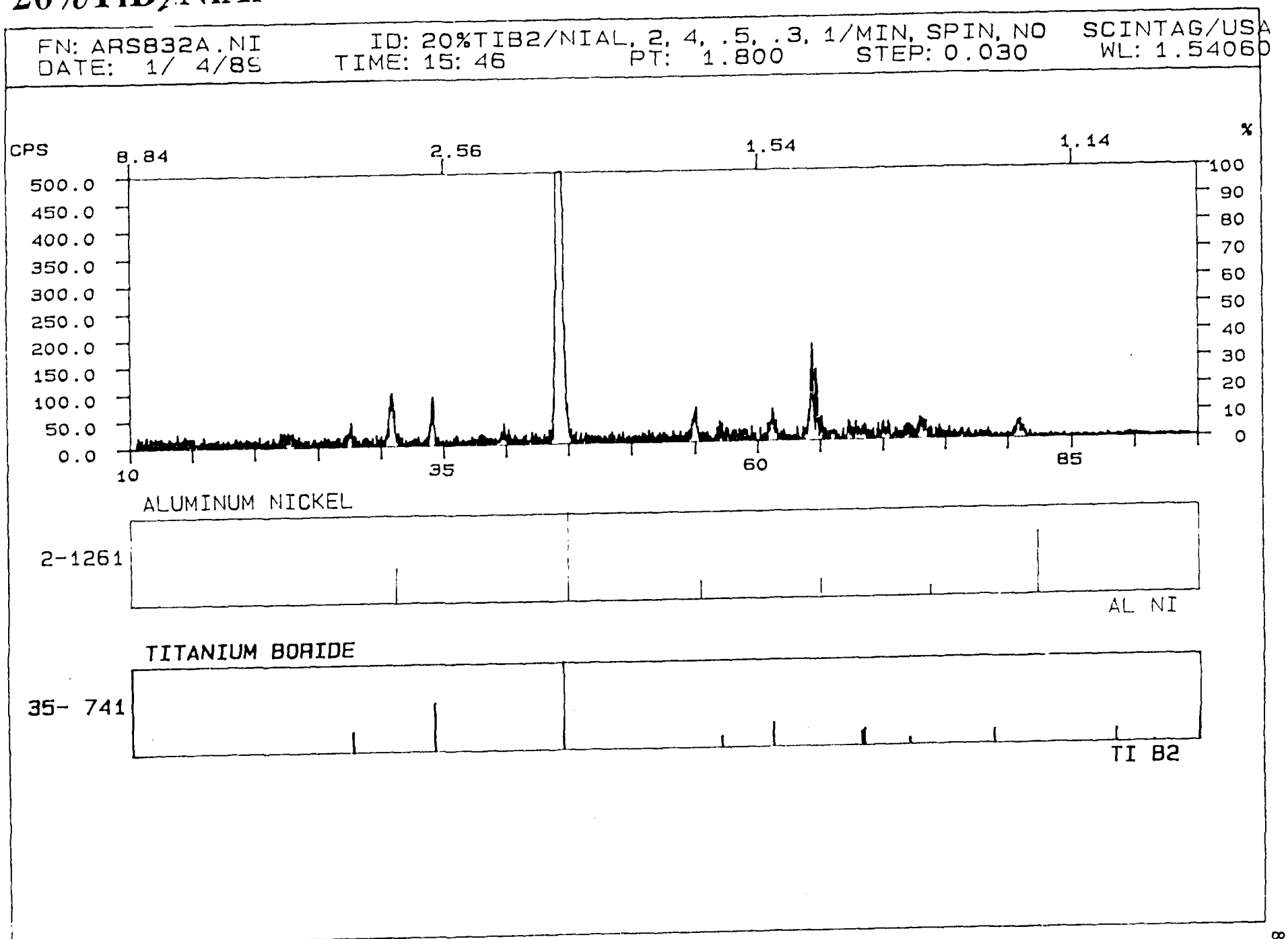

Fig. 7 X-ray powder diffraction pattern obtained from 20 V% TiB_2/NiAl powder sample.

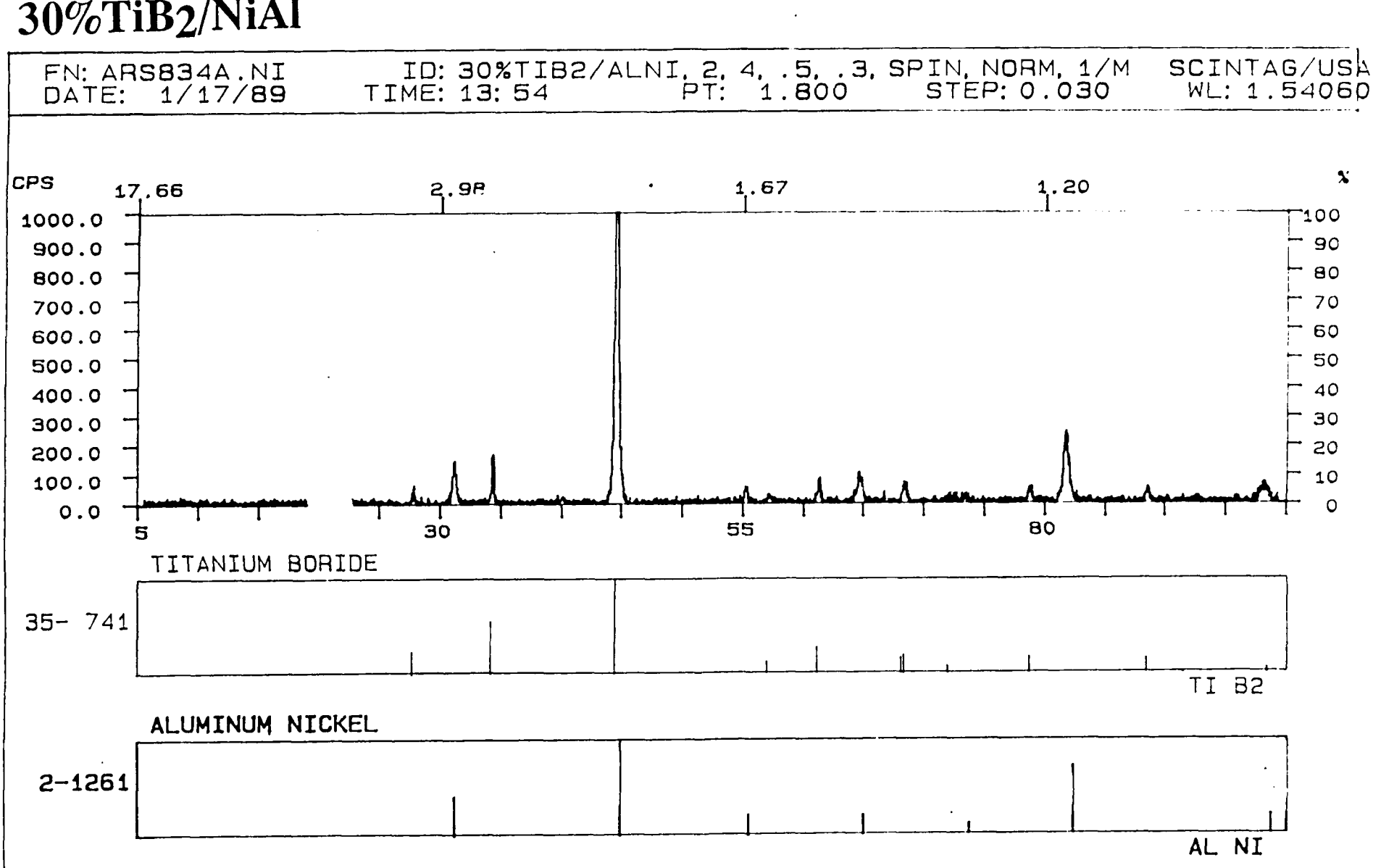

Fig. 8 X-ray powder diffraction pattern obtained from 30 V% TiB_2/NiAl powder sample.

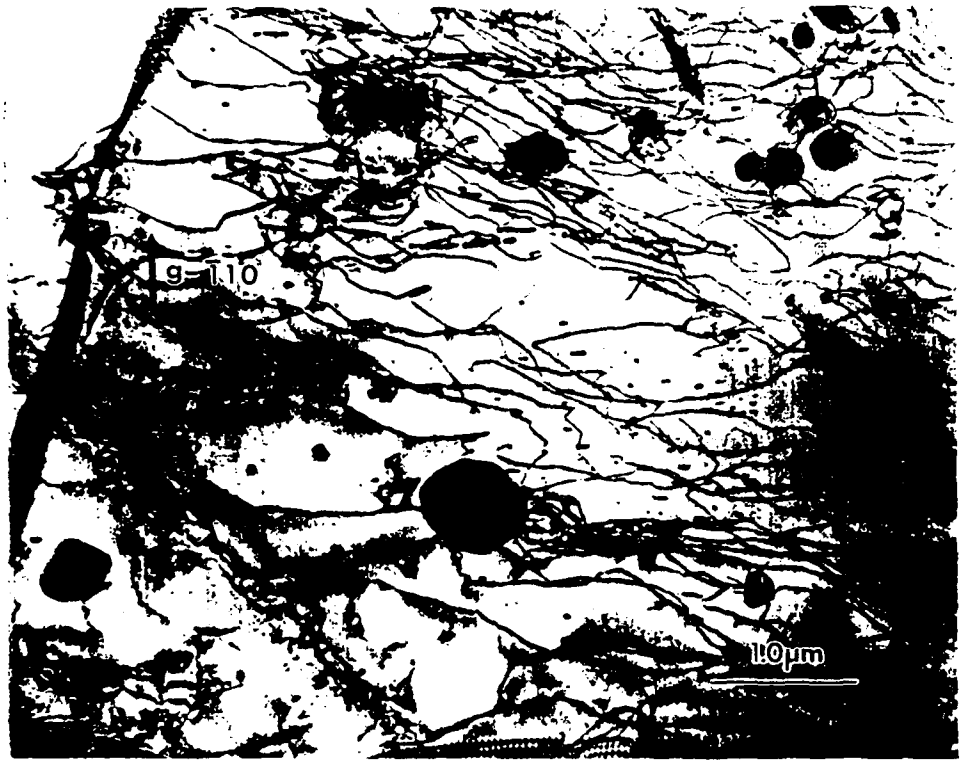

Fig. 9 Transmission electron microscope micrograph of 0 V% TiB_2/NiAl sample, 30% deformed, most of the dislocation having Burger's vector of a[100].

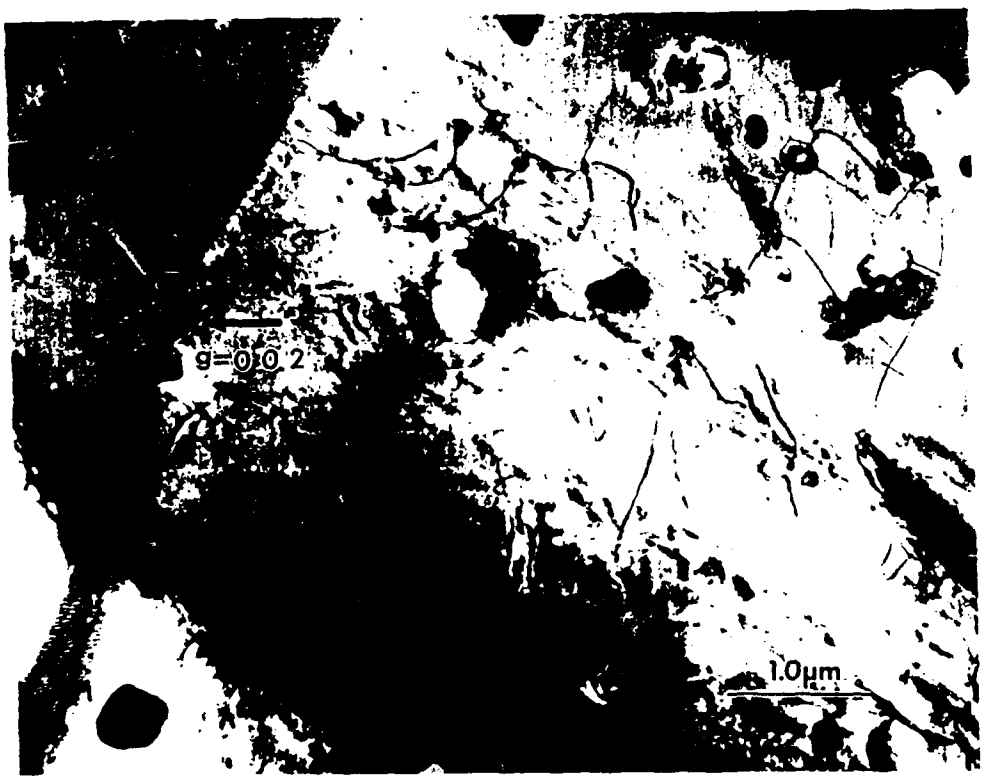

Fig. 10 Transmission electron microscope micrograph of 0 V% TiB_2/NiAl sample, 30% deformed, most of the dislocation having Burger's vector of a[100].

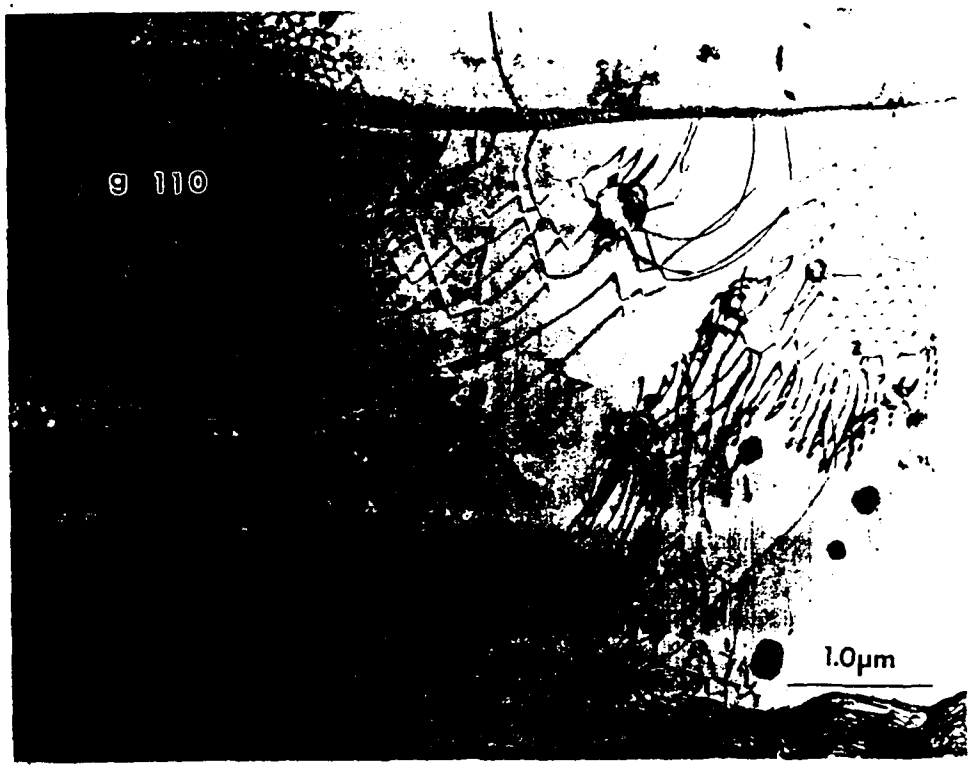

Fig. 11 Transmission electron microscope micrograph of 0 V% TiB_2/NiAl sample, 30% deformed. Networks formed by reactions of [100]+[010]=[110] and[010]+[001]=[011].

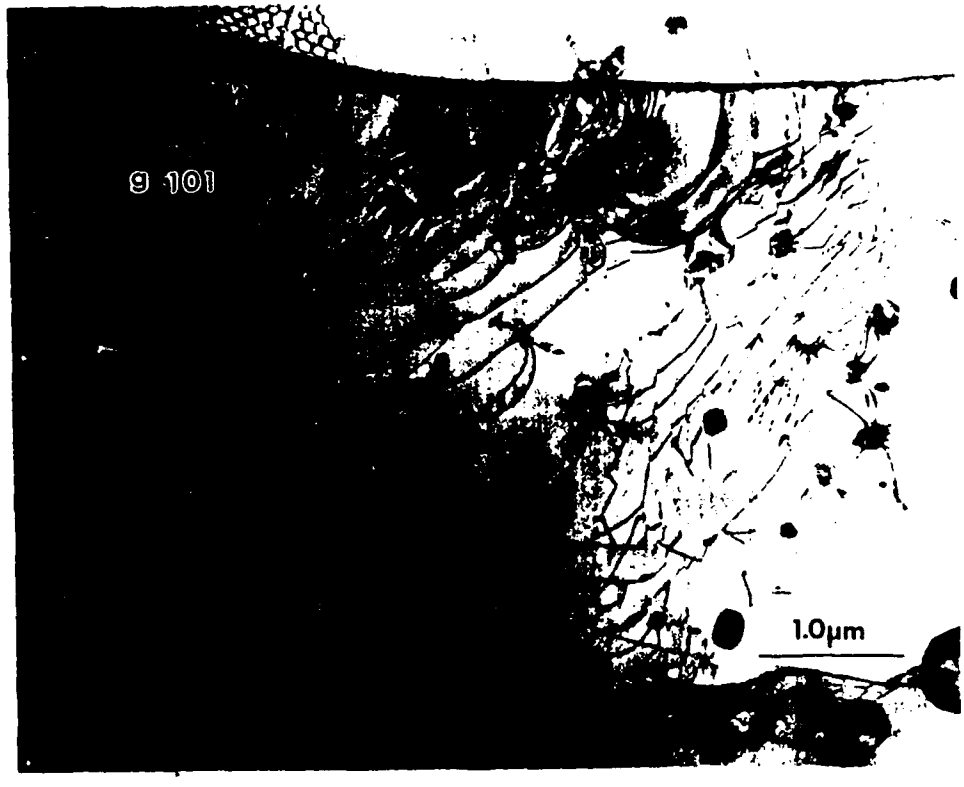

Fig. 12 Transmission electron microscope micrograph of 0 V% TiB_2/NiAl sample, 30% deformed. Networks formed by reactions of [100]+[010]=[110] and[010]+[001]=[011].

Fig. 13 Schematic illustration for convoluted shaped dislocations.

Fig. 14 Transmission electron microscope micrograph of 0 V% TiB_2/NiAl sample, 30% deformed. Shear bond structure.

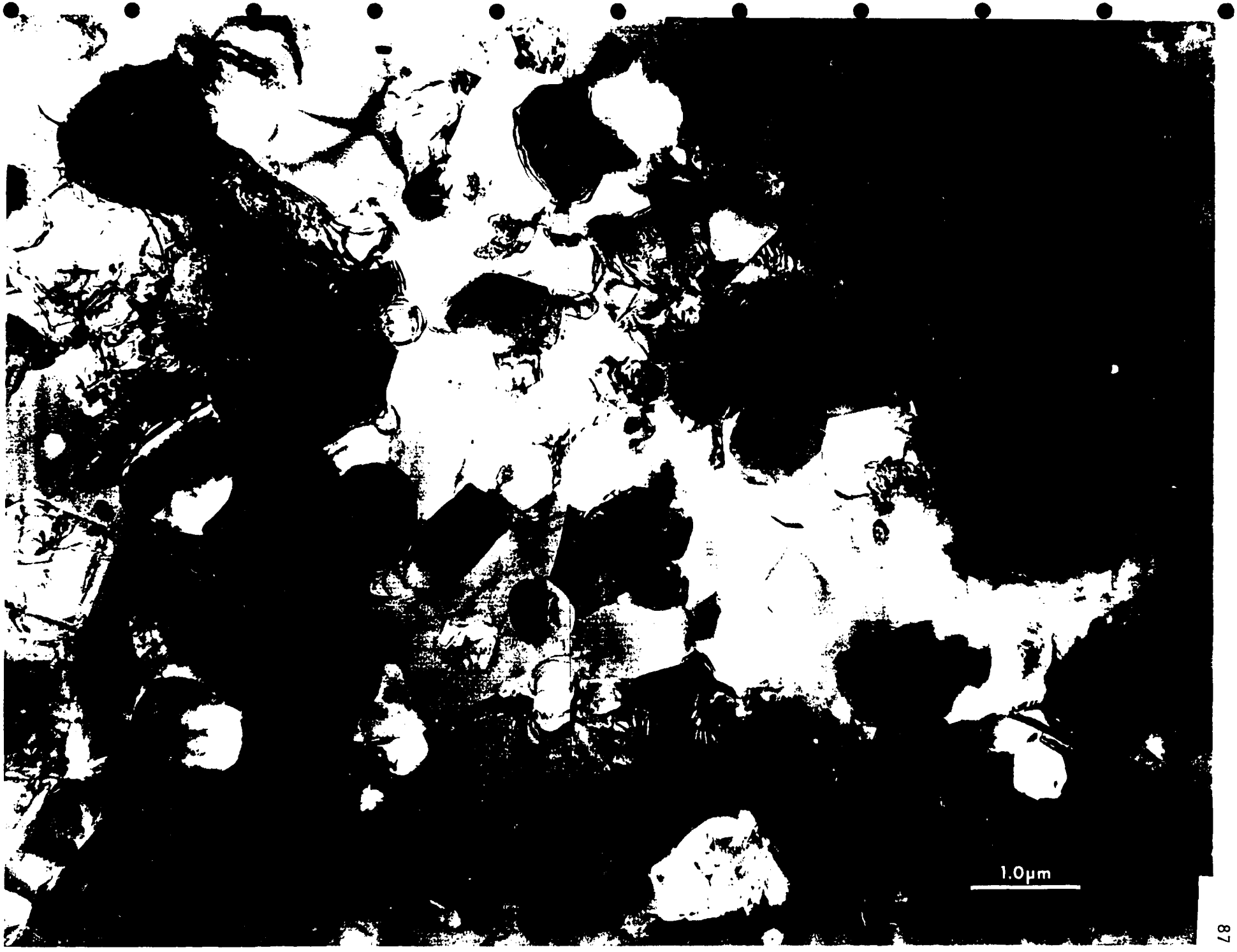

Fig. 15 Transmission electron microscope micrograph of 20 V% TiB_2/NiAl sample, 30% deformed.

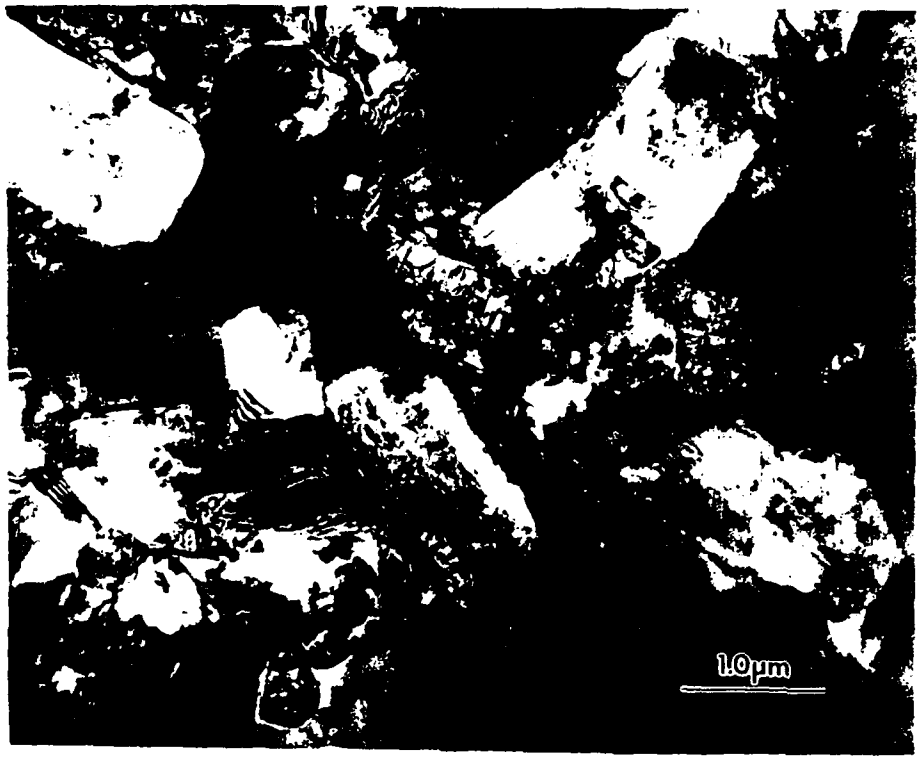

Fig. 16 Transmission electron microscope micrograph of 20 V% TiB_2/NiAl sample, 30% deformed. Highly concentrated TiB_2 area.

Fig. 17 Transmission electron microscope micrograph of 20 V% TiB_2/NiAl sample, 30% deformed. Low concentrated TiB_2.

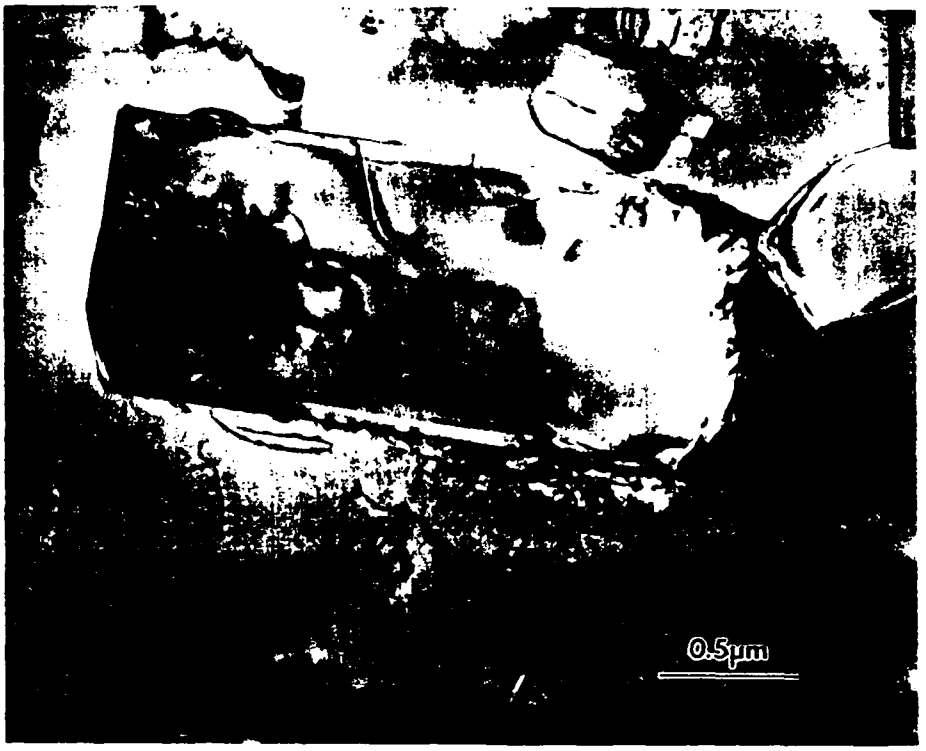

Fig. 18 Transmission electron microscope micrograph of 20 B% TiB_2/NiAl sample, 30% deformed. Not uniformly deformed TiB_2 particle. Deformed matrix always in contact with the dislocation-free end of the TiB_2 particle.

Fig. 19 Transmission electron microscope micrograph of the same area as in Fig. 17, except deformed end of TiB_2 particle with a practically dislocation-free area surrounding matrix.

Dislocations in Titanium Diboride*

L. Wang and R.J. Arsenault

Metallurgical Materials Laboratory, University of Maryland, College Park, MD 20742

ABSTRACT

In this investigation, it was shown that titanium diboride would plastically deform at temperatures of 1300 K and at a stress level much lower than predicted by previous experimental data. The crystal structure of titanium diboride is a topologically hexagonal structure which allows for a number of possible slip systems. Experimentally, it was observed that three slip directions were present; [0001], $<2\bar{1}\bar{1}0>$ and $<2\bar{1}\bar{1}1>$. The probable slip planes are (0001), $\{10\bar{1}0\}$ and $\{10\bar{1}1\}$.

§ 1. INTRODUCTION

Titanium diboride (TiB_2) is an interesting material. It has a high temperature strength which is greater than other ceramics such as silicon carbide (SiC) and aluminum oxide (Al_2O_3) (Ramberg and Williams 1987). Also, TiB_2 is a reinforcement candidate in high temperature composite for it is inert with respect to potential matrix materials. One of the composite sy .is which has received some attention is TiB_2 in nickel aluminide (NiAl) (Wang and Arsenault 1989). It was found that the addition of 30 volume percent particulate TiB_2 resulted in a five-fold increase in the yield stress at 1300 K. The reason why this increase occurs is not evident.

A microstructural investigation was undertaken of these composites to determine the effect of the addition of TiB_2 on the dislocation arrangement and density within the NiAl matrix. It was assumed that the TiB_2 did not deform at 1300 K, for the yield stress at 1300 K which is obtained by a lower limit extrapolation would be 2000 MPa. The stress concentration in the TiB_2 that could occur due to load transfer would not be large enough

* This research was supported by the Office of Naval Research under contract No. N00014-85-K-0007.

to cause yielding of TiB_2 at 1300 K. However, it should be pointed out that the TiB_2 used by Ramberg and Williams (1987) contained titanium carbide (TiC) precipitates.

In the investigation of dislocation configuration and density (Wang and Arsenault 1989) in the NiAl matrix of TiB_2/NiAl composites deformed at 1273 K, it was observed that there was a high density of dislocations within TiB_2 particles. Therefore, a question arose as to what type of dislocations are within the TiB_2 particles. There appears to be a large number of possibilities.

Nakaro, Imura and Takenchi (1973) and Nakaro, Matsubar and Imura (1974) in an investigation of the high temperature hardness of TiB_2 concluded that the primary slip system was $\{1010\}<\bar{1}2\bar{1}0>$. However, Ramberg and Williams proposed two other systems $\{10\bar{1}0\}[0001]$ and $(0001)<10\bar{1}0>$.

The reason that so many possibilities exist is related to the crystal structure of TiB_2 which is schematically shown in fig. 1. The crystal structure could be defined as a topologically hexagonal structure (Parthe 1967), in which the boron atoms form a net connection only. For the case of packing of touching spheres (Laves 1956), the ideal c/a = 1.07, and the c/a = 1.063 for TiB_2. From an examination of fig. 1, it is evident that there is no well defined close packed plane, but the closest packed plane is (0001) and the shortest repeat distance in this plane is $[11\bar{2}0]$.

The purpose of the present investigation was to determine if an increase in dislocation density did indeed occur upon deformation of the TiB_2/NiAl composite, and to characterize the various types of dislocation Burgers vectors that were assumed to be present in the TiB_2 particles within the deformed TiB_2/NiAl composite.

§2. MATERIALS AND EXPERIMENTAL PROCEDURES

The TiB_2/NiAl composite used in this investigation was purchased from Martin Marietta Corporation. The composite contained 10 or 20 volume percent TiB_2 and the TiB_2 particles were of various shapes and size, but on average, the largest dimension was

3 μm.

Prior to testing, the compression samples with a length to diameter ratio of 2 were annealed at 1273 and 1673 K for periods of time of 2-12 hours. Variation in annealing times had no effect on the strength of the composite. Surprisingly, annealing at 1673 K resulted in a slight increase in strength. They were tested at 1273 K at various strain rates (details of the testing are given elsewhere (Wang and Arsenault 1989). The transmission electron microscopy (TEM) foils were obtained from the deformed composite samples and examined at both 100 kV and 1 MeV. Further details of the foil preparation are given elsewhere (Wang and Arsenault 1989). Since it is assumed that there will be a large number of possible Burgers vectors, it is necessary to use a number of operating diffraction vectors. However, if the relative intensity of the operating diffraction vector is so low, then the dislocations would be in very low contrast. Therefore, all micrographs in this paper were taken under operating conditions where the relative intensity is large enough to show the difference between the residue contrast of invisible dislocations and the image of visible dislocations.

§3. RESULTS AND DISCUSSION

The initial portion of the investigation was to determine if the dislocation density within the TiB_2 increased as a result of deformation of the composite. In annealed samples, there is low dislocation density both in the matrix and TiB_2, as shown in Fig. 2(a), except in the case where some of the particles are in contact with each other. A comparison of TEM micrographs of annealed samples and deformed samples clearly shows that density of dislocation within the TiB_2 is significantly higher in the deformed composite sample, as shown in figures 2(a) and 2(b).

It was found that straight edges of a TiB_2 particle were almost always parallel to the (0001) plane. The dislocations labeled A and B do not lie on the plane of the foil, but lie on a plane which is parallel to the bottom edge of the particle. In other words, dislocations A

& B lie on the (0001) plane which is perpendicular to the plane of the foil. Under conditions of 0001 and $\bar{2}0\bar{2}1$ operating diffractions, dislocations labeled A in fig. 3(a) are almost completely invisible. Therefore, the A-labeled dislocations have Burgers vectors of $a[1\bar{2}10]$. Dislocations labeled B in fig. 3(a) and 3(c) which are only invisible under the operation diffraction 0001 has a Burgers vector of $a[\bar{2}110]$ or $a[11\bar{2}0]$.

If the electron beam is exactly parallel to the basal plane, then the projection of dislocation on the basal plane should be straight lines. However, there are exceptions if climb occurs as indicated by the arrow in fig. 3(a). Also, it has been found that stacking faults exist on the basal plane in TiB_2 (Merso, Lynch and Vahldiek 1968) Again, if the electron beam is parallel to the basal plane as in fig. 4(a), the dislocation on the basal plane should project as a straight line labeled A. If the sample is tilted as shown in fig. 4(b), then stacking fault ribbons are evident. The presence of stacking faults is not universal, only a few TiB_2 particles contained stacking faults.

It is suspected that prism slip also occurs and that prismatic punching into the TiB_2 particles from the interface occurs, i.e. the dislocations labeled C in figs. 5(a) and 5(b). If different operation diffractions are used ($\bar{1}010$ and $\bar{2}110$), then prismatically punched dislocations become invisible (figs. 5(c) and 5(d), in areas that the Burgers vector of prismatically punched dislocations is c[0001].

There are dislocations with other Burgers vectors within this particle. The dislocations labeled E in figs. 5(a) and 5(c) are out of contrast under the diffraction vector 0001 [fig. 4(d)]. The dislocations which have Burgers vectors of $<\bar{2}110>$ obviously do not lie on the basal plane. Therefore, it is possible that slip directions of the $<\bar{2}110>$ type can occur on other slip planes.

Besides dislocations with Burgers vectors of $<\bar{2}110>$ and [0001], there are still other dislocations with different Burgers vectors, for example, the dislocations labeled D in fig. 5. It was difficult experimentally to find extinction conditions for these dislocations. Every operating diffraction condition was employed which had a required intensity in the

$(1\bar{2}10)^*$, $(\bar{0}110)^*$, $(0\bar{1}11)^*$ and $(1\bar{2}13)^*$ reciprocal planes. Not one of these operating diffraction conditions could make dislocations labeled D invisible. It is possible to obtain the Burgers vector of dislocations labeled D by considering the dislocation reaction which occurs at the arrow in fig. 5(b), (c) and (d). Dislocations labeled A which have a Burgers vector $[\bar{2}110]$, reacted with dislocation labeled D which results in the short segment of dislocation indicated by the arrow in these pictures.

This short segment of dislocations has a Burgers vector [0001], for it followed the same extinction conditions as the dislocation labeled C which has a Burgers vector of [0001]. Therefore, the reaction can be written as

$$b_A + b_D = b_C$$

The subscripts denote the dislocations labeled in fig. 5. Since b_A is $[\bar{2}110]$ and b_c is [0001], then the dislocations labeled D must have a Burgers vector of the type $<\bar{2}111>$. The reason why it is so difficult to find extinction conditions for these is that only $0\bar{1}10$ diffractions satisfy extinction conditions and the intensity requirement mentioned above.

The possible combinations of slip directions and slip planes are listed in Table 1. The three directions were determined in this investigation, and the planes listed are the three of highest atomic packing.

§4. CONCLUSIONS

From the data obtained in this investigation, it is possible to arrive at the following conclusions.

- The TiB_2 particles within a deformed TiB_2/NiAl composite can be plastically deformed as evidenced by the increased dislocation density within the TiB_2 particles.
- Three slip directions were observed within the TiB_2 particles; they are $<\bar{2}110>$, [0001] and $<\bar{2}111>$.
- Dislocations with Burgers vectors of the type $<\bar{2}110>$ on the basal plane could split

into two particles with a stacking fault between the particles.

- Most of the dislocations in TiB_2 had Burgers vectors of [0001] or $<\bar{2}111>$.

ACKNOWLEDGEMENTS

The authors wish to acknowledge the continued encouragement of Dr. S. Fishman of the Office of Naval Research and the assistance of Dr. E. Ryan of the Argonne National Laboratory High Voltage Electron Microscopy Facility.

Table 1

Slip Systems in Titanium Diboride

	Slip planes		
Slip Directions	(0001)	$\{10\bar{1}0\}$	$\{10\bar{1}1\}$
[0001]		Yes	
$<\bar{2}110>$	Yes	Yes	Yes
$<\bar{2}111>$			Yes

REFERENCES

LAVES, F., 1956, "Theory of Alloy Phases," ASM, Cleveland, OH.

MERSOL, S.A., LYNCH, C.T. and VAHIDIEK, F.W., 1968, "Anistropy in Single-Crystal Refractory Compounds," Plenum, New York, 41.

NAKNO, Kikuo, IMURA, Toru and TAKENCHI, Shin, 1973, J. Appl. Phys. **12**, 186.

NAKNO, Kikuo, MATSUBAR, Hirom and IMURA, Toru, 1974, J. Appl. Phys. **13**, 1005.

PARTHE, Erwin, 1967, "Intermetallic Compounds[illegible] York, 212.

RAMBERG, J.R. and WILLIAMS, W.S., 1987, J. Mater. Sci. **22**, 1815.

WANG, L. and ARSENAULT, R.J., 1989, 11th Annual DMMC, Park City, UT.

WESTBROOK, J.H., 1967, "Intermetallic Compounds," John Wiley, New York, 138.

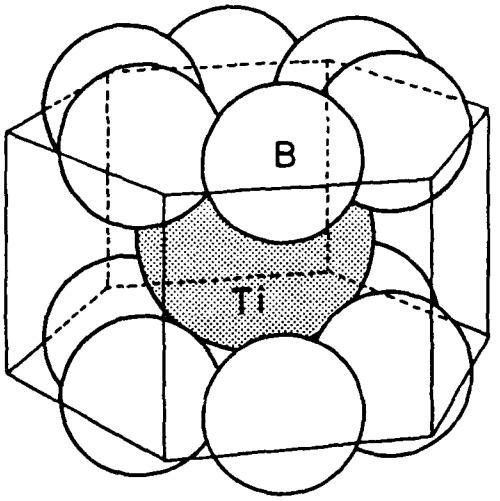

Fig. 1 Ball model of TiB_2. Boron atoms form a net connection only. Titanium atoms sit in the open center of the net. (Westbrook 1967).

Fig. 2(a) TEM micrograph of annealed 20 V% TiB_2/NiAl composite, low dislocation density both in matrix and TiB_2.

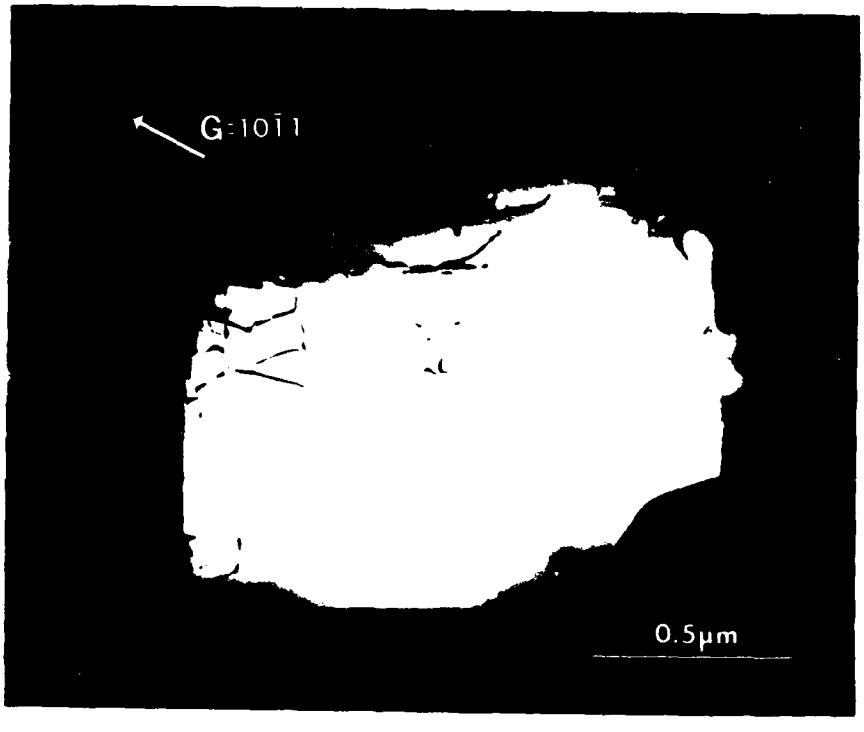

Fig. 2(b) TEM micrograph of a TiB_2 particle in annealed 20 V% TiB_2/NiAl composite.

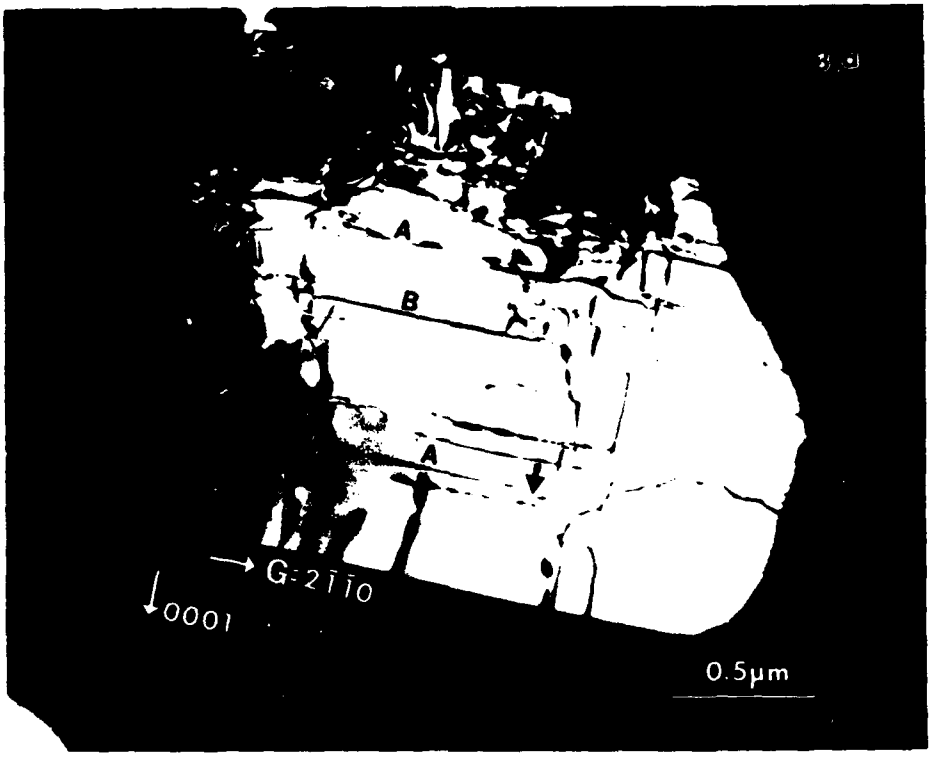

Fig. 3(a)

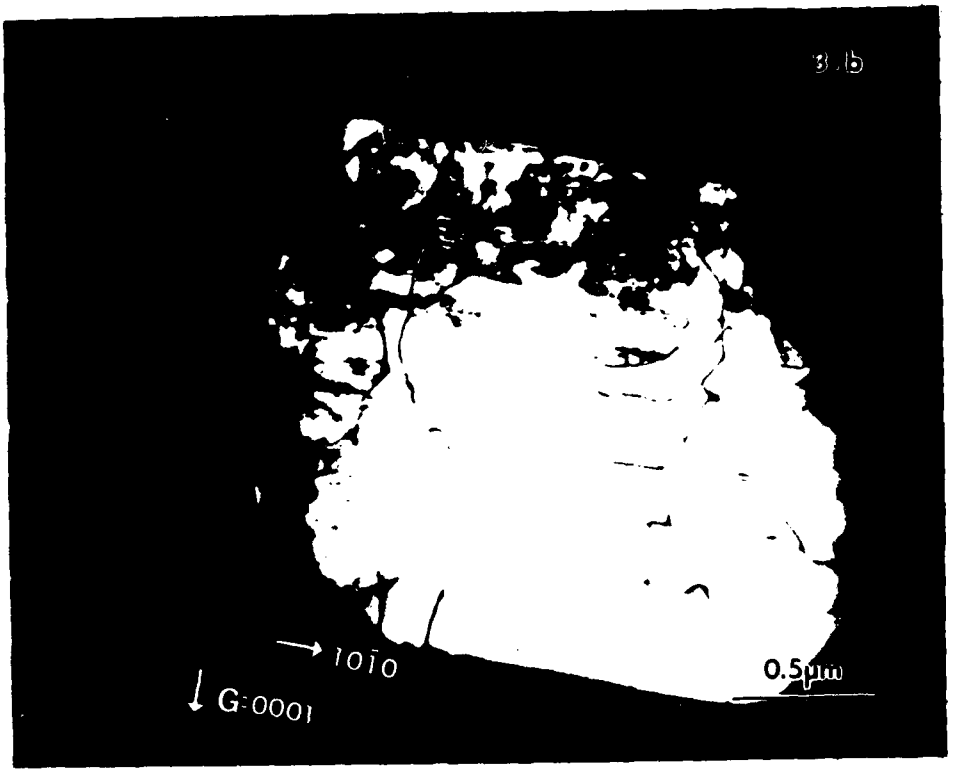

Fig. 3(b)

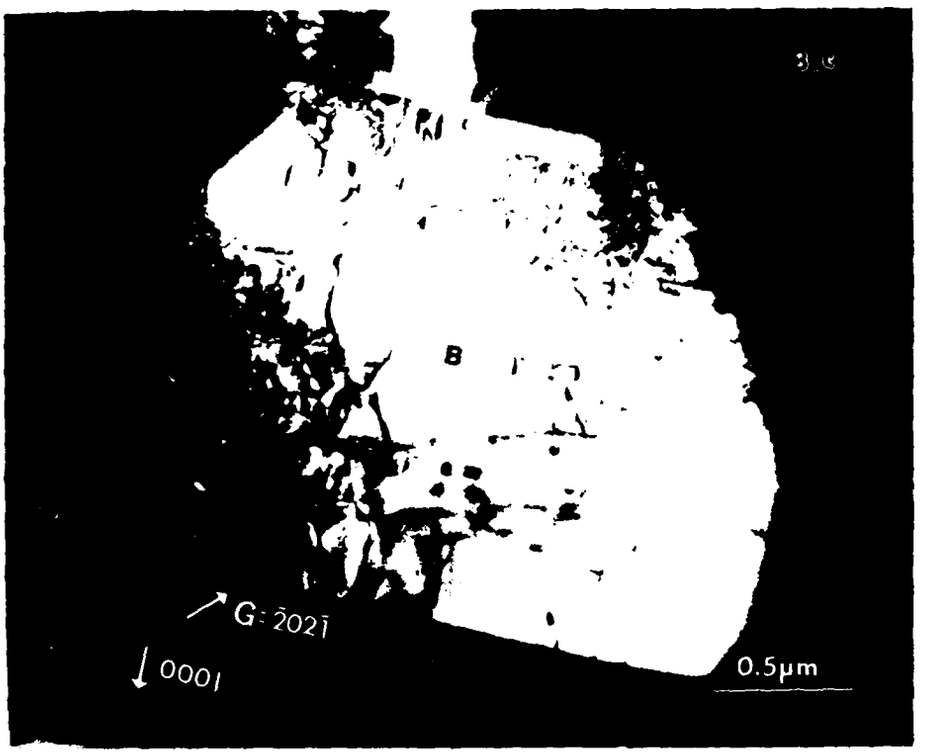

Fig. 3(c)

Fig. 3(a-c) TEM micrographs of a TiB_2 particle in deformed 20 V% TiB_2/NiAl composite with different operating diffractions, (a) dislocation with Burger's vector of a$<\bar{2}110>$ type on the basal plane are visible, (b) all a$<\bar{2}110>$ type dislocations are invisible, (c) only dislocations with Burger's vector of a$[1\bar{2}10]$ are invisible.

Fig. 4(a)

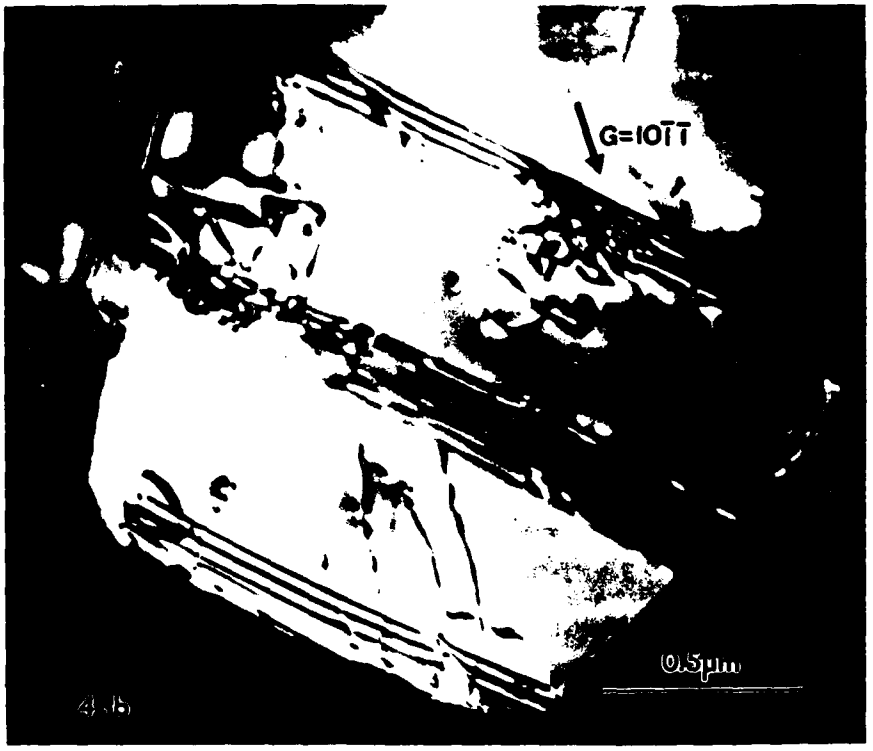

Fig. 4(b)

Fig. 4(a-b) TEM micrographs of a TiB_2 particle in deformed 20 V% TiB_2/NiAl composite. Stacking faults on the basal plane, (a) basal plane is parallel to the electron beam, (b) basal plane is not.


0001
10I0
E
E
D
E
D
A
C
C
C
C
C
C
C
0.5μm
5.a

Fig. 5(a)

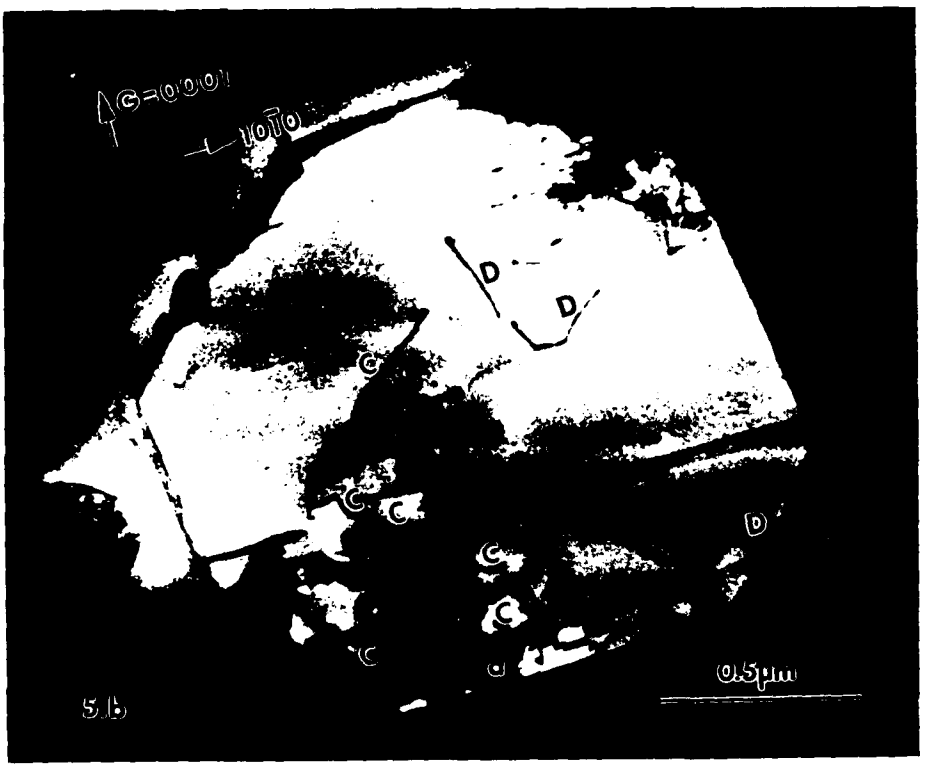
c-0001
10T0
D
D
C
C
C
C
C
C
D
0.5μm
5.b

Fig. 5(b)

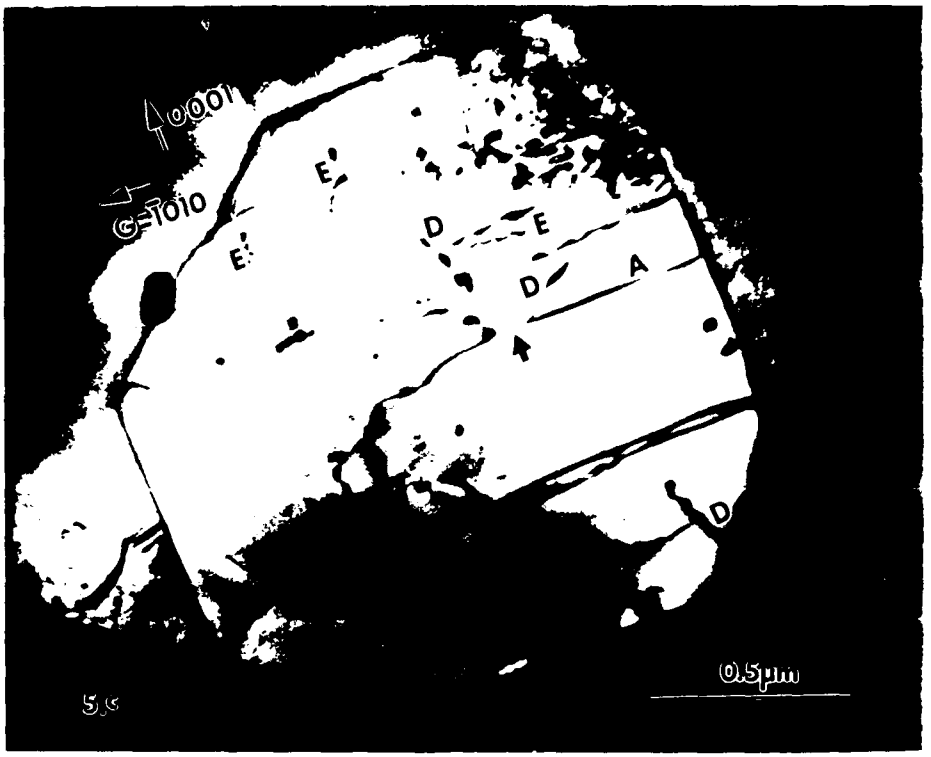

Fig. 5(c)

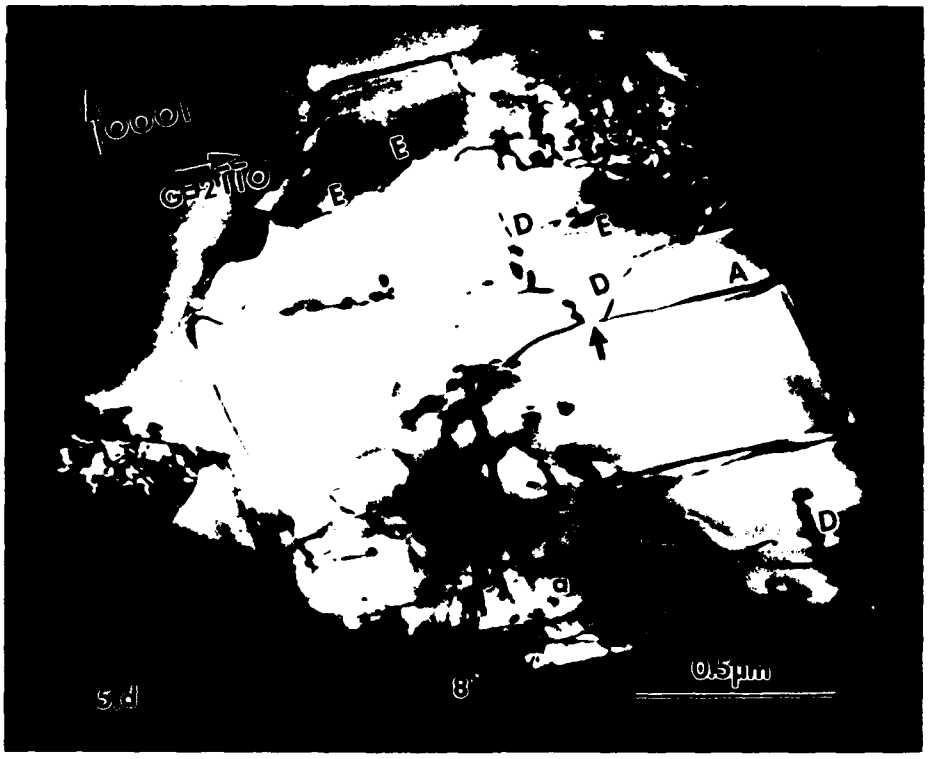

Fig. 5(d)

Fig. 5(a-d) TEM micrographs of a TiB_2 particle in deformed 20 V% TiB_2/NiAl composite, (a) many beams condition. All the dislocations are visible, (b) all of the $<\bar{2}110>$ type dislocations are invisible, (c) and (d) prismatically punched dislocation out of contrast.

LOCALIZED DEFORMATION OF SiC/Al COMPOSITES*

R.J. Arsenault, N. Cai, C.R. Feng and L. Wang
Metallurgical Materials Laboratory, University of Maryland, College Park, Maryland 20742-2115

Abstract

Tensile tests of SiC/6061 Al composites containing various volume fractions of whiskers or particulates (20, 5 and 0V%) showed that for high volume fraction samples (20 V%), the fracture process was very localized, i.e. a very narrow neck. As the volume fraction of whiskers or particles decreased, the deformed region spread out. One might expect that the microstructure should correspond to the macroscale changes. In the highly deformed region the dislocation density is expected to be higher, in the less deformed regions the dislocation density should be lower, and if the deformation is very localized, then the high dislocation density should also be limited to a very narrow region.

Overall, there is good agreement between the microstructure (dislocation density) change and the macroscale deformation of SiC/Al composite tensile samples. The mechanism proposal to account for this change in deformation behavior as a function of volume fraction of SiC in Al is related to the expansion of the plastic zone (due to differences in thermal coefficients of expansion between SiC and Al) when the external stress is applied. Also, the localized deformation is related to localized clusters of SiC particles. There is a cooperative effect which leads to a region of very localized plastic deformation.

1. Introduction

There are many unusual deformation characteristics of SiC/Al discontinuous metal matrix composites. Also, the ductility and fracture toughness of SiC/Al composites are very low [1]. Generally, examinations of the fracture surface do not reveal the presence of SiC particulates or whiskers in the quantities corresponding to their volume fraction [1]. The fracture process is very localized, very little "necking" is observed (in high volume fraction composites), but the fracture surface has both brittle and ductile characteristics. There is

---

* This research was supported by the Office of Naval Research under Contract No. N00014-85-K-0007.

no indication of fracture of SiC (when the size of SiC is less than 10 μm). The fracture may initiate at large intermetallic inclusions, clusters of SiC particulates or whiskers and voids associated with the SiC particulate or whiskers [1].

The results [2] of the tensile tests of SiC/6061 Al composites with various volume fractions of whiskers or particulates (20, 5 and 0 V%) indicated that for high volume fraction samples (20 V%) the fracture process was very localized. As the volume fraction of whiskers or particulates decreased, the deformed region spread out. Figure 1 demonstrates how "necking" changes with a decrease in volume fraction. In the case of the 20 V% composite the reduction in area at the fracture surface was only 3%, and 5 mm away from the fracture surface the reduction in area was *zero*. However, in the case of 5 V% composites at the fracture surface, the reduction in area was 14% and 5 mm away from the fracture surface, the reduction in area was 4%.

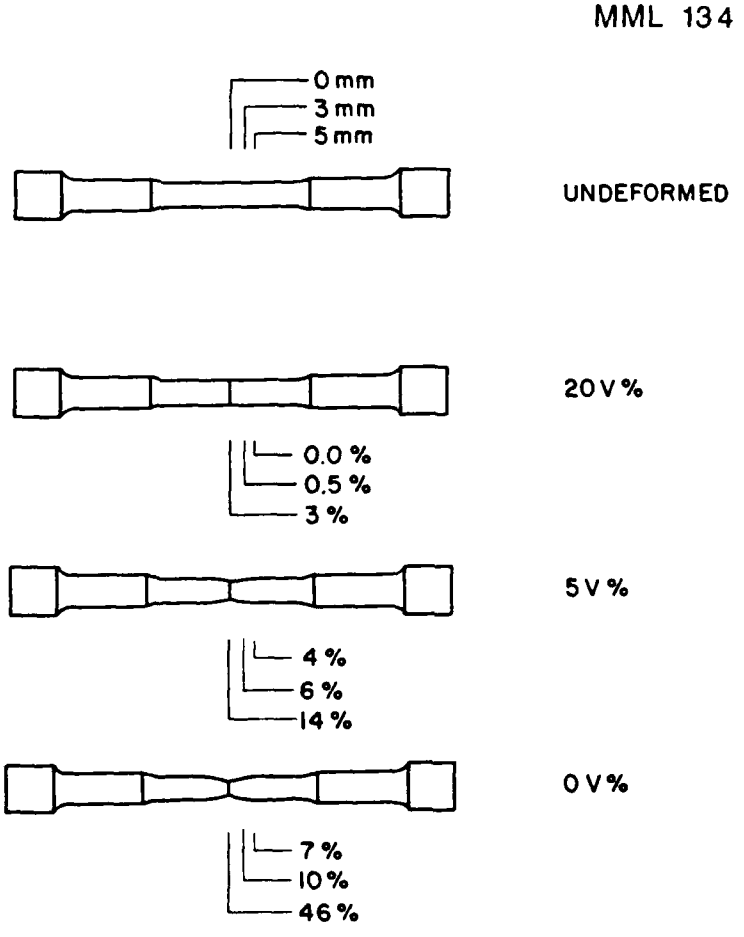

Fig. 1 Reduction in area at various distances from fracture surface for SiC/Al composite tensile samples.

One might expect in a highly deformed region, the dislocation density is expected to be higher and in the less deformed region which is very localized, the dislocation density should be lower. In other words, the high dislocation density should be limited in a very narrow region. It is also of interest to know that

previous work [1] has indicated that along the fracture path, the local density of SiC particles is higher than the average volume fraction of the SiC. In other words, the fracture path is attracted to the particle clusters. However, it is still unclear whether such a "particle friendliness" is only restricted to the fracture process or if it also governs the onset of plastic deformation.

To investigate the underlying mechanism for such a phenomenon, a set of two-dimensional finite element method (FEM) meshes were generated to simulate the effect of inhomogeneous distribution of the SiC reinforcement whisker; that is, the effect of clustering. Furthermore, it is also of importance to know the plastic deformation process around each SiC whisker. Therefore, a three-dimensional FEM mesh was generated to monitor the behavior of plastic zones around whiskers.

There have been numerous investigations and several theories of the ductile fracture of two phase alloys where the second phase is a discrete-non-deforming precipitate or particle [3-19]. All of the theories are based on the assumption that a void nucleates at the interface of the non-deforming particle and then grows, leading to ultimate fracture. An examination of transfer sections by optical and scanning electron microcopy methods indicated there are very few voids near the fracture surface. It is possible that the voids nucleated are very small and can only be observed by transmission electron microscopy techniques.

To determine whether this was a valid assumption, an investigation was proposed to determine the dislocation density along the tensile axis of the gauge section by using the transmission electron microscopy to connect the relation of macroscale and microstructure change to the plastic deformation. Also, the purpose of this investigation was to determine if there was a higher density of voids near the fracture surface in SiC/Al composites.

2. Experimental Procedures

2.1. Materials

SiC whisker or particulate reinforced 6061 Al alloys composites were used for this

investigation. The materials were obtained commercially.

The composites with 20, 5 and 0 V% SiC whiskers (SiC_w/Al) were purchased from ARCO SILAG (presently, Advanced Composite Materials) in the form of extruded rod 15.5 mm in diameter. The composites with 20 and 5 V% SiC particulates (SiC_p/Al) were purchased from DWA Composite Specialties in the form of a plate 15.9 mm thick. All materials were fabricated by the powder metallurgy method. The whiskers [3] were small in diameter, ranging from 0.1 to 1 μm, and the average aspect ratio was 2. The particulates were platelet in shape, 5 to 7 μm long and had an aspect ratio of 2 to 3.

Sample blanks were cut from the rods and plates, then machined into tensile samples. The doubly reduced samples were required to ensure that the fracture occurred in the gauge section and not in the transition region [20]. The dimensions of the samples are

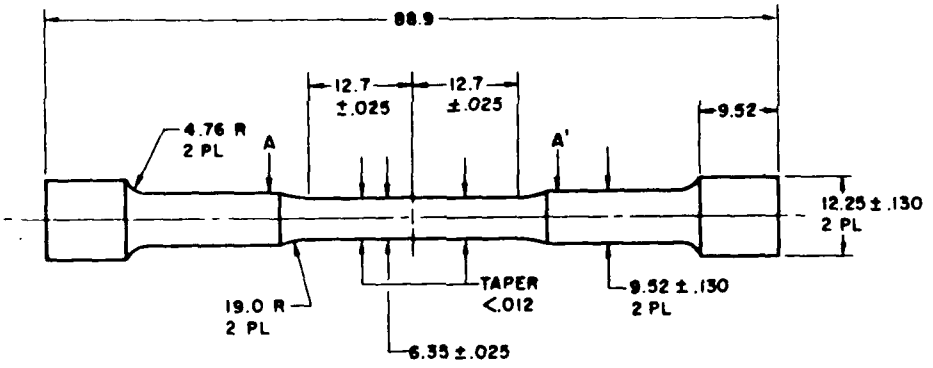

Fig. 2 Dimensions of a round tensile sample (in millimeters).

given in Fig. 2. Those that were to be heat treated were given a modified T6 heat treatment, which means a solutionizing step of three hours (modified) as opposed to the standard one hour. The modified heat treatment was used in case a divorced eutectic formed during the processing. Other were annealed for 12 hours at a solutionizing temperature of 810 K and furnace cooled.

2.2 Tensile testing

All samples were tested in an Instron testing machine at room temperature. Most of

the samples were tested to failure, however, some were tested to a strain where a measurable "neck" occurred in the sample.

2.3 TEM thin foil preparation and examination

After the tensile test, a 3 mm diameter cylinder was electrical-discharge-machined and cut longitudinally (parallel to the tensile axis) out from the gauge section. Then several slices of a thickness of ~0.6 mm disk were cut transversely (along the tensile axis) from the cylinder by a low speed diamond saw. Each disk was fixed on a brass block by DUCO cement, then mechanically thinned on a rotating water flooded wheel covered with 600 grit paper to remove the diamond saw cutting damage and reduce the thickness to approximately 0.12 mm. The reason for using DUCO cement rather than wax (the ordinary way) was to avoid heating the 3 mm disk during the mounting and dismounting of disks from the holders. Again by using DUCO cement, the disk was fixed on a holder and then the disk was dimpled by using diamond paste down to one micron in size forming a disk with a thickness of about 0.025 mm at the center of the dimpled region. The final thinning was carried out by using argon ion plasma bombardment operating at five kV and an ion current of 25 microamperes and a disk inclination of 11 degrees to the ion beam.

All thin foils were observed in a AEI EM7 type high voltage electron microscope operated at 1 MeV at the Argonne National Laboratory. Some of the thin foils were also observed in a JEOL 100 CX electron microscope at 100 kV. The liquid nitrogen cold trap was used to minimize contamination. The double tilt stages were used in both microscopes. However, both microscopes are not equipped with an eucentric stage.

There are several factors which will influence the accuracy of the value of the dislocation density, such as difficulties in determining the foil thickness. Other than this difficulty, one major problem in this part of the investigation was that, in case of very high dislocation density ($> 10^{15} m^{-2}$), the measurement will be less accurate because of the uncertainty of the real positions of dislocations on the TEM micrographs.

2.4 Dislocation density calculation

The dislocation densities were determined by the method proposed by Keh [21]. In this method, a grid of two sets of lines normal to each other, but with different spacing, is placed over the TEM micrograph and then the intersections of dislocation if given by

$$\sigma = (N_1/L_1 + N_2/L_2)t \quad (1)$$

where L_1 and L_2 are the length of the grid lines normal to each other, N_1 and N_2 are the intersections along the lines and t is the thickness of the area where the micrograph was taken.

All the micrographs were taken from the area away from the foil edge to avoid underestimating the dislocation density. Generally, three to four different locations in each foil were examined, and micrographs were taken from three to five different areas in each location.

The upper limit [22] of dislocation density calculated by using Eq. (1) is about $10^{15} \sim 10^{16}\,m^{-2}$. In some micrographs, dislocations were so dense, it was impossible to see the individual dislocation. The dislocation density was estimated by using the width of the micrograph divided by width of the dislocation image. Clearly, the value of dislocation density was underestimated.

2.5 Slip line analysis

From melted 250 μm SiC particulate reinforced composite, rectangular samples 8 mm wide by 50 mm long and 1.5 mm thick were electrical-discharged-machined and polished. The samples were glued to a E. Fullam tensile substage model No. 18202 JEOL JSM-35. The substage was mounted onto a specially constructed holder to fit on to a Zeiss ICM-405. The entire effective gauge was photographed. Then the sample was deformed a small amount and the area which contained slip lines was re-photographed, and again the sample was deformed and re-photographed where slip lines occurred. This process was repeated

until the sample fractured.

2.6 FEM procedures

2.6.1. Two-dimensional FEM procedures

In the present study, the composites are represented by a periodic array of transversely aligned whiskers as shown in Fig. 3, i.e. an infinite two-dimensional array of SiC whisker embedded in the aluminum matrix in plane strain condition. In order to consider the effect of clustering, the array is transformed in such a manner that an array of periodic geometric cluster centers was constructed and the neighboring whiskers (in this case, four whiskers [Fig. 4]) were attracted toward their cluster centers so that a periodic array of clusters were formed as shown in Fig. 5. The degree of clustering was defined by the value of S_V/V and S_h/H in Fig. 5.

Applying above geometric transformation scheme, a commercially available ADINA finite element materials (FEM) code was employed. To represent the reality, the material is assumed to be stress-free at annealing temperature, i.e. 773 K, and is subsequently cooled to room temperature. Therefore, the effect of thermal residual stresses is implicitly considered. After thermal treatment, the composites, clustered and unclustered, were uniaxially loaded in whisker directions. Due to the periodic arrangement, the condition of symmetry can be so utilized that a "unit cell" was selected as a basic building block such that only a quadrant of whisker (cluster) is contained as shown in Figs. 6(a) and (b) , and multi-constraint boundary conditions were employed to represent the symmetry conditions at the boundary.

2.6.2. Three-dimensional FEM procedure

In this case, the reinforcement particles are hexagonally distributed through three-dimensional space. Because of the symmetry, the response of the composite can be fully represented simply by considering a building block which only contains one-eighth of the reinforcement particle, as shown in Fig. 7 and, in consideration of symmetry, multipoint constraint equations were employed in the boundary conditions. As in the case of two-

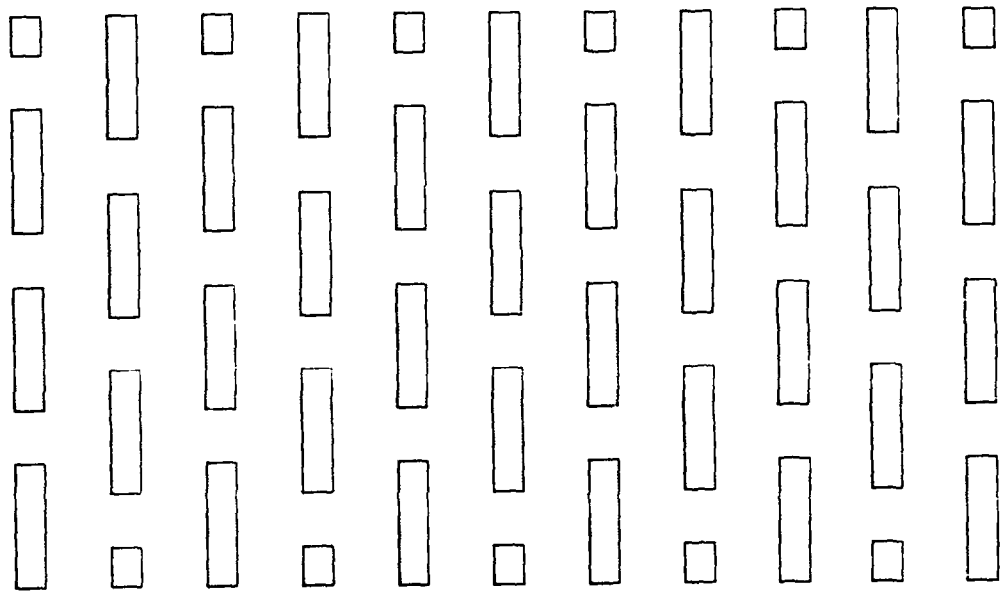

Fig. 3 Periodic hexangonal arrangement of the SiC reinforcement of the whisker. The shaded areas are SiC whiskers.

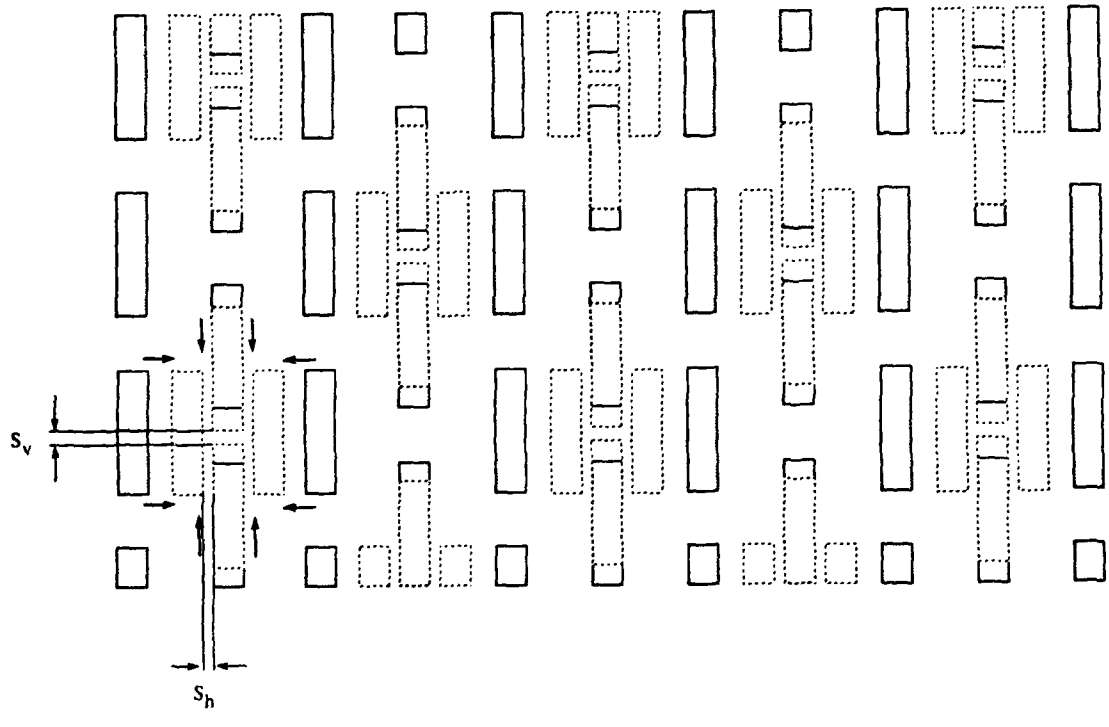

Fig. 4 This figure shows how SiC whiskers move to their geometric cluster center to form a periodic array of clusters. Whiskers with dotted boundaries represent the final locations of the whiskers after the movement indicated by the arrows in the figure, and S_v and S_h show the degree by vertical and horizontal clustering.

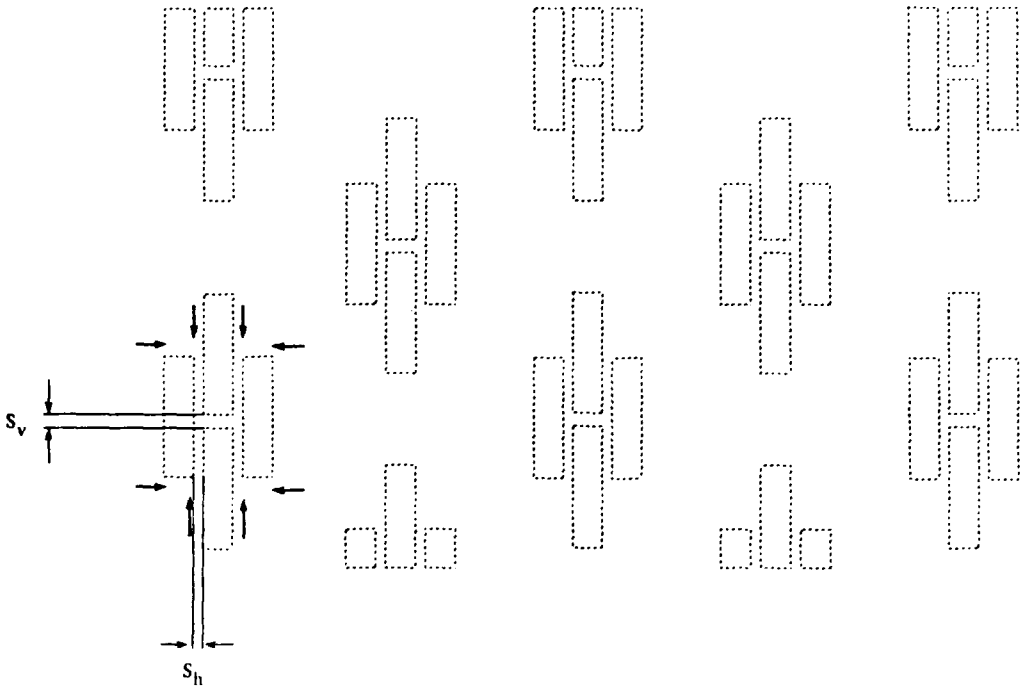

Fig. 5 The configuration of clustered composites.

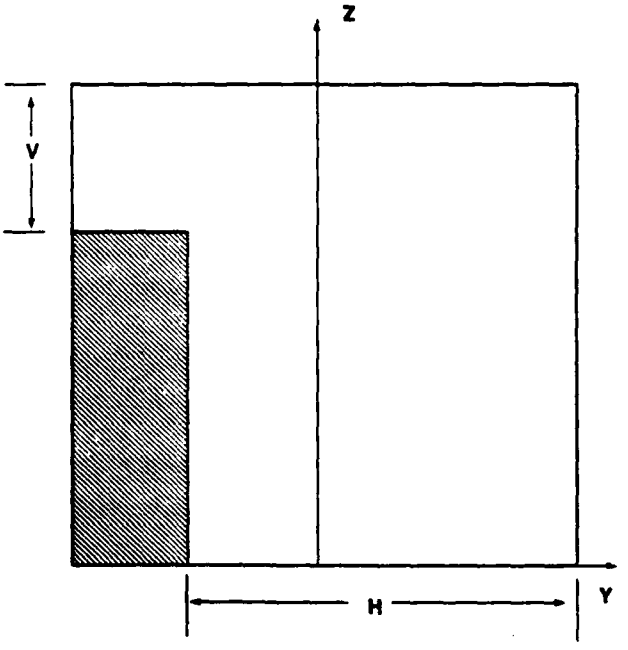

Fig. 6(a) A unit cell for the uniform distribution of the whiskers employed by the FEM analysis where *h* and *v* stand for the horizontal and vertical half spacing.

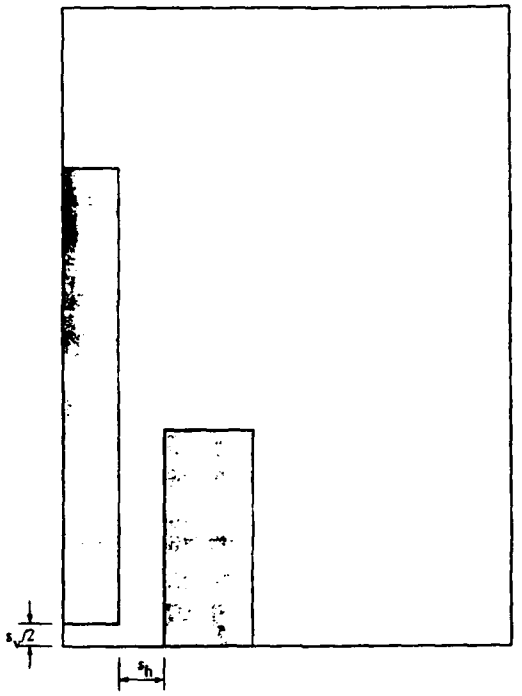

Fig. 6(b) A unit cell for the clustered whisker configuration employed by the FEM analysis where S_v and S_h are defined the same way as in Fig. 4.

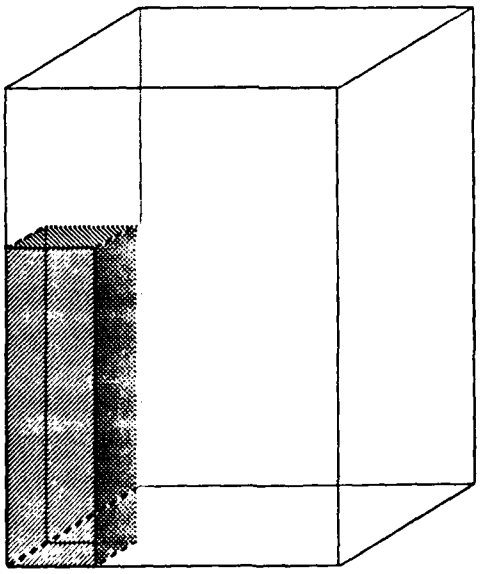

Fig. 7 A unit cell employed for three-dimensional analysis.

dimensional analysis, the composites were assumed stress-free at 773 K which is the annealing temperature for SiC/Al composites, and then the sample was subsequently cooled down to room temperature. Due to a large difference in thermal expansion coefficient between SiC and Al, severe thermal residual stress would be generated around particles. As a result, it is apparent that a plastic zone will form around each particle. Upon further uniaxial loading, such a plastic zone will certainly respond to the external load. Depending on how such a response would be, it will be helpful to understand the deformation mechanism of the composites. Therefore, it is our intention to monitor the geometric change of the plastic zone as a result of external load. This can be done simply by imaginarily slicing the sample longitudinally along the loading direction and monitoring the two-dimensional change of the plastic zone in each plane.

3. Experimental Results

The discussion of the experimental results will be divided into four parts: (a) dislocation density vs. distance, (b) slip line analysis, (c) FEM results, and (d) voids.

3.1. Dislocation density vs. distance

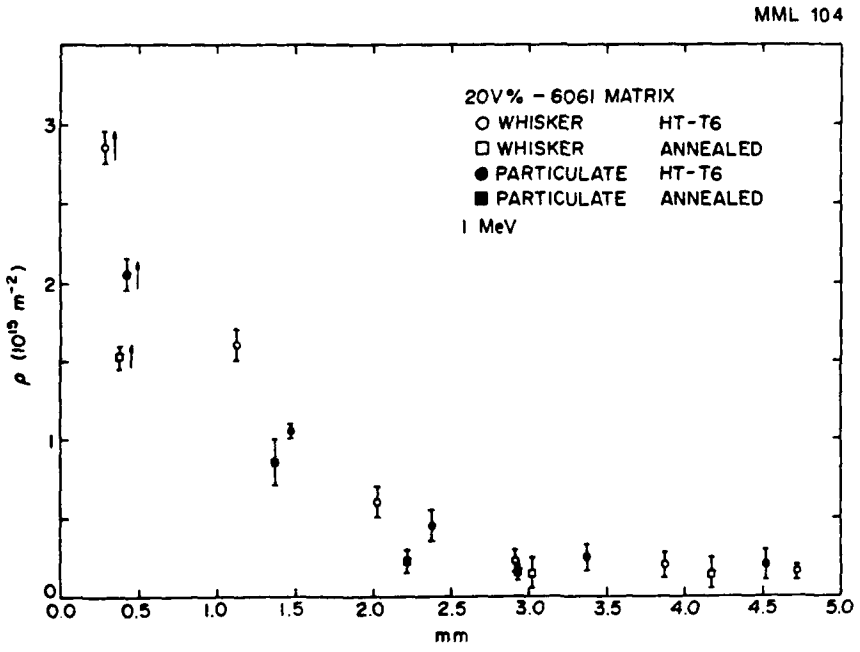

Fig. 8 Dislocation density vs. distance from fracture surface for 20% SiC/Al composite.

3.1.1. 20 V% SiC/Al composite

The plot of dislocation densities (ρ) versus distance from the fracture surface (χ) is shown in Fig. 8. The value of ρ is higher near the fracture surface region and decreases as χ (i.e.

the distance from the fracture surface) increases. When the distance is 3 mm and beyond, ρ is constant and the value of ρ is approximately equal to the value of ρ of an undeformed sample. This value is about one order of magnitude lower than that at the $0.3 \sim 0.5$ mm region, i.e. near the fracture surface region.

In general, the values of ρ are higher in the whiskered and heat treated samples.

The difference between the dislocation densities of each micrograph in the same foil increases as x increases, which means the dislocation densities are more uniformly distributeed near the fracture surface region.

In some foils, the difference in the dislocation densities is quite large (may exceed two orders of magnitude). To avoid confusion, the reported data are the average values of micrographs taken from each location rather than those of a single micrograph, i.e. there will not be two orders of magnitude difference deviation shown in the plot.

Several attempts were made to deform 20 V% SiC/Al composites until a "neck" occurred, then stopping the test prior to fracturing the sample, and then cutting TEM foils from the sample in the "neck" region. All attempts were failures; either the sample fractured before the test was stopped or upon examination of the TEM foils. There was no difference in density between the perceived "neck" region and away from the "neck".

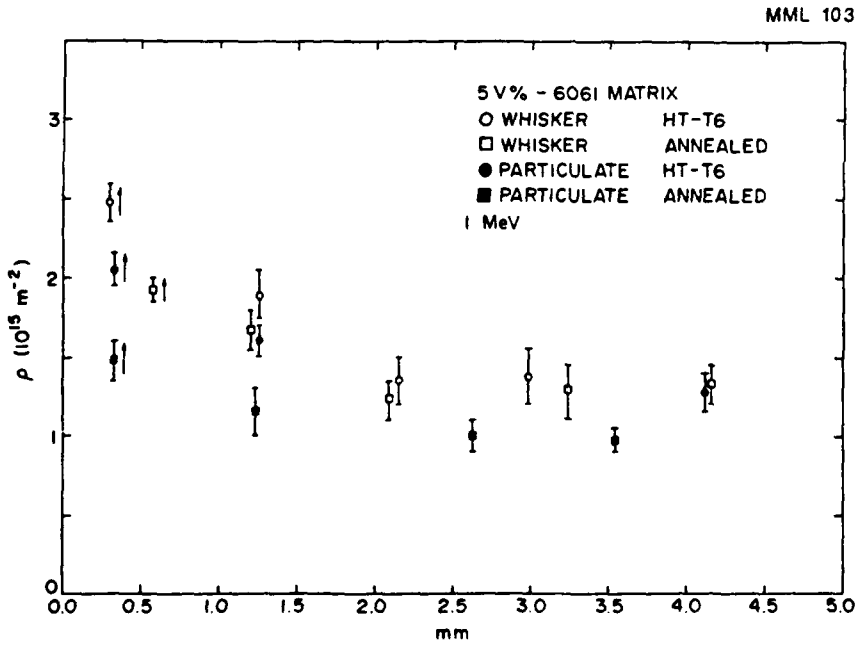

Fig. 9 Dislocation density vs. distance from fracture surface for 5 V% SiC/Al composite.

3.1.2. 5 V% SiC/Al composites The plot of dislocation

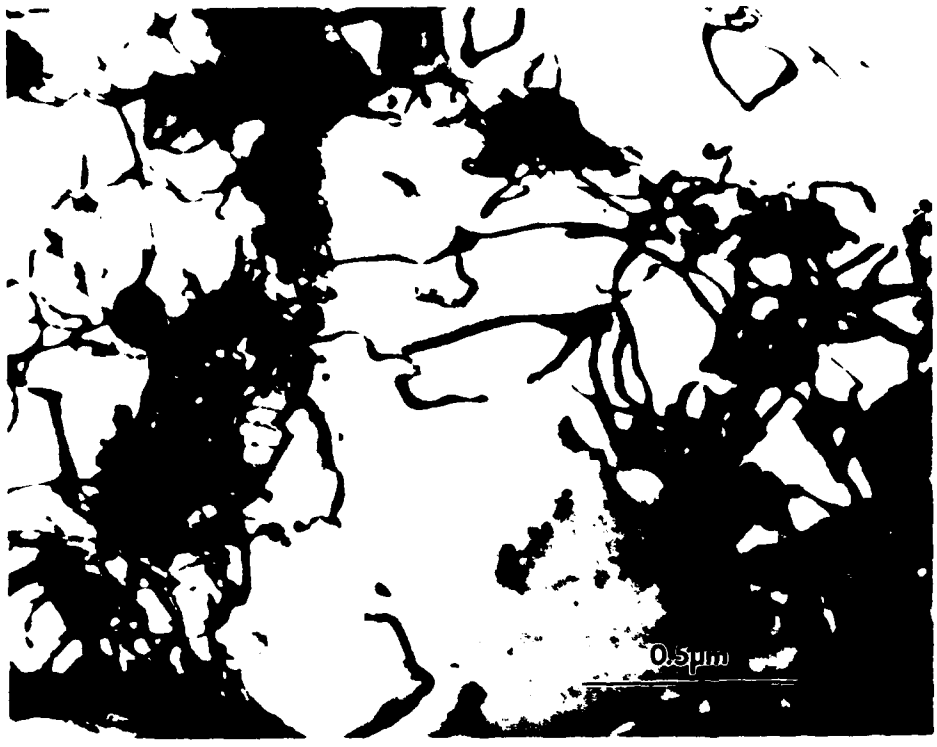

Fig. 10(a) A transmission electron microscopy micrograph of foil taken from the end section of 5 V% whisker SiC/Al tensile sample.

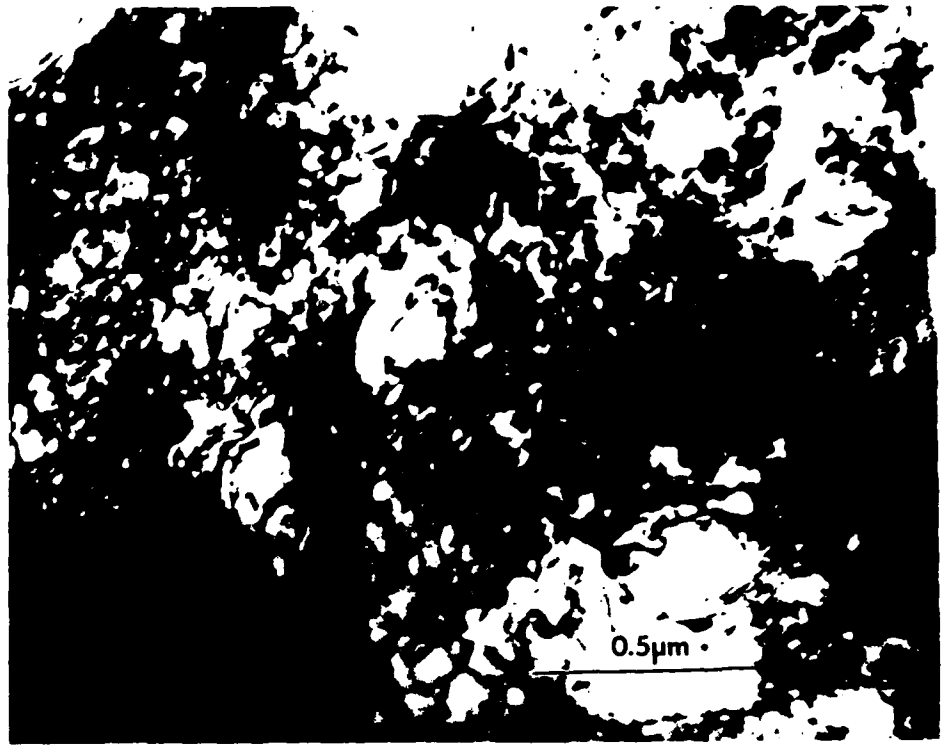

Fig. 10(b) A transmission electron microscopy micrograph of foil taken from the neck section of 5 V% whisker SiC/Al tensile sample.

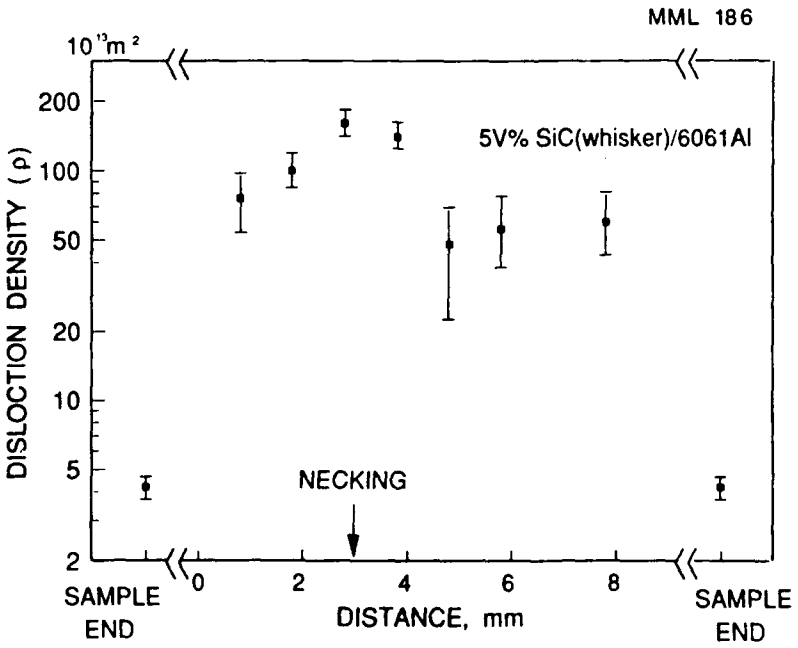

Fig. 11 A plot of dislocation density in the neck region and the end sections of a tensile sample which has been deformed to produce a neck.

densities (ρ) vs. distance from the fracture surface (x) is shown in Fig. 9. Similar to 20 V% (Fig. 4) at 0.3 ~ 0.5 mm, i.e. near the fracture surface region, ρ is higher and approximately equals the 20 V% samples at the same region, then ρ decreases as x increases. But contrary to 20 V%, at 3 mm and beyond, ρ rather than staying constant and the values of ρ are 3 to ~5 times higher than that of undeformed samples.

Also, in agreement with 20 V%, ρ is higher in whiskered and heat treated samples.

As in the case of 20 V% SiC/Al composite, several samples were tested until a "neck" had formed. Then, TEM foils were cut from the "neck" region and the ends of the samples. Figure 10(a) is a TEM micrograph of the end region of the sample and Fig. 10(b) is a TEM micrograph showing the high dislocation density in the "neck" region. The variation of the dislocation density from the "neck" region to the ends of the sample is shown in Fig. 11.

3.1.3. 0 V% SiC/Al samples

The plot of dislocation densities ρ vs. distance from the fracture surface (x) is shown in Fig. 12. Near the fracture surface region (0.3 to ~ 0.5 mm), ρ is higher, but the value of ρ is about one third of 20 V% samples at the same region and unlike the 20 and 5 V%

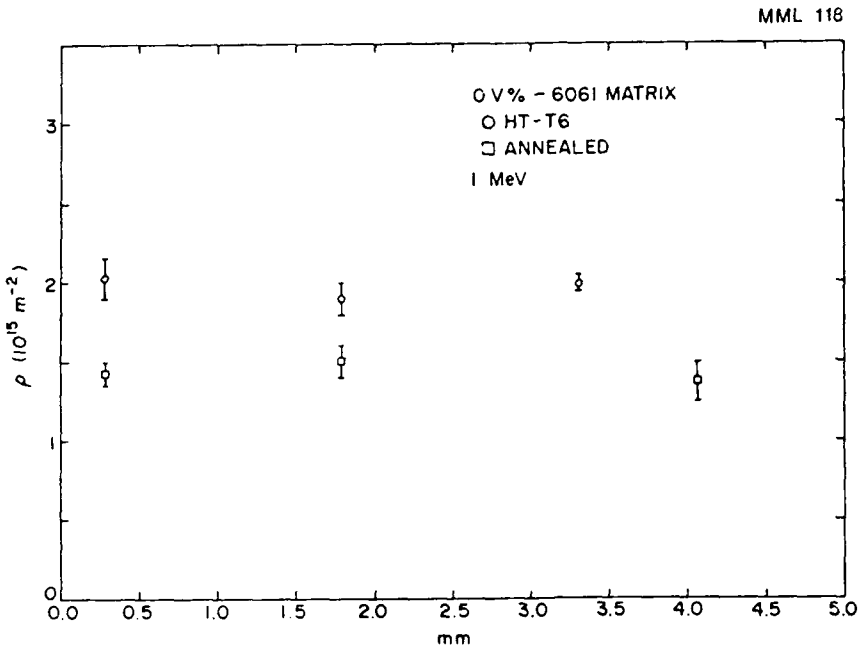

Fig. 12 Dislocation density vs. distance from fracture surface for 0 V% SiC/Al composite.

samples, as x increases ρ decreases in a much slower rate. The values of ρ in this plot are about 2 orders of magnitude higher than an undeformed sample.

Similar to 20 and 5 V% samples, ρ is higher in heat treated samples.

3.2 Slip line analysis

The development of slip lines, i.e. the initial slip lines, began in a region which contained a higher than average density of SiC particles (that is, a cluster). The very first slip lines which occur in this higher density of SiC particle region, occur at the corners of SiC particles, as shown in Fig. 13. Figures 14, 15, 16 are micrographs taken at successive loadings. In other areas of the sample there are no or very few slip lines.

3.3. FEM

3.3.1. Two-Dimensional FEM

The global stress-strain curves of the composites produced by calculation are shown in Fig. 17. It is clear that the more the whiskers are clustered together, i.e. the smaller the S_v and S_h in Fig. 6b, the lower the yield stress. This is consistent with the experimental data described from previous section; that is, plastic deformation is initiated within the region where there is a higher localized particle concentration (cluster). If a periodic arrangement

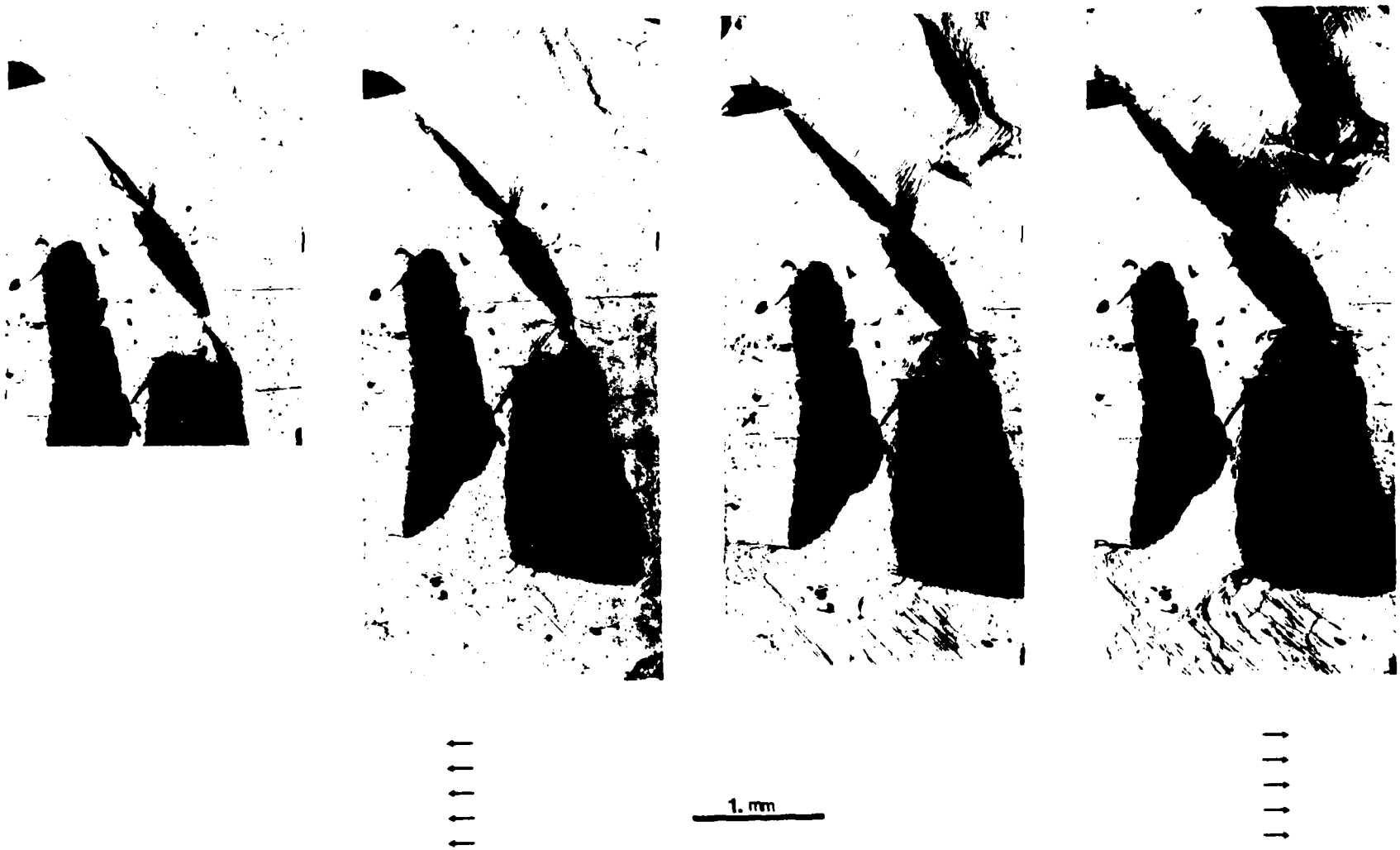

Fig. 13 The sequence of the slip line formation as a result of incremental loading along the direction shown by the arrows. As load increases (from left to right) slip lines first formed around the corners of the SiC particles, and then as the load further increased, slip lines formed around each particle will propagate and interconnect and finally form a set of densely packed slip bands.

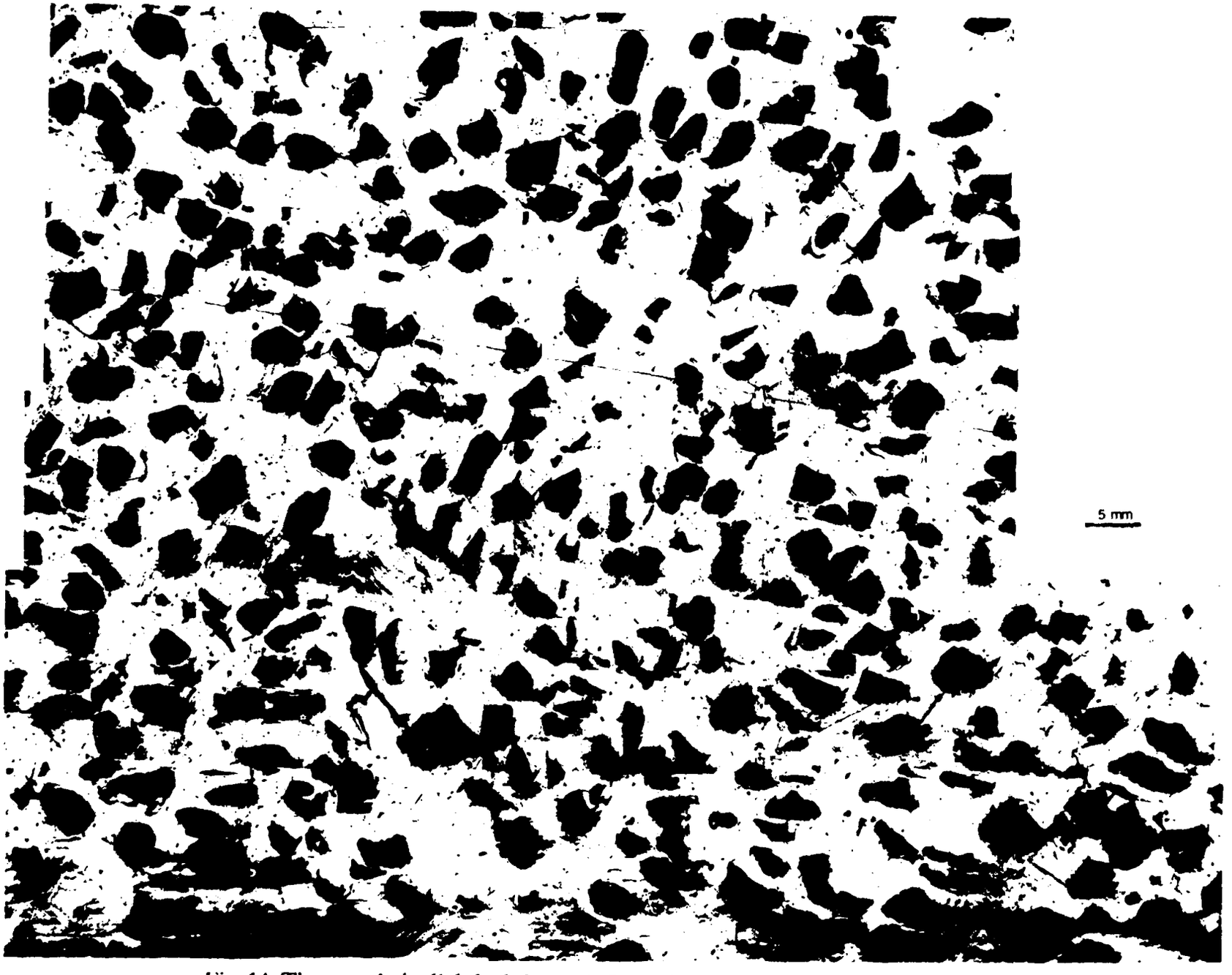

Fig. 14 The sample is slightly deformed. It can be seen that slip lines begin to emerge from the particle matrix interface and the slip line density is higher where there is higher localized particle density.

Fig. 15 Upon further straining, the density of the slip lines increases. However, they are limited to the localized region where it has higher particle volume fractions. (The arrows indicate direction of loading.)

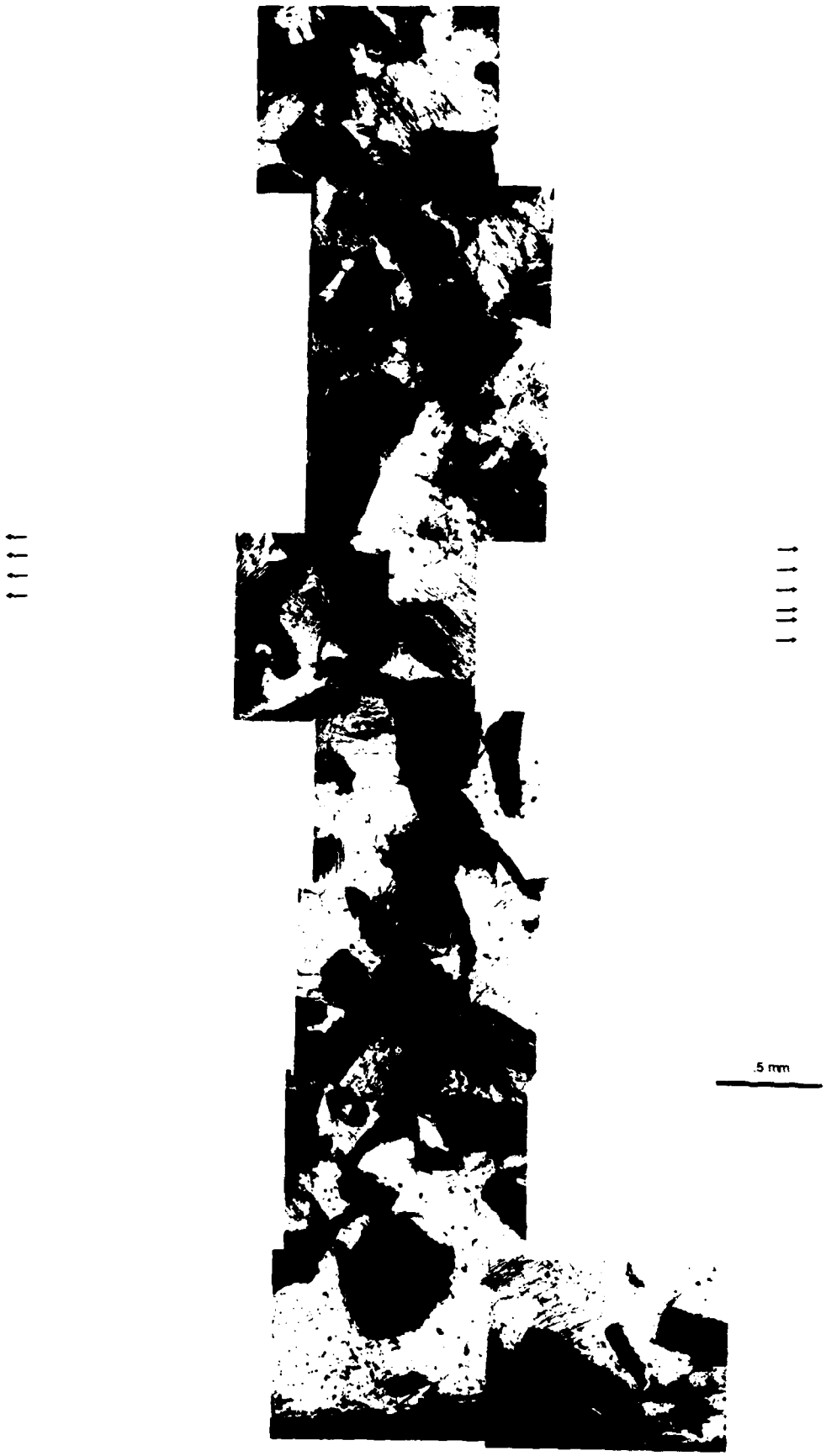

Fig. 16 As the external load increases, plastic deformation becomes more localized, and finally a crack is formed within such a highly deformed region. (The arrows indicate direction of loading.)

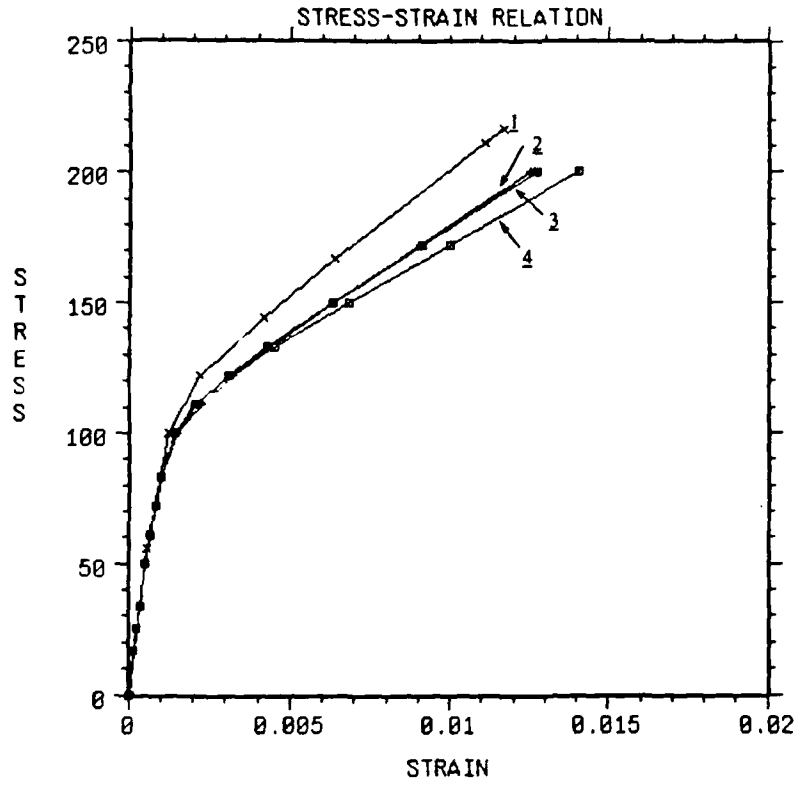

Fig. 17 Stress strain curves produced as a result of clustering where curve 1: $S_v/2V = 1$, $S_v/2H = 1$; Curve 2: $S_v/2V = 0.75$, $S_h/2H = 0.429$, Curve 3: $S_v/2V = 0.5$. $S_h/2H = 0.143$; Curve 3: $S_v/2V = 0.5$, $S_h/2H = 0.143$; Curve 4: $S_v/2V = 0.25$, $S_h/2H = 0.071$.

of the reinforcement particles represents a more uniform plastic deformation best achievable by the composites, clustering of these particles would lead to nonuniformity of plastic deformation, that is, highly localized dislocation generation and, in this case, motion within the cluster of whiskers. It would, therefore, result in reduction of composite flow stress.

3.3.2. Three-Dimensional FEM

It was found that the plastic zone extended about one particle diameter from the edge of the particle which is in agreement with the experimental results [23]. Also, it was found that the plastic zone expanded transversely upon loading the sample in tension which is in agreement with the slip line analysis, whereas longitudinally it contracts near the whisker ends due to the compressive nature [24] of the plastic zone at that part of the matrix. However, this process generally means the generation of dislocations of opposite sign; annihilation of dislocations does not make a significant contribution to the process.

3.4. Voids

The TEM micrographs were examined to determine the density of voids at the interface between the matrix and the SiC whiskers or particle. Voids were found, however, the density of voids near the fracture surface was greater than the density of voids in the non-deformed regions of the samples.

4. Discussion and Conclusions

The discussion of the experimental results will be related almost exclusively to explaining how and why the deformation is so localized in the SiC/Al composites. There will be a brief discussion of the lack of voids.

The evidence obtained from the dislocation density and the slip line investigation is overwhelming: deformation in higher volume fraction composites is very localized. From an analysis of the configuration of SiC particles in the samples which were used for the slip line analysis, it is evident that slip lines began in regions which contained a clustering of SiC particles. The slip propagated from one cluster region to another and deformation in the remainder of the samples is almost zero. The phenomena of localized deformation was duplicated in a FEM analysis.

Although, by considering the fact that plastic deformation initiates within the cluster, the drop in yield stress can be easily explained. The question still remains to be addressed: Why should plastic deformation initiate in the clustered region where there is a local high volume fraction of reinforcement whereas it is obvious the higher the volume fraction of reinforcement, the stronger the material and the less prone to plastic deformation?

To fully explain this phenomenon, it is necessary to consider the fact that deformation compatibility has to be satisfied when there is an inhomogeneous distribution of reinforcement particles, i.e. clustering. Since the clusters are stiffer, upon satisfying compatibility, the stress would be distributed in such a way that the clusters would bear more load than the rest of the matrix. Secondly, since the local volume fraction is higher within clusters, for the same amount of deformation, it must activate more slip systems in the matrix to accommo-

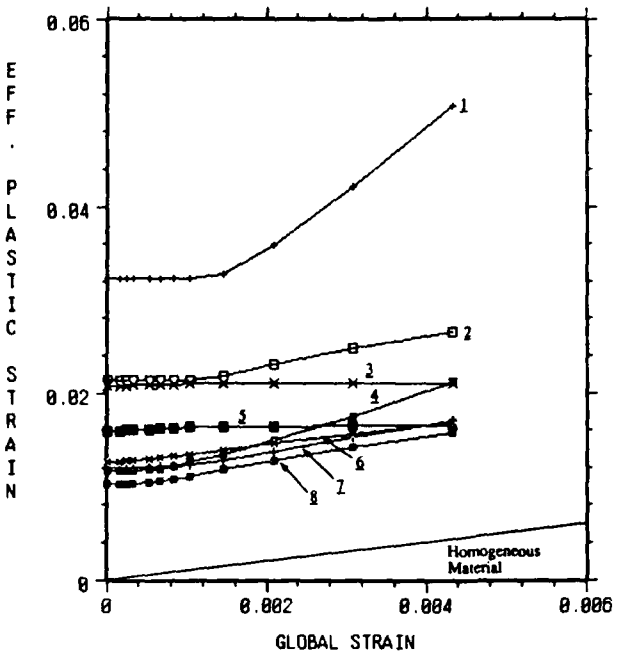

Fig. 18(a) This shows localized effective plastic strain at various locations vs. global strain. "Homogeneous material applies to a homogeneous material subject to a tensile load.

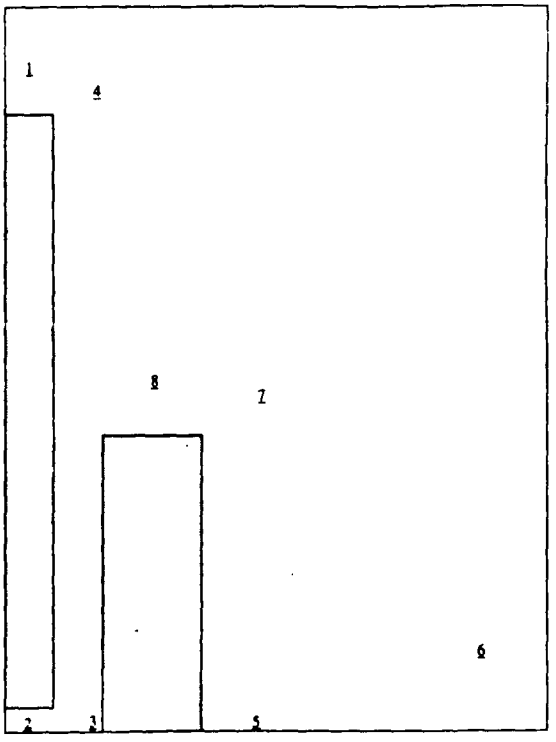

Fig. 18(b) Locations where effective plastic strain is taken.

date the same amount of deformation. Figure 18(a) shows effective plastic strain at various locations within the matrix [Fig. 18(b)] as a function of global strain. If a sample of homogeneous material was tested in tension, then the local strain would be the same as the global strain. This behavior is indicated by the line labeled

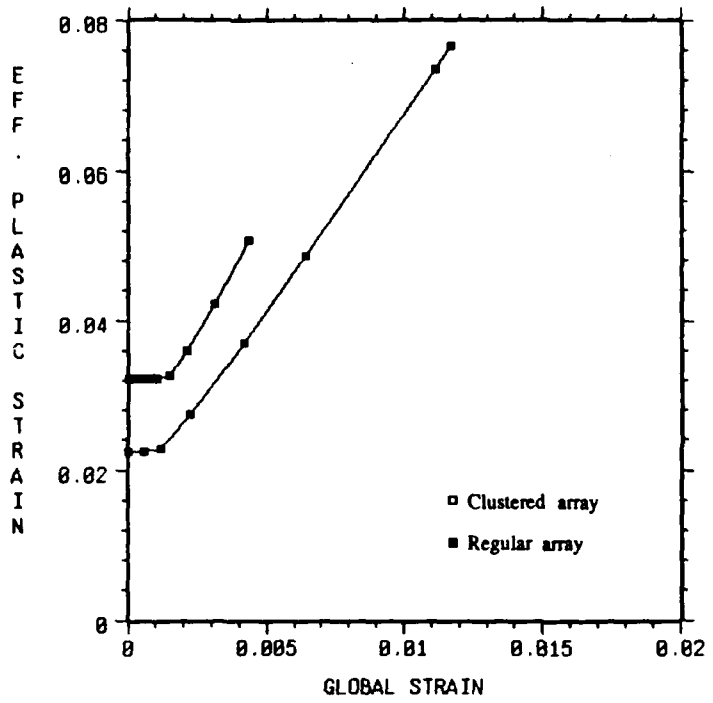

Fig. 18)c) Effective plastic strain vs. global strain at whisker ends for clustered and regular arrays (at location 1) for clustered array as shown in Fig. 18(b). It is clearly indicated that the clustered array has a higher effective plastic strain rate for the same global strain increment, which simply means clustered arrangement of the reinforcement particles is more susceptible to external loading in terms of plastic deformation.

homogeneous material" in Fig. 18(a). From the plot, it can be easily seen that plastic strain rate between the fiber ends in the cluster is much higher than elsewhere in the matrix. Fig. 18(c), shows a comparison of the regular and a cluster whisker distribution. The regular distribution also has a higher plastic deformation rate at the whisker ends, but the cluster distribution has a higher rate. This signifies that each cluster is being treated as a reinforcement particle since apparently it has a higher it has a higher Young's modulus, which is in agreement with earlier work [24], and the stress level in the matrix within the cluster. Therefore, more plastic deformation will be induced.

The lack of voids at the matrix/whisker interface is probably related to several phenomena. First, it has been shown [25] that the bond between SiC and Al is very good. This bond is several times stronger than the bond between Fe_3C and Fe. Second, there is a region of cold work, i.e. a high dislocation density region, around the whisker. As a result of

this hardened region around the whisker, a triaxial stress develops in the matrix some distance away from the whisker. It is into this region that the crack propagates. The end result is that very few voids are found at the interface between SiC and Al.

Acknowledgement

This research was supported by the Office of Naval Research under contract No. N00014-K-85-0007. The positive interactions with Dr. S. Fishman of the Office of Naval Research are to be greatly acknowledged. The authors wish to acknowledge the assistance of Dr. S.B. Wu in the performance of the tensile tests. The authors wish to acknowledge the continued support of the Argonne National Laboratory HVEM facility, especially, Dr. E. Ryan.

References

1. R.J. Arsenault and Y. Flom, K.N. Subramanian and M.A. Iman (eds) *Structure and Deformation of Boundaries*, AIME (1986) p. 261; Y. Flom and R.J. Arsenault, *J. Metals* (1986) p. 31.
2. Unpublished results, Metallurgical Materials Laboratory, University of Maryland (1986).
3. B.I. Edelson and W.M. Baldwin, *Trans. ASM 55* (1962) p. 55.
4. J. Gurland and J. Plateau, *Trans. ASM 56* (1963) p. 442.
5. A. Gangullee and J. Gurland, *J. Trans. Metal. Soc. AIME 239* (1967) p. 269.
6. J. Gurland, *Trans. Metal. Soc. AIME 227* (1963) p. 1146.
7. C.T. Liu and J. Gurland, *J. Trans. Metal. Soc. AIME 224* (1968) p. 1535.
8. C.T. Liu and J. Gurland, *Trans. Metal. Soc. AIME 61* (1968) P. 156.
9. J. Gurland, Fracture of Metal-Matrix Particulate Composites, (eds) L.J. Broutman and R.H. Krock, *Modern Composite Materials*, Addison-Wesley, NY, (1969).
10. I.L. Mogford, *Metal. Reviews 114* (1967) p. 12, 49.
11. R.H. Van Stone, R.H. Merchant and J.R. Low, Jr., *ASTM STP 556* (1974) p. 93.
12. T.B. Cox and J.R. Low, *Metal. Trans. 5* (1974) p. 1457.
13. G.T. Hahn and A.R. Rosenfield, *Metal. Trans. A 6* (1975) p. 653.
14. G.G. Garret and J.F. Knott, *Metal. Trans. A 9* (1978) p. 1187.

15. K.H. Schwalbe, *Eng. Frac. Mech. 9* (1977) p. 795.

16. G. LeRoy, J.D. Embury, G. Edwards and M.F. Ashby, *Acta Metal. 29* (1981) p. 1509.

17. R.C. Bates, Modeling of ductile fracture by microvoid coalescence for prediction of fracture toughness, (eds.) J.M. Wells and J.B. Landes, *Proc. 113th AIME Conf.* (1985) p. 117.

18. W.W. Gerberich, Interaction of microstructure and mechanism in defining K_{IC}, K_{ISCC} or K_{th} values, (eds.) J.M. Wells and J.B. Landes, *Proc. 113th AIME Conf.* (1985) p. 49.

19. D. Firrao and R. Roberti, On the mechanism of ductile fracture nucleation ahead of sharp crack, (eds.) J.M. Wells and J.B. Landes, *Proc. 113th AIME Conf.* (1985) p. 165.

20. R.J. Arsenault, *Mater. Sci. Eng. 64* (1984) p. 171.

21. A.S. Keh, *Direct Observation of Lattice Defects in Crystals*, Wiley-Interscience, NY (1962) p. 213.

22. P.B. Hirsch, A. Howie, R.B. Nicholson, D.W. Pashely and M.J. Whelan, *Electron Microscopy of Thin Crystals*, Butterworths, London (1965) p. 416.

23. Y. Flom and R.J. Arsenault, *Mater. Sci. Eng. 75*, (1985) p. 151.

24. N. Shi, M. Sarfarazi, R.J. Arsenault, submitted to J. Int. Plasticity for publication.

25. Y. Flom and R.J. Arsenault, *Mater. Sci. Eng. 77* (1986) p. 191.

STRENGTHENING OF COMPOSITES DUE TO MICROSTRUCTURAL CHANGES IN THE MATRIX*

By

R.J. Arsenault, L. Wang and C.R. Feng
Metallurgical Materials Group
University of Maryland
College Park, Maryland 20742-2115

ABSTRACT

The addition of discontinuous silicon carbide (SiC) to aluminum (Al) alloys can result in a five-fold increase in the yield stress. The magnitude of the increase is obviously a function of the volume fraction and the particle size of the SiC. Previously, it was proposed that the strength increase due to SiC addition to Al alloys was the result of change in the matrix strength, i.e. an increase in dislocation density and a reduction of subgrain size. The data obtained from a series of experiments indicate that dislocation density increases with an increase in volume fraction of SiC and decreases with an increase in particle size. The subgrain size decreases as the volume fraction increases and increases as the particle size increases.

There is a good correlation between the microstructural changes in the matrix and the changes in the yield stress of the composites.

1. INTRODUCTION

The concept of strengthening due to an increase in dislocation density has been in existence for several decades, probably since shortly after the original proposal of edge dislocations by Orwan, Polyani and Taylor [1]. Over the subsequent years, there have been numerous investigations which have correlated a strength increase with an increase in dislocation density. The strengthening due to a reduction in subgrain size is not as old as the concept of strengthening due to an increase in the dislocation density [2]. However, the correlation has been demonstrated quite clearly by several individuals; in particular, by

---

* This research was supported by the Office of Naval Research under contract No. N00014-85-K-0007.

McQueen et al. [3].

It had been proposed by Arsenault [4] a few years ago that the strengthening of Al and Al alloys due to the addition of discontinuous SiC reinforcements occurred as a result of generation of dislocations which produced an increase in dislocation density and a reduced subgrain size in the matrix. The generation is due to a difference in thermal coefficient of expansion between the matrix and the reinforcement (ΔCTE). The presence of the high dislocation density within the matrix has been demonstrated along with a very small subgrain size. An in situ investigation has demonstrated the validity of the ΔCTE mechanisms as a means by which the high dislocation density is produced within the matrix [5].

Further, it has been shown that a very simple model based on prismatic punching is capable of producing an adequate dislocation density [6]. However, it should be clearly pointed out that this model will only predict the lower limit of the dislocation density. Attempts to calculate the upper limit of the dislocation density due to the ΔCTE effect have proven unsuccessful, for all of the calculations predicted a very high dislocation density, i.e. approaching infinity, which obviously is not correct.

However, there remain several questions pertaining to the details of the strengthening mechanism of discontinuously reinforced metal matrix composites based on the strengthening of the matrix due to a change in the microstructure of the matrix.

The first question is related to transmission electron microscopy (TEM) procedures for determining dislocation densities; a) Does the sample preparation technique, i.e. dimpling and ion milling, introduce damage into the TEM foil? and b) If a thin region of the foil is examined (i.e. the viewing region) at 100-200 KV, will a lower dislocation density be observed? There have been a few investigations which have determined the dislocation density as a function of foil thickness and the most recent are by Fajita et al. [7-9]. In the case of pure Al, it was found that the foil thickness had to be greater than 1 μm to obtain a bulk dislocation density. The question arises, since SiC/Al is not high purity Al, does this requirement of foil thickness still apply?

The second question: Is there an overall relationship between dislocation density (ρ), subgrain size (λ), reinforcement particle size (D) and volume fraction (V), and the increase in the yield stress of the composite? There have been several investigations where the dislocation density was determined for a specific particle size and volume fraction, but there have been no systemic investigations of these parameters. Also, there are no systematic investigations of the subgrain size as a function of particle size and volume fraction.

Another question: Is it possible to increase the strength of the matrix sufficiently to account for the strengthening? In other words, if the Al matrix alone (with no SiC present) had the same dislocation density as in the composite, would the Al matrix have the same strength as the composite? Is it possible to increase the dislocation density and reduce the subgrain size within the Al alloy matrix by cold working to approach the yield strength of a composite containing 20 V% reinforcement in the same Al alloy matrix.

An investigation was undertaken to address the questions raised above.

2. MATERIALS AND TESTING

A discussion of materials and testing will be divided into three portions corresponding to:

2.1 Composite Materials

2.2 Cold Rolled 0 V% 1100 Al Alloy

2.3 High Parity Al

2.1. Composite Materials

All of the composite materials were produced by a powder metallurgical procedure. The Al alloy powders were mixed with particulate or whisker SiC, hot-compacted and hot-extruded into 12.7 mm diameter rods or hot pressed into a plate. The 0, 5 and 20 V% SiC whiskers/6061 Al alloy composites plus the 0 V%/1100 Al alloy composites were purchased from ARCO Silag*. The 20 V% SiC-250 μm particulate/1100 Al alloy composite

---

* Now, Advanced Composite Materials of Greer, South Carolina.

was purchased from DWA* in the form of a plate. The remainder of the material was produced in the Metallurgical Materials Laboratory of the University of Maryland in the form of an extruded rod.

From the extruded rod and plate, tensile samples were machined into a configuration as described elsewhere [4]. Prior to tensile testing, the samples were annealed for 12 hours at 803 K and furnace cooled. All of the tensile testing was conducted at room temperature at a strain rate of $10^{-4}\,sec^{-1}$.

Short sections of extruded rod (12 mm) and portions of as-pressed plate were annealed at 803 K for 12 hours and furnace cooled. From these sections and portions, 0.5 mm thick disks were electrically discharge machined. The procedure for thinning the TEM foils and the method of determining the dislocation densities is given elsewhere [5]. The electron microscopy investigation involved the use of two microscopes, a JEOL CFX1 100 operating at 100 KV and the Argonne National Laboratory 1 MEV microscope operated at 1 MV.

2.2 Cold Rolled 0 V% 1100 Al Alloy

The cold rolled strips were produced by taking 0 V% 1100 Al alloy material purchased from ARCO Silag and rolling without any intermediate annealing until a reduction in thickness of ~90% was obtained. From the cold rolled strips, "dog bone" shaped tensile samples were machined with a 24.5 mm gage length and a width of 2.6 mm and a thickness of 1.42 mm.

The tensile sample preparation and testing were the same as described in Part A. This also applies to the TEM foil preparation and examination.

2.3. High Purity Al

Relatively high purity Al (99.99%) was obtained in the form of a rod, 12.7 mm dia. from ALCOA as a gift. This material was annealed for 12 hours at 803 K and furnace cooled. The TEM foils of high purity Al were produced by two different procedures. Some

---

* Composite Specialties of Chatsworth, California.

of the foils were produced using the electrical discharge machine, dimpling and ion milling procedure, using the same operating parameters as used for the composite TEM foils (Part 2.1). The other samples, after cutting into 0.5 mm thick disks by electrical discharge machining, were electrochemically thinned using a jet polishing device. The foils were examined at 100 KV and 1 MV.

3. Results

The discussion of the results will be divided into four portions:

3.1 Yield Strength vs. Particle Size and Yield Strength vs. Volume Fraction

3.2 Dislocation Density Determination

3.2.1. Dislocation Density Due to Foil Preparation Procedures and TEM Operating Voltages

3.2.2. Dislocation Density and Subgrain Size vs. Particle Size and Volume Fracture

3.3. Changes in Dislocation Density and Subgrain Size due to Cold Rolling and the Determination of the Yield Strength

3.1 Yield Strength

Of interest is the incremental increase in the yield stress (which is defined as the stress at a plastic strain of 0.2%) due to the addition of the reinforcement. Therefore, the yield stress of the 0 V% matrix alloy is subtracted from the yield stress of the composite. The incremental yield stress ($\Delta\sigma_y$) is what is plotted and listed in all cases. The variations in $\Delta\sigma_y$ of the SiC whisker/6061 Al alloy composites were considerably less than in the SiC/1100 Al alloy composites. This is simply due to the greater homogeneity of the reinforcement within the matrix in the 6061 Al alloy composites.

As expected, as the size of the SiC particulate increased, the strength decreased, as shown in Fig. 1. The squares represent the average of at least three tests and there could be as many as ten tests for a given particle size. The arrow bars define the range of scatter. The ultimate strength is only slightly larger than the yield strength indicating that the work hardening rate past yielding is small. The uniform strain was fairly constant, between 3 and

4% for the 0.5 to 9 μm composite materials, then increasing to 6-7% uniform strength for the 20 and 70 μm particulate and slightly larger on average for the 250 μm particulate size composites.

Increasing the volume fraction of SiC resulted in an increase in strength (Fig. 2), but not linearly as predicted by the classical-continuum-load transfer-shear lag model [10], which is indicated by the dashed line in Fig. 2.

3.2 Dislocation Density Determinations

3.2.1. Dislocation Density Due to Foil Preparation Procedures and TEM Operating Voltages

The two different series of investigations were undertaken to determine if the TEM foil preparation procedure was introducing damage into the composite. The first investigation involved preparing TEM foils from annealed and furnace cooled high purity Al rods by two difference routes. The first involved electrical discharge machining, followed by dimpling using 0.25 μm diamond paste and then followed by ion milling, i.e. the same procedure which is used in the composite. The second technique involved electrical discharge machining and then followed by electro-chemically thinning. Figure 3(a) is a micrograph taken of an ion milled thinned sample and Fig. 3(b) is taken from a sample which was electrochemically thinned. As can be seen, the dislocation densities are low in both cases. The only recognizable difference between the ion milled and the electro-chemically thinning is the "mottled" appearance of the ion milled micrograph. This mottled appearance is the result of the non-uniform thickness of the ion thinned foil; the reason for the non-uniformity is not known.

However, it is safe to conclude that the dimpling and ion milling do not introduce any detectable increase in the dislocation density.

The second investigation was related to foil thickness (viewing thickness) as related to dislocation density. If the operating voltage of the TEM is 100 KV, the thickness of the foil in which dislocations may be viewed is 0.2 to 0.4 μm. However, if the operating voltage is

1 MV, the thickness of the foil increases to 1 to 2 μm. If we consider the micrograph shown in Fig. 4, we can see the effect of foil thickness on the dislocation densities. Figures 4(a) and (b) are micrographs taken at 100 KV and the foil thickness in Fig. 4(b) in which a few dislocations are visible is 0.3 μm and the dislocation density is $1.6\times10^{13}\,m^{-2}$. Fig. 4(c) and (d) are micrographs taken at an operating voltage of 1 MV. The dislocation density in Fig. 4(d) is $4.5\times10^{13}\,m^{-2}$ and the foil thickness is 0.9 μm. Figures 4 (a), (b), (c) and (d) are micrographs taken from the same area of a foil under the same operating diffraction condition, only a thinner area around the brim of the hole is transparent for the 100 KV microscope. This is a general result for all composites examined. If a low operating voltage is used, i.e. 100-200 KV, the apparent dislocation density is low compared to the dislocation density obtained from foils examined at 1 MV.

Therefore, in order to obtain realistic measures of dislocation density, it is necessary to examine thickness foils which needs a operating voltage (800 KV to 1 MV).

3.2.2. Dislocation Density and Subgrain Size vs. Particle Size and Volume Fracture

The determination of dislocation density by TEM is fraught with many perils. Two of the many possibilities have already been addressed, i.e. introduction of dislocations during sample preparation and the effective viewing of the foil thickness on the observed density. There are certainly several others, especially if numerous slip systems are operative as they certainly are in composites. In a two-beam condition, this means that several operative g-vectors have to be considered, but when operating at 1 MV, a many-beamed condition can easily be used and a larger fraction of the dislocations present become visible. However, it is still necessary to tilt the sample and take several different pictures. Also, there is an inherent variation of dislocations from place to place within the matrix. For example, the dislocation density is higher near the particles and decreases with distance away from the particle. This variation is especially critical in large particle size and low volume fraction samples. In order to overcome this difficulty, it is necessary to take measurements of many micrographs. The procedure for measuring the dislocation density is given elsewhere [5].

The data given for each condition (i.e. particle size or volume fraction) in Figs. 5 and 6 represent tens to hundreds of micrographs of a given foil and 5-6 different foils were examined for each condition. The dislocation densities reported are the average dislocation densities in the matrix of annealed samples. As stated above, the dislocation density is not uniform in the matrix.

Upon increasing the volume fraction, the dislocation density increases, but upon increasing the volume fraction, the subgrain size decreases as shown in Fig. 5, and upon increasing the particle size, the opposite is the case, the dislocation density decreases (and the subgrain size increases) as the particle size increases (Fig. 6).

3.3 Effect of Cold Rolling

The yield strength and the dislocation density were determined of a 0 V% 1100 Al alloy which had been cold rolled ~ 90%. The cold rolling reduced the subgrain size slightly from 5-10 μm to 2 μm, but there was a significant increase in dislocation from less than 10^{10} m to 1.5×10^{13} m. The cold rolling increased the yield strength from 30 MPa to 146 MPa. If a comparison is made with the 9 μm SiC particle size to 20 V% 1100 Al alloy matrix composite, it can be seen that the $\Delta\sigma_y$ is greater for the cold rolling material than that of the SiC_p/1100 Al alloy composite (Table I). However, the interesting point is that the dislocation density in the composite is much greater than that of the 0 V% 1100 Al alloy cold rolled material.

4. DISCUSSION

The discussion will follow along the lines of the questions raised in the Introduction.

4.1 Dislocation and Subgrain Size Determinations

From the investigation of high purity Al, it was shown that the dislocation density in the foils, produced by dimpling and ion milling was the same as that in the electro-chemically produced foils. A main concern of ion milling is that the heat generation occurs and that this heat generation would result in a decrease in the dislocation density. In terms of dimpling, which involves grinding the foil with 0.25 μm diamond paste, this could

plastically deform the sample, i.e. introduce dislocations. These dislocations would have an entirely different appearance as compared to the remnant dislocations which remain from the long term high temperature annealing. The outcome of this investigation is that the dimpling and ion milling do **NOT** introduce any dislocations into the TEM foil.

If the foil thickness increases, the density of dislocations should increase up to center foil thickness and remain constant. For if we consider a homogeneous material, for example, high purity Al. The reason for the decrease in the density in a thinner foil is that the presence of the image force should move a proportionally larger number of dislocations from the thinner foil.

In the case of SiC/Al alloy composites, we are not dealing with a homogeneous material. There are thermal residual stresses within the sample prior to thinning. If we consider points labeled 2 in Fig. 7, there is a tensile residual stress acting in the direction C^1, A^1 and B^1. If the sample is cut along the lines A-A^1 and B-B^1, the stress at the surfaces will have to relax to zero. A simple manner of stress relaxation is by dislocation motion, i.e. dislocation motion out of the foil. Again, the thinner the foil, the more extensive the proportional dislocation loss out of the sample. The image force is still present and would tend to reduce the dislocation density still in the thinner area of the foil, just as in the homogeneous material. Therefore, in order to obtain reasonable measures of the dislocation density, it is necessary to examine thicker portions of the TEM foil, which means examining the foil at 1 MEV. The determination of the subgrain size is not as dependent on foil thickness or the foil preparation procedure.

4.2 CORRELATION BETWEEN MICROSTRUCTURAL CHANGES AND YIELD STRESS

The increase in the yield stress with an increase in the volume fraction or the decrease of yield stress with an increase in the particle size is to be expected. Correspondingly, the dislocation density and the subgrain change in the expected manner. However, it is necessary to consider if **THE CHANGES IN THE YIELD STRESS CAN BE RELATED TO THE**

CHANGES IN DISLOCATION DENSITY AND THE SUBGRAIN SIZE.

Before considering these correlations, it is necessary to point out again that dislocation density within the matrix is not uniform, and secondly, there can be a significant difference in stress at the proportional limit and the yield stress defined at a plastic strain of 0.2%. This would indicate that there is significant work hardening on a local scale occurring within the matrix. The reason for stating that it is on a local scale is due to the fact that very little plastic strain is occurring between the proportional limit and the defined yield stress. Investigations have shown that it is very difficult to determine any changes in the overall dislocation density at yielding [11]. It is not known at the present time where the predominance of dislocation motion has occurred when a tensile plastic strain of 0.2% has been obtained, a FEM analysis [11] seems to indicate that the predominance occurs in the higher dislocation density region. Therefore, a assumption is made that the average increase in the dislocation density is small due to the initial loading to a plastic strain of 0.2%, and that the stress field which opposes dislocation motion had a strain of 0.2% which is due to the average dislocation density of the annealed undeformed sample. Therefore, we can use the well-established relationship

$$\Delta\sigma_y = \propto \mu b \sqrt{\rho}$$

where $\Delta\sigma_y$ is the increase in the yield stress of the composite over that of the 0 V% matrix material, $\propto$ is a constant and Hansen [12] has shown that for Al, this 1.25, μ is the shear modulus of the matrix (2.64×10-4 MPa), **b** is the Burgers vector (2.86×10^{-10} m) and ρ is the dislocation density.

Then we can calculate the incremental increase in the yield stress due to the presence of the increase in dislocation density. This is the increase which should be added to the annealed 0 V% Al alloy matrix yield stress. In Table II are listed the incremental increases in the strength due to an increase in dislocation density as a function of changes in particle size at a constant volume fraction of 20%.

If we consider the increase in dislocation density with the increase in volume fraction, it is obvious that the strengthening due to the increase in dislocation density alone is very large (Table III). In this case, it is necessary to subtract out the dislocation density of the 0 V% material, for this is appreciable when considering smaller volume fractions. In a case of particle size increase, this subtraction is not necessary. for the dislocation density of the 0 V% annealed 1100 Al alloy matrix was very low.

In terms of strengthening due to a reduction in subgrain size, it is necessary to rely on the data of McQueen. In Table II are listed the predicted increase in strength due to a reduction in the subgrain size $\Delta\sigma_{SG}$. The subgrain size of the 1100 Al matrix is much larger than the subgrain size of the composite so a subtraction is not necessary. The amount of strengthening due to a reduction in subgrain size in the small particle size range is greater than that in the large particle size range. If we consider the effect of volume fraction on the change in the subgrain size, in this case, it is necessary to subtract the increment of 0 V%. The increase in strength due to the reduction in subgrain size becomes predominant at 20 V%.

In general, the predicted increase in the yield strength is much larger than the experimentally determined yield strength. There are several possible explanations for this discrepancy; a) the value taken for the constant α in Eq. 1 is too large. The values reported in the literature for α range from 0.5 to 1.25. The second possibility is that the assumption of using an average dislocation density is not valid for the plastic strain at 0.2% and may be due to the motion of dislocations in the matrix where the dislocation density is much lower than the average density. This certainly could account for the discrepancy in the 250 μm particle size composite and the 1 V% composite where the variation in the dislocation density is the greatest.

4.3 STRENGTHENING OF THE MATRIX

As discussed in the Introduction, there is a question as to whether the matrix can be strengthened to the required levels by changes in the microstructure, i.e. can there be a

sufficient increase in the dislocation density or a sufficient decrease in the subgrain size?

The cold rolled investigation has shown that the 0 V% 1100 Al alloy material can have a yield stress which is comparable in strength to a 20 V% SiC/Al alloy composite.

5. CONCLUSIONS

This investigation had as its purpose to address several questions concerning the observed strength of discontinuous SiC/Al alloys, especially related to the mechanism proposed which is based on the changes in the microstructure of the matrix due to differences in thermal coefficient of expansion between the reinforcement and the matrix.

From a consideration of the data, several conclusions were obtained:

- The observed strength of the discontinuous SiC/Al composite can be accounted for in terms of a mechanism based on a change in the microstructure of the matrix.
- This change in the microstructure, i.e. an increased dislocation density and a reduced subgrain size as compared to 0 V% matrix alloy, is due to the difference in coefficient of expansion between the reinforcement (SiC) and the matrix (Al).
- The procedure of TEM foil preparation of the composites which involves electrical discharge machining, dimpling and ion milling does not introduce dislocations into the matrix.
- In order to obtain realistic values of the dislocation density, it is necessary to view thick foils, i.e. an operating voltage of 1 MV.

Acknowledgement

This research was supported by the Office of Naval Research under contract No. N00014-K-85-0007. The positive interactions with Dr. S. Fishman of the Office of naval Research are to be greatly acknowledged. The authors wish to acknowledge the assistance of Dr. S.B. Wu in the performance of the tensile tests. The authors also wish to acknowledge the continued support of the Argonne National Laboratory HVEM facility, especially that of Dr. E. Ryan.

References

1. G.I. Taylor, *Proc. Roy. Soc. A 145* (1934) 362, *J. Inst. Met. 62* (1938) 307.
2. G. Boas, *Helv. Phys. Acta 23* (1950) 159.
3. H.J. McQueen and J.E. Hackett, *Metal. Trans. 1* (1970) 2997.
4. R.J. Arsenault, *Mater. Sci. Eng. 64* (1984) 171.
5. M. Vogelsang, R. Fisher and R.J. Arsenault, *Metal. Trans. 17A* (1986) 379.
6. R.J. Arsenault and N. Shi, *Mater. Sci. Eng. 81* (1986) 175.
7. H. Fujita, Y. Kawasali, E. Furubayashi, *Japan J. Appl. Phys. 6* (1967) 214.
8. H. Fujita, T. Tabata, K. Yoshida, N. Summida and S. Katagiri, *Japan J. Appl. Phys. 11* (1972) 1522.
9. H. Fujita, T. Tabata, *Japan J. Appl. Phys. 12* (1973) 471.
10. M. Taya and R.J. Arsenault, *Scripta Metal. 21* (1987) 349.
11. R.J. Arsenault, N. Shi, L. Wang and C.R. Feng, "Localized Deformation of SiC/Al Composites," submitted for publication in *Mater. Sci. Eng.*
12. N. Hansen, *Acta Metal. 25* (1977) 863.

TABLE I

Comparison of 9×10^{-6} m Particle Size 20 V% SiC/Al Composite with Cold Rolled 0 V% 1100 Al Composite

Material	Dislocation Density $\rho\times10^{14}$ m^2	Subgrain Size $\lambda\times10^{-6}$ m	Δ Experiment Yield Stress $\Delta\sigma_{y_{0.2}\%}$ MPa	ΔCalculate Yield Stress MPa
20 V% SiC_p	1.1	2	88	168
0 V% CR	.15	2	116	106

Δ calculated yield stress = the predicted increase in strength due to an increase in ρ and a decrease in λ.

Δ experimental yield stress = the yield stress of the composite minus the yield stress of 0 V% matrix.

TABLE II

Predicted Increase in Yield Strength of 20 V% SiC 1100 Matrix and Experimentally Measured Values

Particle Size D (μm)	$\Delta\sigma_\rho$ MPa	$\Delta\sigma_{SG}$ MPa	$\Delta\sigma_{y_{pred}}$ MPa	$\Delta\sigma_{y_{exp}}$ MPa
0.5	126.6	131	257.6	153
9	99	69	168	88
70	79	20	20	69
250	59.7	0-13.8	59.7-73.5	26

Keys

$\Delta\sigma_{y_{exp}}$ The yield stress defined at 0.2% plastic strain minus the 0.2% yield stress of the 0 V% 1100 matrix

$\Delta\sigma_\rho$ The predicted increase due to the increased dislocation density

$\Delta\sigma_{SG}$ The predicted increase due to the reduced subgrain size

$\Delta\sigma_{y_{pred}}$ The sum of $\Delta\sigma_\rho + \Delta\sigma_{SG}$

TABLE III

Predicted Increase in Yield Stress of 6061/Al Alloy as a Function of Volume Fraction of SiC Whisker

Volume Fraction V%	$\Delta\sigma_\rho$ MPa	$\Delta\sigma_{SG}$ MPa	$\Delta\sigma_{y_{pred}}$ MPa	$\Delta\sigma_{y_{exp}}$ MPa
1	37.7	0	37.7	6.9
5	56.6	7.0	63.6	52
20	70	48.3	118.3	100

Keys

$\Delta\sigma_{y_{exp}}$ The yield stress defined at 0.2% plastic strain minus the 0.2% yield stress of the 0 V% 1100 matrix

$\Delta\sigma_\rho$ The predicted increase due to the increased dislocation density

$\Delta\sigma_{SG}$ The predicted increase due to the reduced subgrain size

$\Delta\sigma_{y_{pred}}$ The sum of $\Delta\sigma_\rho$ x $\Delta\sigma_{SG}$

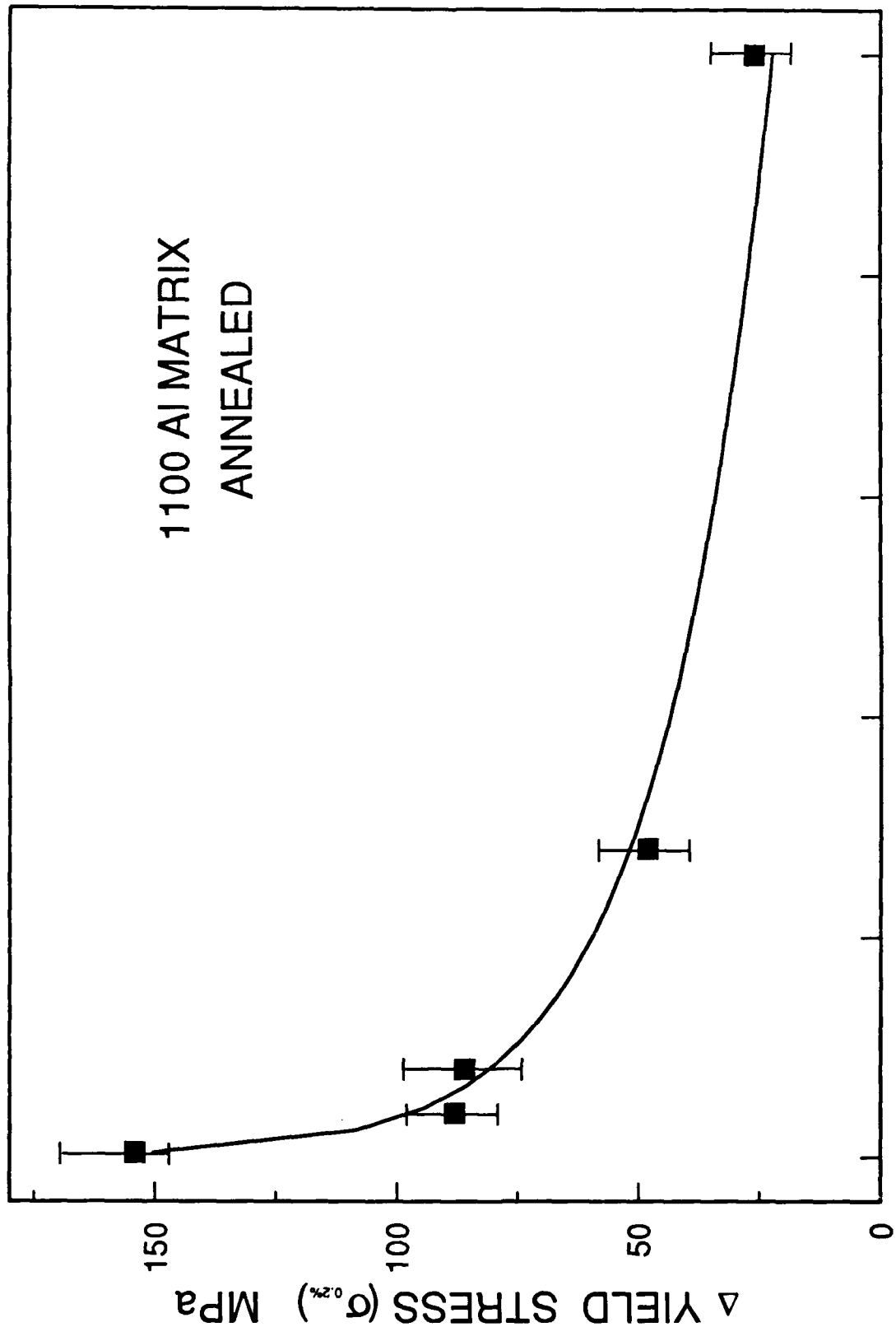

Fig. 1 The change in the yield stress as a function of SiC particulate size. The matrix is a 1100 Al alloy. The composite is in the annealed condition.

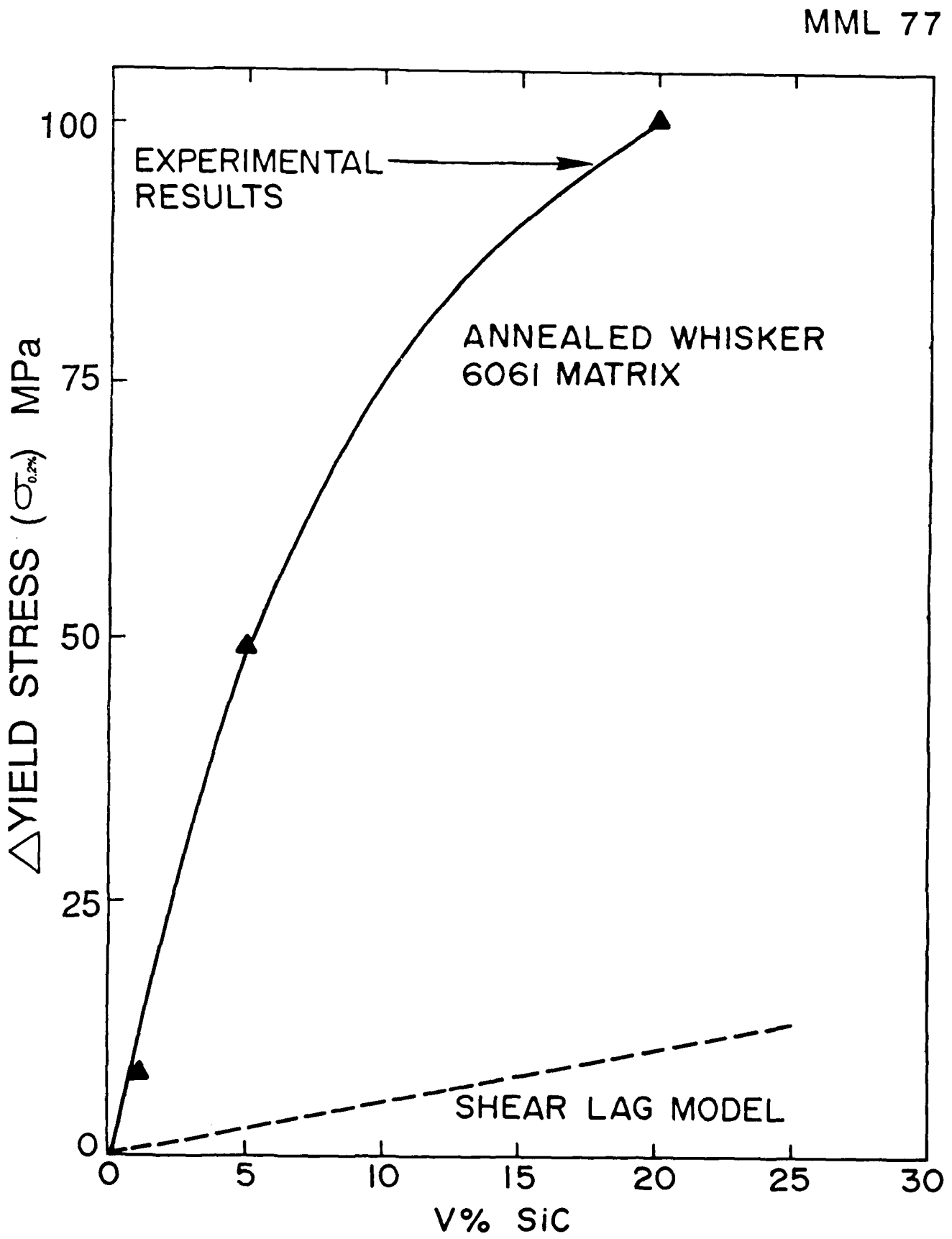

Fig. 2 The change in the yield stress as a function of the volume fraction of SiC (SiC particulate is ~ 5 μm in dia.). The matrix is a 6061 Al alloy. The composite is in the annealed condition.

Fig. 3(a) A transmission electron micrograph of high purity Al in the annealed condition thinned by dimpling and ion milling.

Fig. 3(b) A transmission electron micrograph of high purity Al in the annealed condition thinned by dimpling and jet polished.

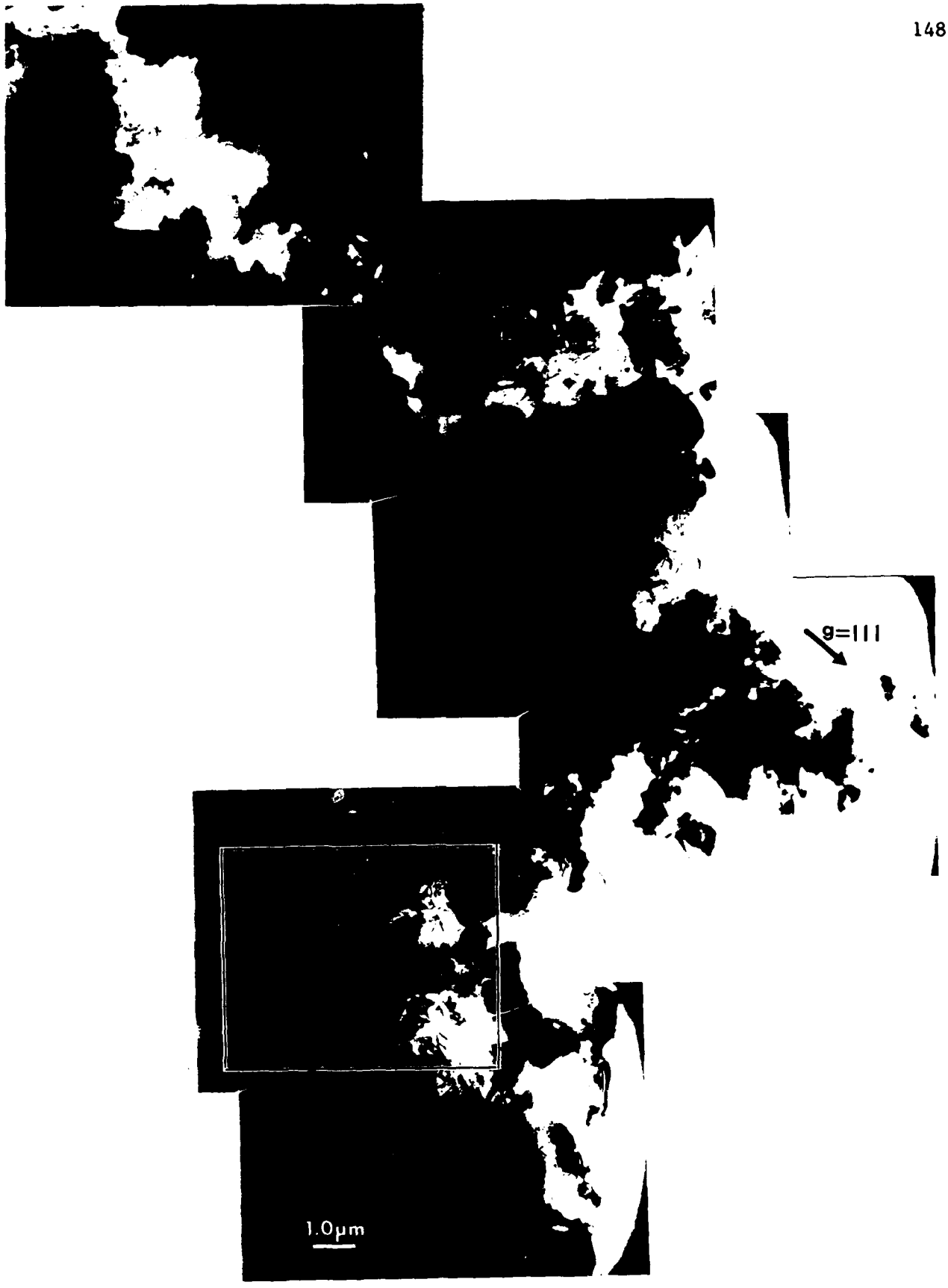

Fig. 4(a) A transmission electron micrographs taken at an operating voltage of 100 KV.

Fig. 4(b) A transmission electron micrographs taken at an operating voltage of 100 KV. This micrograph is of the enclosed area in Fig. 4(a).

Fig. 4(c) A transmission electron micrographs taken at an operating voltage of 1 MV.

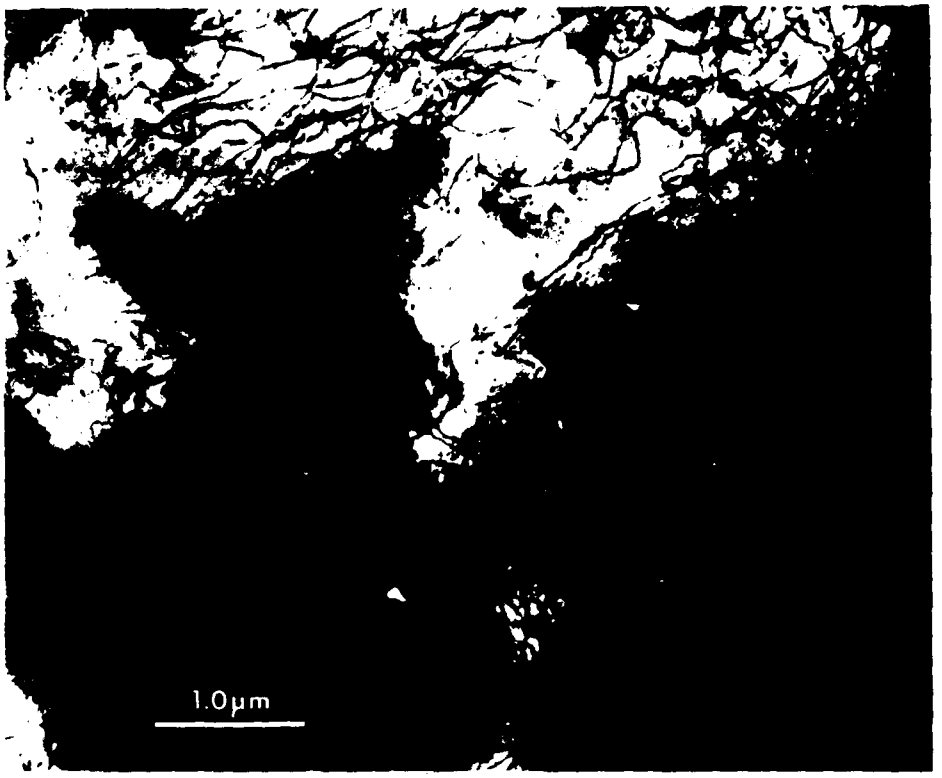

Fig. 4(d) A transmission electron micrographs taken at an operating voltage of 1 MV. This micrograph is of the enclosed area in Fig. 4(c).

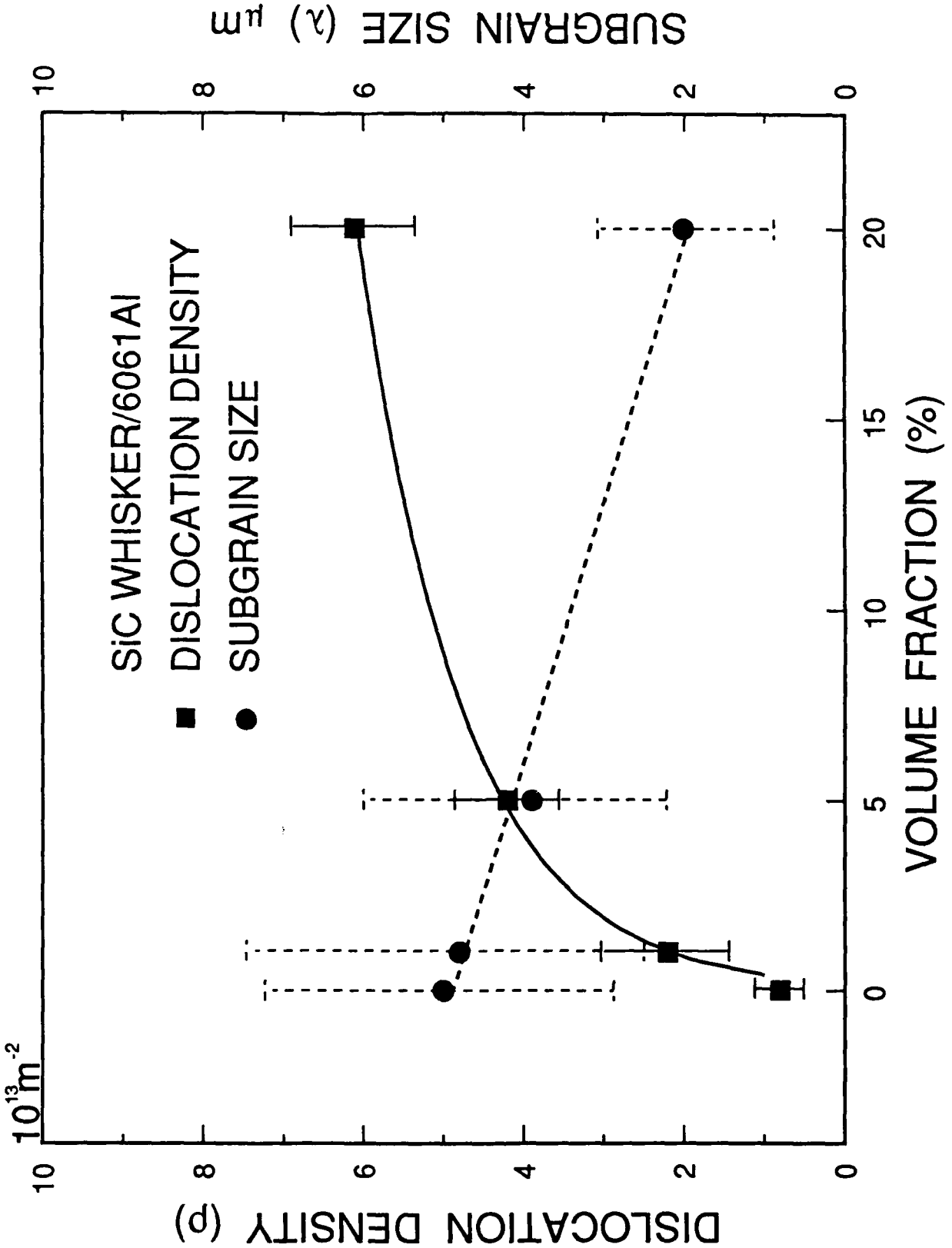

Fig. 5 The change in dislocation density as a function of volume fraction of SiC (SiC whiskers have a length to diameter on average of ~ 2 and the dia.~ 0.5 μm).

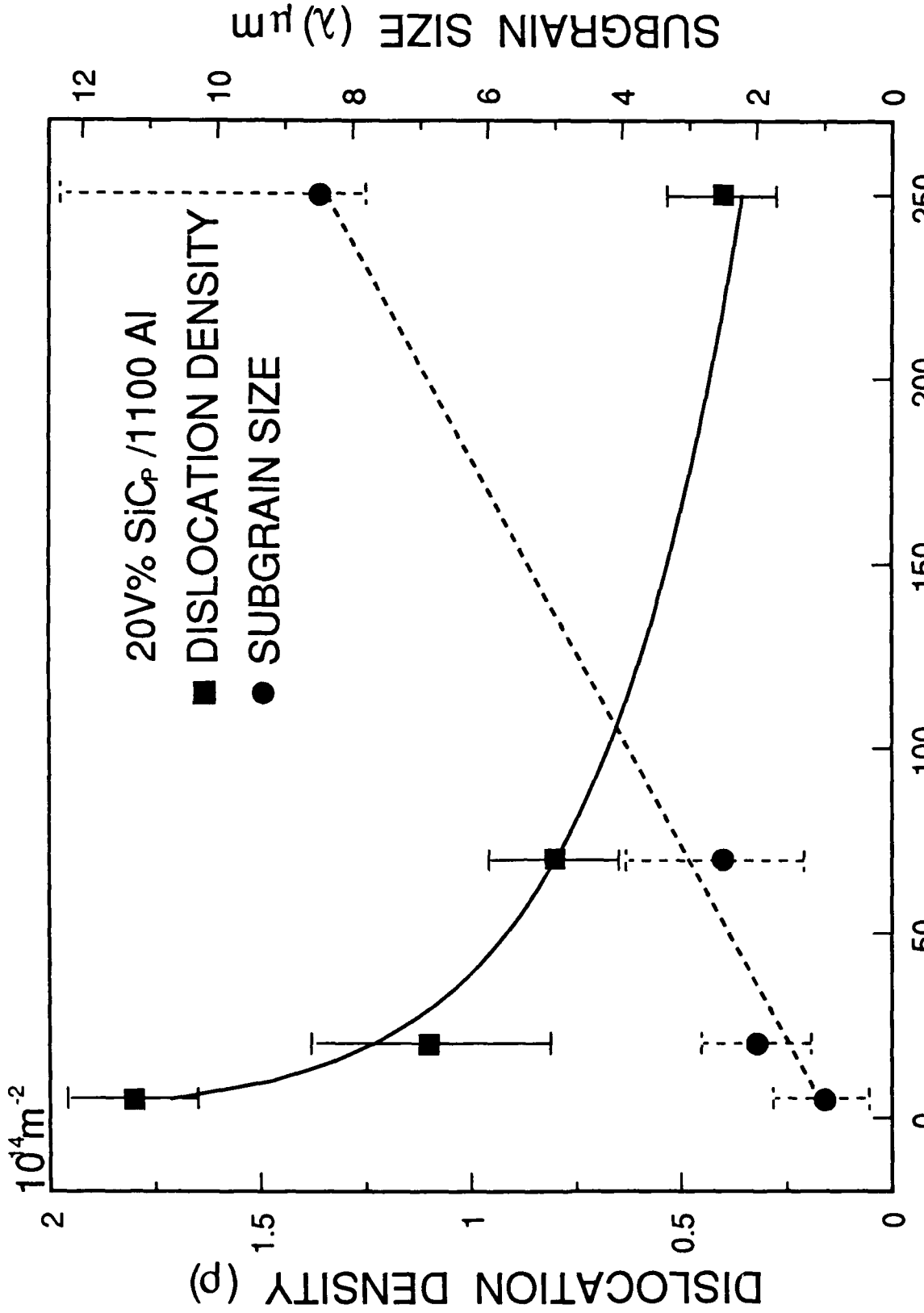

Fig. 6 The change in dislocation density as a function of particulate size.